MEASURING COFFEE EXTRACTION KINETICS AT EARLY TIME SCALES

The University Of Sheffield.

Matthew James Maille

Chemical and Biological Engineering

University of Sheffield

May 2024

A thesis submitted for the degree of

Doctor of Philosophy

Acknowledgements

I would like to express my profound gratitude to my advisor, Professor Jim Litster, for providing this opportunity to pursue my dreams and helping me achieve this significant milestone in my life. You always fostered an environment full of encouragement, kindness, and patience. You supported me, guided me, and helped me grow as a professional and as an engineer, for which I will always be grateful.

I would like to thank Keurig Dr Pepper for sponsoring my entire PhD program. Dan Fletcher and Patricia Carulli-Hauser, thank you for championing my sponsorship at the senior leadership and executive leadership levels. Scott Moffitt, thank you for providing the executive approval in this investment in me as an individual and recognizing the strategic value this work would bring to the company. I thank Dr. Alberto Azeredo, Jeff Allard, Switlana Wojcickyj, and Kevin Madina for your continued financial support over the years in this endeavor.

Over the past six years, numerous individuals at Keurig helped me through this journey in various ways; the most important was Dr. Alberto Azeredo. Alberto, your unwavering, continuous support and advocacy is one of the principal reasons I was able to complete my PhD. You advocated and ensured my funding was there for every year of this program, which was an enormous undertaking. It required personal sacrifice to influence several senior leaders to maintain Keurig's investment in this program. You secured and provided the resources and time necessary for me to complete the research. I will forever be grateful for your support, sacrifice, investment, and advocacy.

I would like to thank Kyle Sala for being an amazing colleague, friend, and my sounding board on so many fronts; you were instrumental in my post graduate journey. A special thanks to past and current colleagues Edward Fuchs, Chuck Opferman, Dwight Noyes, Olivia George, Vince Cruz, Jordan Cormier, Brittany DeWind, Hannah Zukswert, Chris O'Brien, and Dr. Paul Milne for your support and contributions. I would also like to thank Dr. David Scott for your technical guidance and our various discussions. Additional mentors I would like to thank are Professor Rachel Smith, Dr. James Michaels and Dr. Willie Hendrickson. I would like to thank Dr. Bryan Ennis for suggesting I do a PhD; without you suggesting this in the first place, I'm not sure I would've ever considered pursuing one. This is evidence that a simple comment from one interaction can inspire and change a person's career and life.

Lastly, but most importantly, I thank my amazing wife Dr. Laura Werner for your consistent support, love, and patience over the last six plus years of this journey. To my parents, Charlene A. Maille and George A. Maille Jr, and all my family thank you for your endless love and support. God has blessed me with a loving family, and with many supportive friends, mentors, and colleagues.

Abstract

Measuring Coffee Extraction Kinetics at Early Time Scales

By Matthew James Maille

Research Supervisor: Professor James Litster

The single-serve coffee market has experienced significant growth over the past 25 years with over tens of billions of single-serve coffee units sold annually worldwide. Single serve pods are very popular due to the extreme convenience of brewing a fresh, full cup of coffee in a minute or less, at the touch of a button. Despite the growing adoption and use of single serve coffee appliances and pods, there is very little literature which explores the coffee extraction kinetics at the time scales of a single serve brew method, specifically 5 to 30 s.

This thesis develops a new method for measuring early time scale coffee extraction kinetics in a well-mixed batch reactor. This is accomplished by the unique sampling approach to fractionate coffee extract at previously unachievable time scales. Coffee extraction kinetics for caffeine, chlorogenic acid (3-CQA), citric acid, malic acid, and quinic acid are measured between 5 s and 600 s with 80% of the extraction data collected under 35 s.

Individual chemical compounds with nearly identical molecular weights had very different extraction kinetics in the first 30 s. Two compounds, caffeine and 3-CQA, showed a 3 to 4 s delay in extraction. For the three other compounds, extraction began immediately. This is the first data set to capture this behavior. 50% of the citric and malic acid concentration was found to extract within the first 10 s, highlighting the criticality of understanding extraction kinetics at early time scales.

[redacted]

The extraction data collected by the new method provided direct evidence of two distinct extraction regimes during brewing; an initial rapid extraction regime followed by a slower extraction regime. A new two term empirical model to describe these two extraction regimes is introduced. The characteristic time of the rapid extraction regime varies between 5 and 15 s, whereas the characteristic time for the slow extraction regime varies between 20 and 150 s for the various chemical compounds measured. This model yielded excellent fits to the measured kinetic data, with mean percent errors under 10%, and in many cases 5% or less.

Understanding short time kinetics can lead to improved sensory attributes and coffee extraction efficiency, differentiate products on shelves, and increase revenue growth and profit.

[redacted]

Table of Contents

List of Figures

List of Tables

List of Variables and Abbreviations

Variable	Description	Units
a	Dimensionless, non-zero intercept term (*Eqn* 2.2)	-
a'	Inverse of dimensionless residence time	-
a_{sf}	Volume specific surface area	$m^2\ m^{-3}$
A_{sp}	Specific surface area	$m^2\ kg^{-1}$
Bi_m	Mass transfer Biot number	-
c	Dimensionless constant in BET analysis (*Eqn* 3.3)	-
C	Concentration	$kg\ L^{-1}$
$C_{aliquot,1}$	Aliquot concentration of the first sample	$kg\ L^{-1}$
$C_{aliquot,i}$	Aliquot concentration of the i^{th} sample	$kg\ L^{-1}$
C_∞	Bulk solution concentration at infinite time	$kg\ L^{-1}$
C_t	Concentration at time t	$kg\ L^{-1}$
$C_{s,0}$	Initial solute or solid concentration	$kg\ L^{-1}$
$C_{l,0}$	Initial bulk liquid concentration	$kg\ L^{-1}$
$C_{l,sat}$	Saturation concentration of the solute in the solvent	$kg\ L^{-1}$
$C_{sys}(t)$	Concentration of the system at time t	$kg\ L^{-1}$
$C_{sys,j}$	Concentration of the system at the time of the j^{th} sample	$kg\ L^{-1}$
Ca	Dimensionless Café number	-
δ	Thickness of a Nernst layer	m
d_c	Diameter of a single coffee cell	m
d_{cell}	Diameter of a single plant cell	m
d_p	Diameter of a particle	m
d_{pore}	Diameter of a pore within a particle	m
$d_{3,2}(Co.)$	Sauter mean diameter for the coarse fraction of a volume distribution	m
$D[4,3]$	Volume mean diameter of a particle size distribution	m
$D[4,3]_i$	i^{th} Volume mean diameter of a particle size distribution	m
$D[3,2]_{dry}$	Sauter mean diameter from Malvern air dispersion method of a particle size distribution	m
$D[4,3]_{dry}$	Volume mean diameter from Malvern air dispersion method of a particle size distribution	m
$D[4,3]_{hybrid}$	Volume mean diameter of the particle size distribution obtained by the combination of the liquid and air dispersion data sets.	m
D_{eff}	Effective diffusivity	$m^2\ s^{-1}$
D_{soln}	Diffusivity in solution	$m^2\ s^{-1}$
ε_{open}	Open porosity within a particle	-
ε_{closed}	Closed porosity within a particle	-
ε_p	Particle porosity	-

ε_v	Void fraction	-
Fo_m	Fourier number for mass transport	-
γ^{lv}	Surface tension of liquid	N m^{-1}
h	Penetration distance into a capillary pore	m
K	Partition Coefficient	-
k	Mass transfer coefficient	m s^{-1}
k_1	Mass transfer coefficient of the first layer of cells in a particle	m s^{-1}
k_c	Mass transfer coefficient of the inner layer	m s^{-1}
k_j	Mass transfer coefficient of the j^{th} layer of cells in a particle	m s^{-1}
k^*	Mass transfer coefficient weighted by specific surface of coffee bed	m s^{-1}
k_{obs}	Observed mass transfer coefficient	m s^{-1}
$\boldsymbol{\lambda}_1$ or $\boldsymbol{\lambda}_{fast}$	Time constant for the rapid extraction regime	s
$\boldsymbol{\lambda}_2$ or $\boldsymbol{\lambda}_{slow}$	Time Constant for the slow extraction regime	s
m	Mass	Kg
$m_{sys,j}$	Mass of the system at j^{th} sample	Kg
μ_f	Dynamic viscosity of a fluid	Pa s
M_w	% Moisture on a wet basis	-
n	Recursive index	-
N	Number of concentric layers of a single cell thickness in a plant particle	-
N_A	Avogadro's number	-
Ω	Coffee test material identifier	-
P	Pressure	Pa
P^o	Saturation pressure of an adsorptive gas	Pa
P_1	Measured pressure of helium in sample cell in pycnometry testing	Pa
P_2	Measured pressure of filled helium expanded into the reference volume	Pa
ΔP	Change in pressure	Pa
φ	Total concentration fraction extractable in the rapid extraction regime	-
Q	Volumetric flow rate	m^3 s^{-1}
r	Radial distance from the origin of an object	m
R_p	Radius of a particle	m
R_{pore}	Effective capillary pore radius	m
ρ	Density	kg m^{-3}
ρ_b	Bulk density	kg m^{-3}
ρ_e	Envelope density	kg m^{-3}
$\rho_{e,corrected}$	Corrected envelope density	kg m^{-3}
$\rho_{e,reported}$	Reported envelope density from mercury intrusion porosimetry	kg m^{-3}
ρ_f	Fluid density	kg m^{-3}
ρ_s	Particle density	kg m^{-3}

ρ_t	True density, the intrinsic density of a solid material	kg m^{-3}
σ^2	Cross-sectional area of the adsorptive molecule	m^2
τ	Observed extraction delay time	s
τ_p	Particle relaxation time	s
t	Time	s
$t_{exp,0}$	Time from the addition of coffee into WMBR to extract flow out	s
$t_{i,corrected}$	Corrected sample time for the i^{th} sample	s
t_j	Time at j^{th} sample	
θ	Contact angle	°
θ_d	Dynamic contact angle	°
θ_{fs}	Fraction of total dissolved solids from surfaces of coarse particles and fine particles	-
$\theta_{hybrid,j}$	Cumulative volume fraction of the hybrid particle size distribution	-
$\theta_{fines\ (liquid)}$	Volume fraction of all particles <186 µm measured by liquid dispersion	-
$\theta_{coarse\ (air)}$	Volume fraction of all particles >186 µm measured by air dispersion	-
$\vartheta_{v,coarse}$	Total volume fraction of the surface of coarse particles contributing to fast extraction	-
$\theta_{v,fines}$	Total volume fraction of all particles below 186 µm.	-
V	Volume	L or m^3
$V_{aliquot,1}$	Initial or first aliquot volume removed	L
$V_{aliquot,i}$	Aliquot volume removed of the i^{th} sample	L
V_c	Calibrated sample cell volume	m^3
V_m	Adsorptive gas monolayer volume	m^3
$V_{pore,P=27.4kPa}$	Pore volume measured by mercury intrusion at a pressure of 27.4 kPa	m^3
V_r	Reference cell volume	m^3
V_s	Sample volume	m^3
V_{ss}	Average volume of aliquots removed during steady state flow & sampling	L
$V_{sys,0}$	Initial system liquid volume	L
$V_{sys,j}$	System liquid volume at the j^{th} sample	L
$v_{i,liquid}$	Class bin volume fraction of the i^{th} bin on Malvern measured by liquid dispersion	-
$v_{i,air}$	Class bin volume fraction of the i^{th} bin on Malvern measured by air dispersion	-
$v_{i,hybrid}$	Class bin volume fraction of the i^{th} bin of the hybrid particle size distribution	-
x	Solute exhaustion degree of the particle	-
x_j	Solute exhaustion degree of the j^{th} spherical layer of the particle	-
$\overline{x_i}$	Arithmetic average of the i^{th} bin class particle diameter	m

Abbreviations	Description
3-CQA	Chlorogenic acid (3-O-Caffeoylquinic acid)
5-CQA	Neochlorogenic acid (5-Caffeoylquinic acid)
BET	Brunauer-Emmett-Teller
BICM	Broken and Intact Cell Model
BIC-SCM	Broken and Intact Cell-Shrinking Core Model
CL	95% Confidence Level
DoE	Design of Experiments
DI	Deionized (Water)
FEM	Finite Element Method
HFS	Horizontal Feed Screw
HPLC	High Performance Liquid Chromatography
HTST	High Temperature Short Time
IPA	Isopropyl Alcohol
LC-MS	Liquid Chromatography-Mass Spectrometry
LDFM	Linear Driving Force Model
LTLT	Low Temperature Long Time
MPE	Absolute Mean Percent Error
PP	Polypropylene
RPM	Revolutions per Minute
RS	Roll Speed
SCA	Specialty Coffee Association
SCM	Shrinking Core Model
SEM	Scanning Electron Microscopy
SFE	Supercritical Fluid Extraction
SSA	Mass Specific Surface Area
TLM	Thin Layer Model
TDS	Total Dissolved Solids
VFS	Vertical Feed Screw
WB	Whole Bean Coffee
WMBR	Well Mixed Batch Reactor

Chapter 1: Introduction

Coffee in its variety of brew methods, drip, espresso, cold brew and so forth, is one of the most consumed beverages worldwide. The consumption of coffee beverages dates back to the 15th century, and in 2023 was more than a $116 billion global market. Coffee is the second most traded commodity, after oil, and has emerged as major economic factor for several countries and communities [Juma, C. 2016, Markets and Research 2024].

The single-serve coffee market has emerged as a dominant player in the food and beverage industry, demonstrating an astonishing 56,000% growth from 2000 to 2014, as shown in Figure 1.1 and Figure 1.2 [Gonzalez, A. 2014, Trefis Team 2016]. As depicted in Figure 1.2, single serve coffee brewing methods have disrupted the US market, changing how at home coffee is prepared with approximately 28% of consumers choosing a single-serve preparation method versus traditional drip brew (37%), espresso machine (10%), bean to cup (8%), French press (2%), or other (15%) methods [National Coffee Association of U.S.A. 2024].

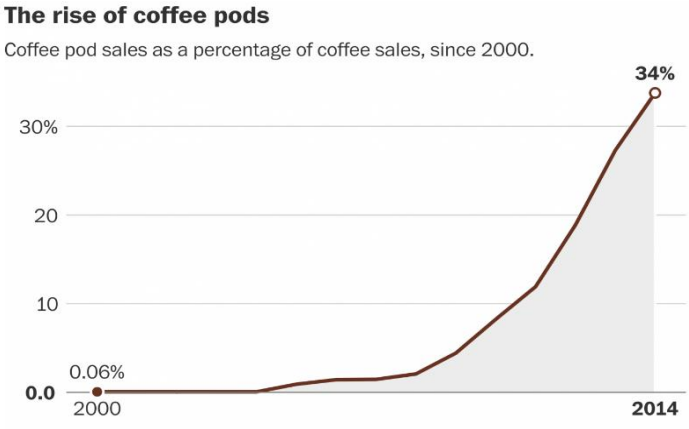

Figure 1.1: Percentage of Coffee Pod Sales of Total Coffee Sales from 2000 to 2014 [Trefis Team 2016].

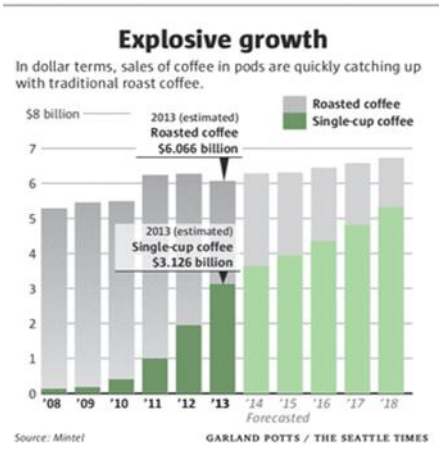

Figure 1.2: Explosive Growth of Single Serve Coffee [Gonzalez 2014].

The success of single serve coffee manufacturers has been due to vast brand selection, availability, and consumer convenience all for customer centricity and customization. As the North American single serve market has become more competitive, industrial emphasis has been placed on market differentiation focusing on coffee quality, price point and coffee design to value. An opportunity for product differentiation is to deliver desired coffee strength out of a single serve pod. A "weak coffee experience" is the greatest barrier to consumer adoption of single-serve coffee technologies [Calderone 2016].

Early research by E.E. Lockhart et al. [1955] concluded that the ideal coffee beverage had strength of 1.15% to 1.35% and a percent extraction of 18-22%. Coffee strength (solubles concentration) is the percent concentration of the coffee total soluble solids in water on a wt/wt basis [Mestdagh et al. 2017]. The strength of the brewed coffee beverage is directly proportional to the coffee to water ratio [Lingle 2011]. Percent extraction (solubles yield) is the percentage of coffee mass extracted from the coffee particles; approximately 28% of the coffee particle will dissolve in water, with the remaining percent mass being comprised of insoluble cellulose fiber. [Lingle 2011].

The work of E. E. Lockhart et al. [1955] was the basis for the Specialty Coffee Association (SCA) brewing control chart relating total dissolved solids to percent extraction for various coffee to water brew ratios when prepared with a traditional drip coffee maker as shown in Figure 1.3. It has been debated whether the SCA chart is applicable to other brewing methods, including the single-serve and other technologies [Melrose et al. 2018].

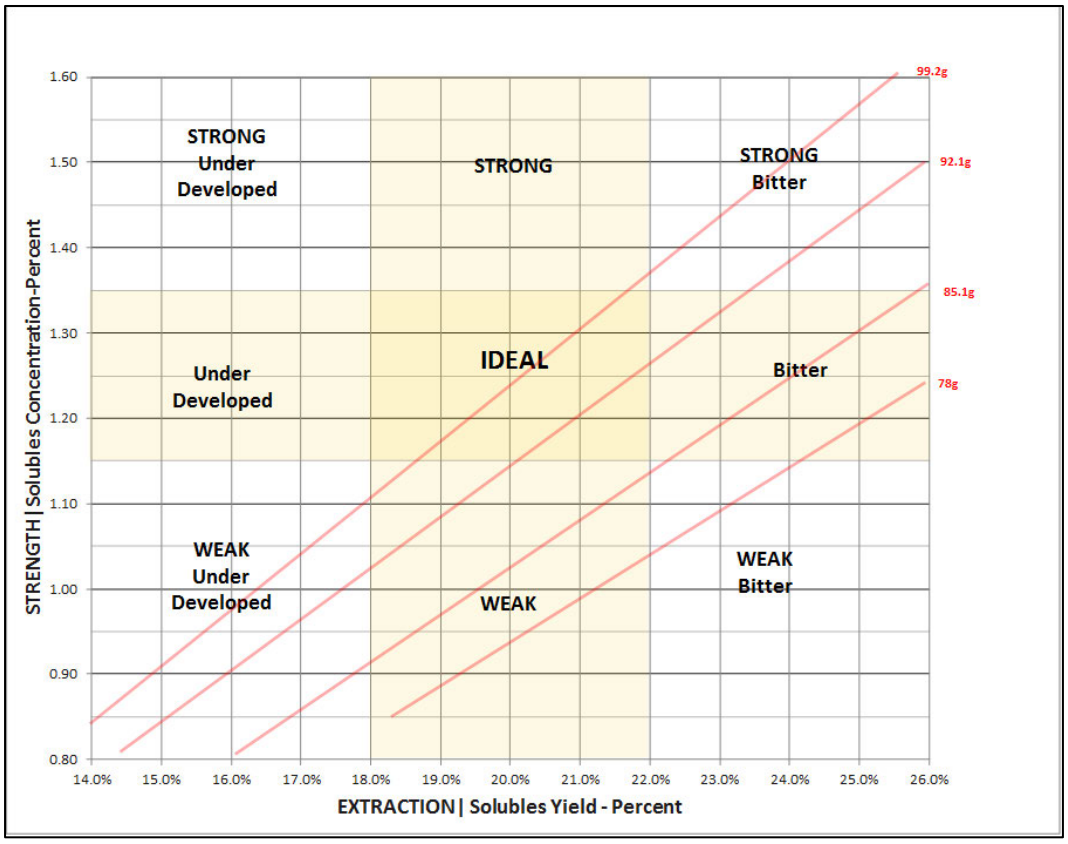

Figure 1.3: Drip coffee brewing control chart [E.E. Lockhart et al. 1955].

Chapter 2:Literature Review

Section 2.1: Introduction to Coffee, Harvesting and Coffee Farm Processing

Green coffee beans are the product of dried seeds from the coffee cherry fruit of a coffee tree. *Coffea Arabica* is the most common species of the coffee plant whose fruit is harvested, pulped, washed, fermented, and seeds dried. After trading, the green coffee beans are post-processed by roasting and grinding [Farah and dos Santos 2015].

Figure 2.1 shows the processing steps of coffee cherries after harvesting. There are three primary processing methods where the endosperm is separated from the rest of the fruit. These three methods are: natural or dry, semi-washed or pulped natural, and wet or washed.

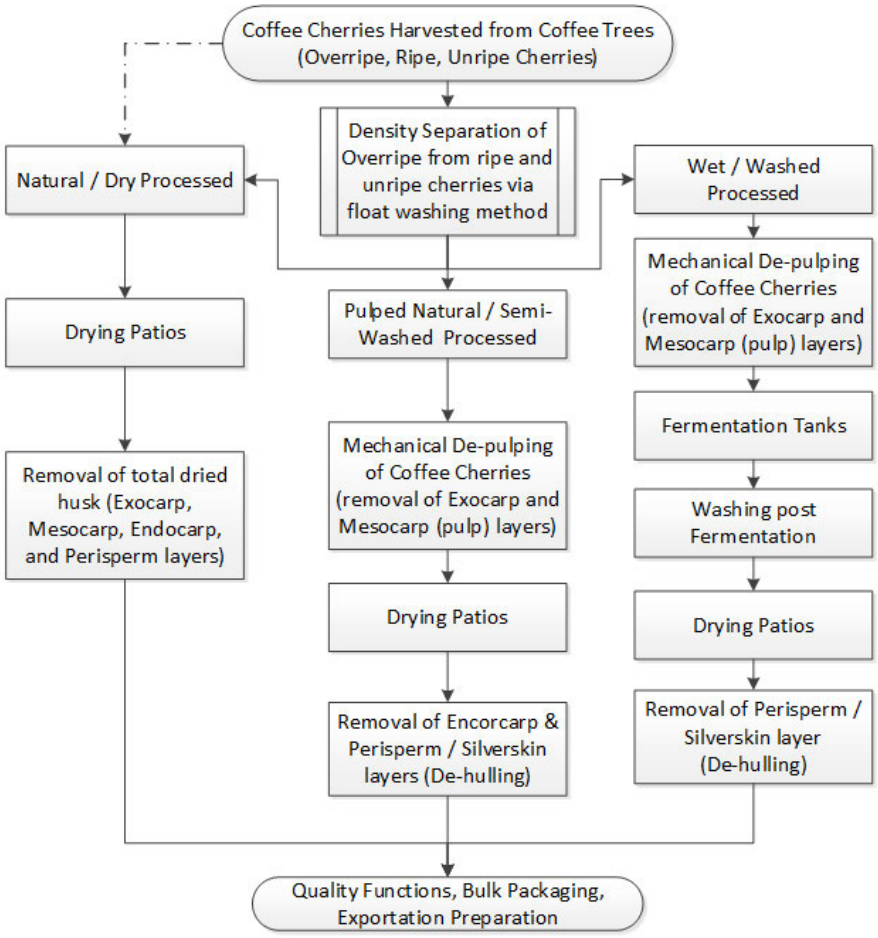

Figure 2.1: Coffee cherry processing steps post-harvest, and an overview of the natural, pulped natural and washed processing methods. [Farah and dos Santos 2015]

At the time of harvesting, overripe, ripe, and unripe coffee cherries are indiscriminately collected. A separation step is used for separating ripe, unripe, and overripe cherries. A water floatation method is the most common process used as overripe cherries float in water, whereas ripe and unripe cherries sink due to density differences. The separation of overripe cherries is critical as they have started to naturally ferment, and therefore mold, which leads to poor coffee quality. The green processing method of the harvested coffee has a large impact on the sensory characteristics of the brewed coffee. For example, green coffee beans processed *via* the washed method have been found to be more acidic [Rao 2014; Farah and dos Santos 2015].

Section 2.2: Overview of Common Coffee Processing Operations

Section 2.2.1: Post-Importation Processing of Green Coffee

After importing green coffee, the next step in the value and operations chains is to turn the green coffee into a finished product. The most common product developed from green coffee is roasted and ground coffee, which is later brewed, and its extract consumed as a beverage. However, there are several other value chain avenues, including decaffeination, producing ready-to-drink coffee, coffee concentrates, and soluble coffee. The unit operations in producing roasted and ground coffee include green bean cleaning (a final effort to remove any additional foreign objects such as stones or other plant matter), roasting, grinding, degassing, and packaging [Clarke (Ed.) 2012b].

Figure 2.2 shows typical processing steps within the value chain after importing green coffee and up to the shipment of finished goods to consumers [Clarke (Ed.) 2012b].

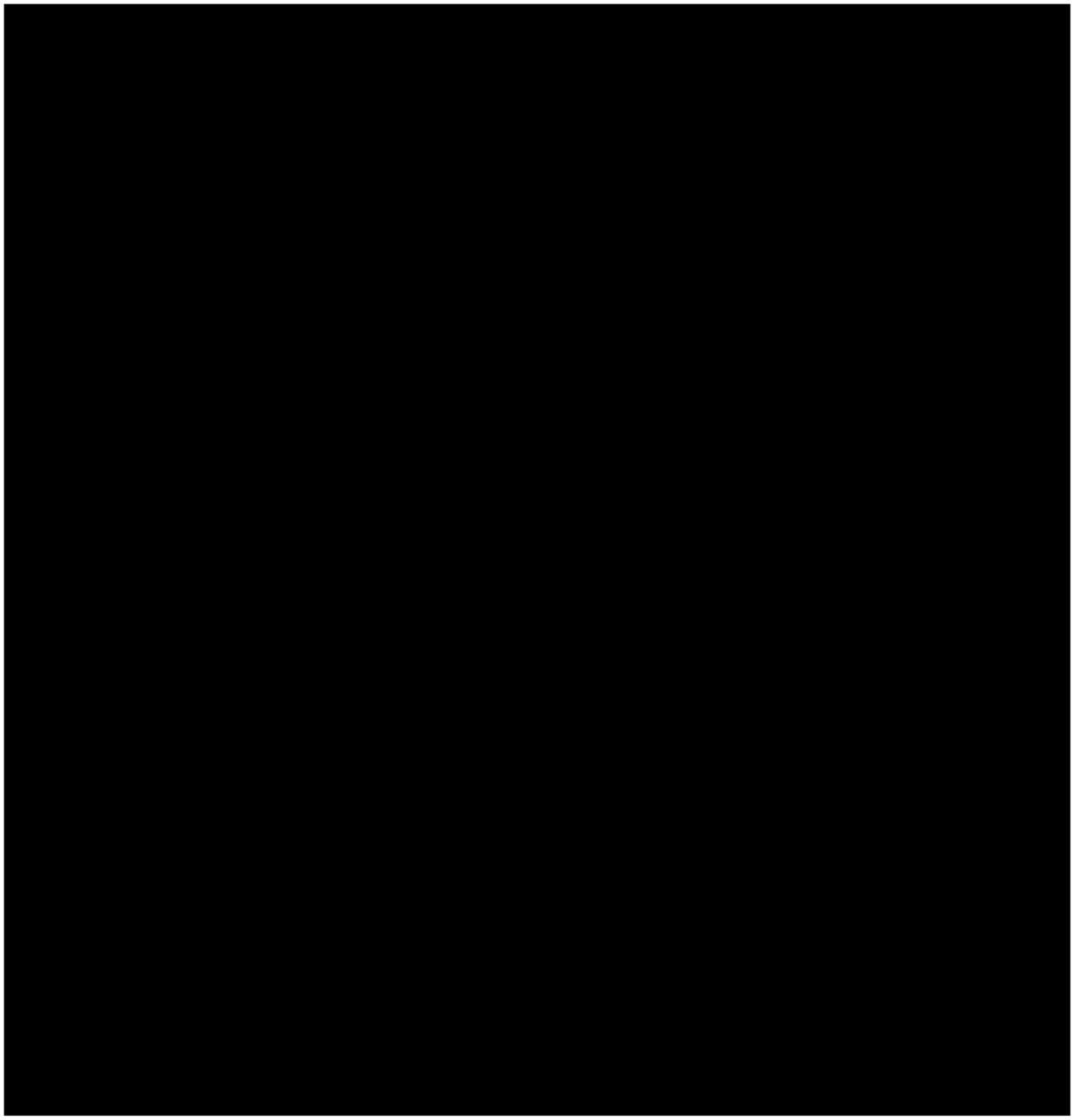

Figure 2.2: Post importation processing of green coffee to various finished goods.

Section 2.2.2 Coffee Roasting

The coffee roasting process is a critical step that influences coffee beverage chemical composition, especially in the development of flavor compounds in the finished beverage [Wei and Tanokura 2015, Buffo and Cardelli-Freire 2004]. A series of complex chemical reactions occur during the roasting process where marked physical changes in the bean appearance and

structure are observed. These chemical reactions include: Maillard, Strecker degradation, and pyrolysis reactions. The change in coffee bean color is a result of the Maillard reactions, whereas water evaporation, Strecker degradation and pyrolysis reactions result in a significant expansion of the coffee bean volume [Wang and Lim 2014, Schenker et al. 2000, Buffo and Cardelli-Freire 2004, Geiger et al. 2005]. A pressure buildup of water vapor and CO_2 generation occurs within the coffee bean during roasting. This pressure develops a porous structure within the coffee bean [Wang 2012]. Figure 2.3 shows the evolution of the coffee bean structure during various stages of roasting.

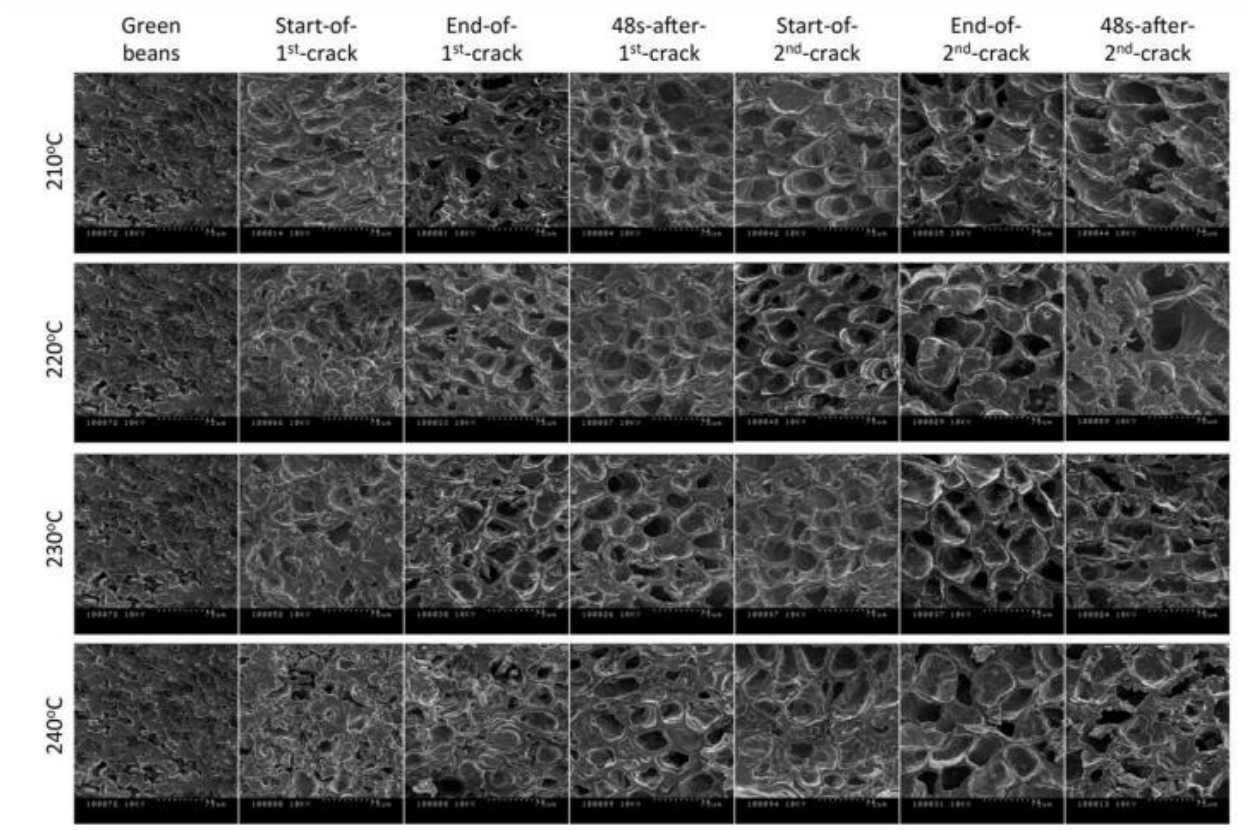

Figure 2.3: SEM images of the internal coffee bean structure at various stages of roasting. The temperatures for each row were the end point roast temperatures. [Wang 2012].

Geiger et al. [2005] claims that the thermo-mechanical behavior and expansion of the coffee bean during a roasting event is due to polysaccharide state transitions. The cellulose structure changes from a glassy to a rubbery state as temperature increases. The authors claim

that it was in the rubbery state that the greatest coffee bean volume expansion was observed. In all studied roasting events, the generation and release of water vapor was always greater than that of carbon dioxide, and thus the main driving force to coffee bean expansion during roasting was attributed to the evaporation of water. Geiger et al. [2005] also reported that in low temperature, long time roasting events (LTLT), more water vapor and carbon dioxide was generated than high temperature short time (HTST) roasting events. These structural changes influence coffee extraction, flavor retention, aroma release, coffee oil migration, and coffee degassing behavior [Geiger 2004].

Bustos-Vanegas et al. [2018] observed that higher roasting temperatures provided greater bean expansion, consistent with the findings of Schenker et al. [2000], Geiger [2004], and Geiger et al. [2005]. The authors found that the coffee bean expansion was isotropic at temperatures around 220^{o}C. Moreover, it was noted that at roasting temperatures of 200^{o}C, the growth rate in each axis was temperature dependent, noting a larger growth rate in the longitudinal axis of the bean.

Coffee is roasted to various degrees, providing different flavor profiles [Buffo and Cardelli-Freire 2004]. Given the collective findings of structural changes during the roasting process, Geiger [2004] claimed that controlling the temperature increase during roasting and pre-conditioning the moisture content of the green beans could be methods to influence the development of a roasted coffee bean structure to a desired state. For example, implementing these steps could lead to a better flavor or aroma, or improved extraction with an engineered coffee particle structure.

Oliveros et al. [2017] expands upon predicting the structure of roasted coffee by including the dynamic development in bean porosity into the heat and mass transfer models. This new addition is claimed to improve the prediction of a particular bean structure during a roasting process based on just the roasting temperature. The inclusion of the dynamic porosity transformations during roasting provided an explanation as to why a slowing of moisture loss is observed during the roasting process, despite porosity increasing. The authors point to the thermal transfer as being the dominate process versus the mass transfer, and the increasing porosity creates an insulating effect, reducing thermal conductivity.

Section 2.2.3: Roasted Coffee Grinding

After roasting, whole bean coffee is permitted sufficient time to cool prior to grinding the coffee. It has often been suggested that it is beneficial to use a cutting method for size reduction of roasted coffee versus other means such as crushing, impact or tearing. The preferred process of a cutting method is believed to give more control over the resulting grind size distribution [Clarke (Ed.) 2012b]. The size reduction technology chosen is intimately tied with the intended beverage to be produced. Various types of coffee beverages have different desired grind sizes. For example, typical coffee grind sizes for percolators are 1130 µm, filtered coffee is 800 µm [Clarke (Ed.) 2012b], single serve pods are 600 µm [Wang et al. 2016], espresso coffees are approximately 320 µm [Melrose et al. 2018], and so forth. A summary of particle sizes and the percent volume of fines (particles <100 µm) found in those distributions for various beverages are seen in Figure 2.4.

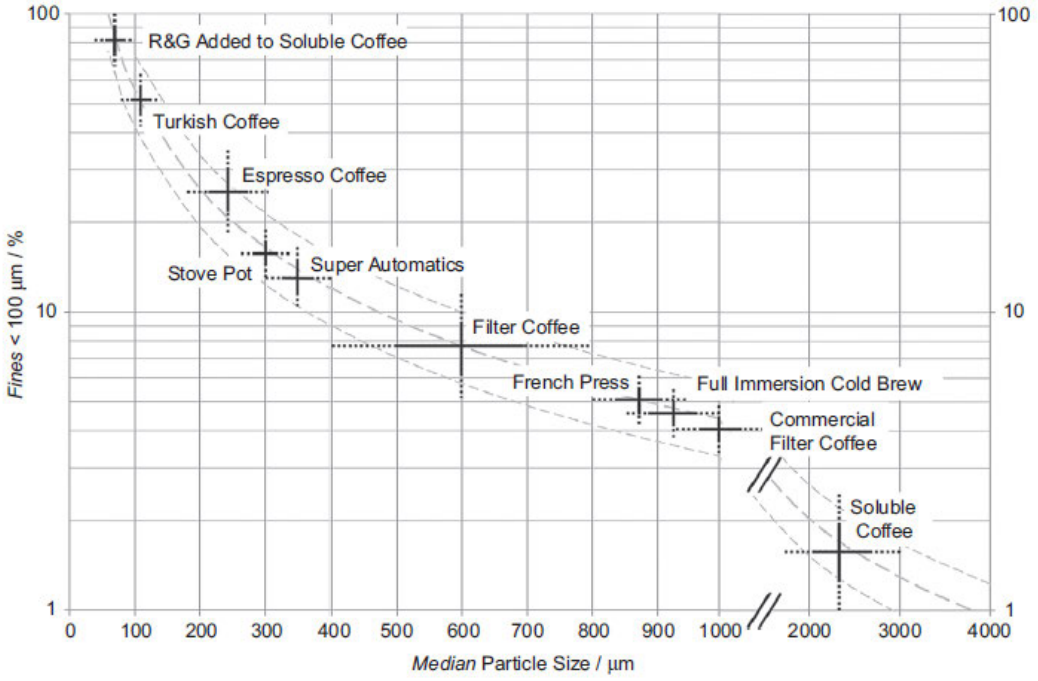

Figure 2.4: The percent volume of fine particles (<100 µm) versus median particle size of grind size distributions for various brewing technologies [von Blittersdorff and Klatt 2017].

Typical grinding equipment found in café shops and large production facilities are those of parallel discs or burrs and of multistage roll mills, respectively. Single stage size reduction

techniques, like those of the common burr grinder, have higher variation in the resulting grind size distributions than those of multistage size reduction such as the three stage roll mills offered by Neuhaus Neotec, MPE, and Probat [von Blittersdorff and Klatt 2017, Clarke (Ed.) 2012b].

Coffee grinding studies have investigated the effects of coffee origin, post-harvest processing methods, and cryogenic temperatures on size reduction of coffee. Uman et al. [2016] reported that coffee origin and different green bean processing methods, such as washed versus natural, had no significant impact on grind size distributions under similar grinding conditions. The authors did report that cryogenically grinding the coffee did produce a narrow size distribution of a finer particle size; experiments were targeting a particle size of *ca* 70 µm. Cryogenic grinding has also been reported to aid in the retention of volatiles and aromatic compounds [Clarke (Ed.) 2012b].

[redacted]

Section 2.2.5: Degassing and Packaging of Coffee

After the roasting process, coffee continues to release carbon dioxide from the bean for several days if it remains in whole bean format [Geiger et al. 2005]. On the other hand, degassing for freshly ground coffee can be on the time scale of hours as degassing rates are attributed to the disruption of the pore structures and increased surface to volume ratio of the particles due to size reduction [Wang and Lim 2014].

Primary packaging considerations for whole bean coffee and ground coffee are important to preserve freshness and quality. Oxidation and moisture ingress are the two primary concerns as both have large influences on coffee becoming stale. Prior to the advent of the one-way valve in multilayer metal or foil bags, a fine balance had to be struck between degassing behavior and packaging, as carbon dioxide continues to escape the coffee over a long period of time in whole bean format. The one-way valve permitted the packaging to release the pressure buildup of degassing coffee while on the shelf, maintaining the appropriate barrier properties for oxidation and moisture [Clarke (Ed.) 2012b]. In single serve pods, there are no valves on the pods to permit degassing, and therefore it is a challenge to ensure appropriate packaging times are coupled with degassing behaviors to preserve the freshness of the coffee.

Section 2.3: Physical and Chemical Properties of Green and Roasted Coffees

Section 2.3.1: Physical Properties of Roasted Whole Bean and Ground Coffee

Previously reported physical attributes of roasted whole bean and roasted ground coffee include whole bean and ground coffee particle porosities, particle sizes, particle true densities, loose bulk density, tapped densities, particle sphericity, and particle pore size distributions. Table 2.1 provides a summary of several physical properties for whole bean coffee.

Table 2.1: Select physical properties of whole bean coffee. Note: LTLT: low temperature, long time roasted; HTST: high temperature, short time roasted; -M: medium roast; -D: dark roast.

Origin	Species	Green or Roasted	Sample ID	Total Roast Loss %	Density (g/mL)	Porosity (%)	Source
Brazil	Arabica	Roasted	LTLT-M	15.7	0.626	*	Wang, X. and Lim, L.T. 2014
Brazil	Arabica	Roasted	HTST-M	14.9	0.585	*	Wang, X. and Lim, L.T. 2014
Brazil	Arabica	Roasted	LTLT-D	18.1	0.561	*	Wang, X. and Lim, L.T. 2014
Brazil	Arabica	Roasted	HTST-D	17.6	0.522	*	Wang, X. and Lim, L.T. 2014
*	Arabica	Green	*	*	*	9.88	Oliveros et al. 2017
*	Arabica	Roasted	*	*	*	34.24	Oliveros et al. 2017
Brazil	Arabica	Green	*	*	1.126	4.75	Pittia et al. 2011
Brazil	Arabica	Roasted	*	16	0.603	41	Pittia et al. 2011
Colombia	Arabica	Roasted	HTST	15.33	0.622	52.8	Schenker et al. 2000
Colombia	Arabica	Roasted	LTLT	15.81	0.747	47.4	Schenker et al. 2000

Many of these physical attributes are dependent on the history of coffee processing steps such as roasting and grinding, as discussed above. Roast and ground particle size distributions are frequently reported as bimodal, and the bimodal description is often found regardless of intentional efforts to create a particle size target mean or median value [Corrochano 2017, Moroney et al. 2015, Uman et al. 2016, Wang et al. 2016, Kuhn et al. 2017, von Blittersdorff and Klatt 2017].

Roasted and ground coffee, a plant-based material, presents itself as a porous cellular matrix. A roasted and ground coffee particle can be described as an irregular shaped, dense

cellular material, with cleaved cells present at the surface of the particle, like that of other beans, seeds or like plant derivatives [Fiori et al. 2009]. These cleaved cells can be measured in a variety of ways, but most readily *via* SEM imaging, and are reported to be 20-60 μm in diameter. Beyond the cleaved, surface cellular layer, the porous structure of coffee is limited to macropores (intact cells) and mesopores between the plant cell walls, or the plasmodesmata, connecting adjacent cells to one another. Robards and Lucas [1990] describe plasmodesmata as critical structures to plant tissue function. These small pores transverse the cell wall forming cell to cell connections and are primarily responsible for water and solute transport through the plant tissue. The tortuous path of one cell being connected to another can be readily envisioned as the shape of an hourglass, where these mesopores range between 10 to 50 nm in diameter [Schenker et al. 2000, Wang and Lim 2014, Corrochano 2017].

Roasted whole bean and roasted ground coffee particle porosity values have been found to vary from 0.34 to 0.65 (Oliveros et al. 2017, Schenker et al. 2000), moreover Schenker et al. [2000] shows the roasted whole bean porosity is dependent on the preceding thermal treatment. The resulting porosity of roasted whole bean coffee is a result of the roasting speed, time, and temperature. Beyond the overall increase in total bean volume during roasting, it was found that the porosity of the cell walls in the HTST coffee was larger, with an average pore radius of 13 nm versus the average pore radius of 11 nm in the LTLT coffee.

Roasted and ground coffee has been reported to contain closed cell porosity, which is interpreted from the data obtained by a combination of helium pycnometry and mercury intrusion porosimetry. Closed cell porosity is the intragranular porosity of the particle that is inaccessible by helium or mercury; this was first reported by Mateus et al. [2007] and Corrochano [2017], respectively. The values of closed cell porosity were reported in the range of approximately 0.20 and 0.45 $cm^3\,g^{-1}$, and were dependent upon particle size, with the latter values being for coarse particles.

Several studies have used x-ray tomography to observe the physical structure of the coffee bean, specifically the intragranular porosity before and after roasting. This was completed by taking several 2D images and compiling them to create a 3D rendering of the structure [Pittia et al. 2011, Frisullo et al. 2012]. It was found by Pittia et al. [2011] that pore

shape, size, and the distribution density of pores varied throughout a roasted coffee bean. Large, roundish pores were predominantly found in the exterior portions of the bean, while smaller pores were concentrated towards the inner, central part of the bean; while not mentioned by Pittia et al. [2011], it is reasonable that this observation is indicative of the heat transfer gradient in the bean during a roasting event. This work dismisses the homogeneous assumptions of a consistent pore network within the bean, and therefore it is reasonable to assume that ground pieces of coffee from the same bean could have different particulate porosities. The authors reported macropores (intact cells) within the roasted whole bean to be between 10-70 µm.

Frisullo et al. [2012] investigated differences between the two most common coffee species, arabica and robusta, and found differences in the porous structure. The arabica coffee had a lower overall porosity based on total pore volume, but a greater number of pores, suggesting a high number of small pores than the Robusta Coffee. The work by Frisullo et al. [2012] confirms the previous work of others showing that all coffees post roasting had increased pore volumes.

The true density of coffee has been reported in the range of 1.1 to 1.36 g cm^{-3} [Singh 1997], while others have reported values within the range of 1.3 to 1.35 g cm^{-3} [Corrochano 2017]. Bustos-Vanegas et al. [2018] have reported relationships of true density of coffee beans as a linear function of the moisture content as a result of the roasting process. However, the equation utilized in those calculations is a measurement of the apparent density of the coffee bean, as the volume is calculated using a semi-ellipsoid calculation where the a, b, and c axes are measured *via* x-ray tomography and incorporates the intra-granular porosity of the particle. Helium pycnometry measurements of true density of various ground coffees with differing moisture contents have not been found in literature. This may be due to standard of identity requirements from government regulatory agencies, such as the USDA, limiting the maximum moisture content of regular roast and ground coffee to 5% [USDA CID A-A20213B], where the typical moisture level of roasted whole bean and roasted ground coffee is 1- 2% [Geiger et al. 2005, Rao 2014]. Given this narrow range of moisture conditions for this material, it would be estimated that the differences in true density due to moisture would be negligible.

The force required to fracture a roasted coffee bean was investigated by Pittia et al. [2001] who measured the breakage force of roasted beans for various thermal treatments; the breakage force ranged from 50-250 N. This study included both arabica and robusta species, roasted to light and dark levels, including the high temperature, short time (HTST) roasting method, and a thermal treatment *via* vacuum oven drying. The authors used an Instron to generate a force-displacement curve for each sample, where the point of fracture was used as a proxy for mechanical strength of the roasted bean. It was found that as heating time and temperature increased, the observed force at failure decreased, indicating a progressive decline in strength as heat treatment continues. All samples demonstrated characteristics of low strength, low toughness, and low deformability, all indicative of a material that is fragile and brittle in nature.

Section 2.3.2: Chemical Composition of Green and Roasted Coffee

Green and roasted coffees are comprised of polysaccharides, oligosaccharides, proteins, lipids, acids and other minor constituents, such as the widely associated molecule found in coffee beverages, caffeine [Clarke (Ed.) 2012a, Povey et al. 2020]. Table 2.2 provides a breakdown of green and roasted coffee content as a percentage of its composition.

Table 2.2: Contents of green and roasted arabica and robusta coffees [Clarke (Ed.) 2012a].

Component	Arabica		Robusta	
	Green	Roasted	Green	Roasted
	% Composition			
Minerals	3.0-4.2	3.5-4.5	4.0-4.5	4.6-5.0
Caffeine	0.9-1.2	~1.0	1.6-2.4	~2.0
Trigonelline	1.0-1.2	0.5-1.0	0.6-0.75	0.3-0.6
Lipids	12.0-18.0	14.5-20.0	9.0-13.0	11.0-16.0
Chlorogenic Acids	5.5-8.0	1.2-2.3	7.0-10.0	3.9-4.6
Aliphatic Acids	1.5-2.0	1.0-1.5	1.5-2.0	1.0-1.5
Oligosaccharides	6.0-8.0	0-3.5	5.0-7.0	0-3.5
Polysaccharides	50-55.0	24.0-39.0	37.0-47.0	*
Amino Acids	2	0	2	0
Proteins	11.0-13.0	13.0-15.0	11.0-13.0	13.0-15.0
Humic Acids	*	16.0-17.0	*	16.0-17.0

Caffeine, chlorogenic acids, and organic acid contents of coffee have been extensively studied and published. Table 2.3 lists previously reported 3-O-Caffeoylquinic acid (3-CQA) content per gram of green or roasted coffee. Caffeine and chlorogenic acid content have been studied for a variety of factors including as function of roasting [Perrone et al. 2010, Jeon et al. 2017], brew method [Moeenfard et al. 2014], coffee origin [Jeon et al. 2017], coffee species and variety [Farah et al. 2005, Perrone et al. 2008b], and between decaffeinated, regular and instant [Perrone et al. 2008a].

Caffeine content in roasted coffee has been found to vary between 850 to 2000 mg/100g of coffee depending on the species. Citric acid content has been found to vary between 1.8-4.2% by dry weight depending on the degree of roast [Clarke (Ed.) 2012a, Perrone et al. 2008b]. Total chlorogenic acid content is greater in green coffee than roasted coffee, degrading from 5.5-8.0% in green coffee to levels below 2.5% in roasted coffee. However, the content of 3-CQA was reported lower by Perrone et al. [2008b] and Farah et al. [2005] for green coffee than very light or light roasted coffee, which is an indication that some of the total chlorogenic acid content, for example 5-Caffeoylquinic acid (5-CQA), initially breaks down into 3-CQA at light roasts.

Table 2.3: 3-CQA content in various coffees for green coffee and a variety of degrees of roast.

Origin or Type	Species	Roast or % Wt Loss	3-CQA (mg/g)	Source
Brazil cv. Mundo Novo	Arabica	Green Coffee	667	Perrone, D. et al. 2008b
Brazil cv. Mundo Novo	Arabica	11.5	1097	Perrone, D. et al. 2008b
Brazil cv. Mundo Novo	Arabica	13.6	721	Perrone, D. et al. 2008b
Brazil cv. Mundo Novo	Arabica	15.4	433	Perrone, D. et al. 2008b
Brazil cv. Mundo Novo	Arabica	16.1	325	Perrone, D. et al. 2008b
Brazil cv. Mundo Novo	Arabica	19.9	52	Perrone, D. et al. 2008b
Brazil cv. Catuai Vermelho	Arabica	Green Coffee	618	Perrone, D. et al. 2008b
Brazil cv. Catuai Vermelho	Arabica	10.4	1030	Perrone, D. et al. 2008b
Brazil cv. Catuai Vermelho	Arabica	11.7	808	Perrone, D. et al. 2008b
Brazil cv. Catuai Vermelho	Arabica	14.1	495	Perrone, D. et al. 2008b
Brazil cv. Catuai Vermelho	Arabica	15.0	328	Perrone, D. et al. 2008b
Brazil cv. Catuai Vermelho	Arabica	17.9	70	Perrone, D. et al. 2008b
Brazil cv. Conillon	Canephora	Green Coffee	1066	Perrone, D. et al. 2008b
Brazil cv. Conillon	Canephora	10.4	1308	Perrone, D. et al. 2008b
Brazil cv. Conillon	Canephora	11.7	1065	Perrone, D. et al. 2008b
Brazil cv. Conillon	Canephora	14.1	711	Perrone, D. et al. 2008b
Brazil cv. Conillon	Canephora	15.0	563	Perrone, D. et al. 2008b
Brazil cv. Conillon	Canephora	17.9	96	Perrone, D. et al. 2008b
Brazil cv. Bourbon	Arabica	Green Coffee	483	Farah, A. et al. 2005
Brazil cv. Bourbon	Arabica	Very Light	996	Farah, A. et al. 2005
Brazil cv. Bourbon	Arabica	Light	816	Farah, A. et al. 2005
Brazil cv. Bourbon	Arabica	Light Medium	459	Farah, A. et al. 2005
Brazil cv. Bourbon	Arabica	Dark Medium	199	Farah, A. et al. 2005
Brazil cv. Bourbon	Arabica	Dark	123	Farah, A. et al. 2005
Brazil cv. Bourbon	Arabica	Very Dark	80	Farah, A. et al. 2005
Ethiopia cv. Longberry	Arabica	Green Coffee	478	Farah, A. et al. 2005
Ethiopia cv. Longberry	Arabica	Very Light	951	Farah, A. et al. 2005
Ethiopia cv. Longberry	Arabica	Light	805	Farah, A. et al. 2005
Ethiopia cv. Longberry	Arabica	Light Medium	344	Farah, A. et al. 2005
Ethiopia cv. Longberry	Arabica	Dark Medium	181	Farah, A. et al. 2005
Ethiopia cv. Longberry	Arabica	Dark	110	Farah, A. et al. 2005
Ethiopia cv. Longberry	Arabica	Very Dark	53	Farah, A. et al. 2005
Uganda cv. Robusta	Canephora	Green Coffee	925	Farah, A. et al. 2005
Uganda cv. Robusta	Canephora	Very Light	1257	Farah, A. et al. 2005
Uganda cv. Robusta	Canephora	Light	1087	Farah, A. et al. 2005
Uganda cv. Robusta	Canephora	Light Medium	623	Farah, A. et al. 2005
Uganda cv. Robusta	Canephora	Dark Medium	334	Farah, A. et al. 2005
Uganda cv. Robusta	Canephora	Dark	219	Farah, A. et al. 2005
Uganda cv. Robusta	Canephora	Very Dark	108	Farah, A. et al. 2005

Section 2.3.3: Impact of Caffeine, Chlorogenic Acid, and Organic Acids on Sensory

Sensory analysis of coffee beverages has been concentrated on the flavor profile of the beverage as experienced by the consumer. The consumer experience is a combination of aroma, mouthfeel, and flavor. There has been a lot of focus on studying the hundreds of volatile compounds in both the aroma and liquid beverages thought to contribute to positive sensory scores in coffee beverages, but not nearly as much on non-volatile compounds [Sunarharum et al. 2014]. The studied non-volatile compounds believed to contribute to sensory impact are caffeine, trigonelline, proteins, polysaccharides, melanoidins, carboxylic acids, chlorogenic acids, lipids and minerals [Buffo and Cardelli-Freire 2004]. Buffo and Cardelli-Freire [2004] state caffeine contributes to bitterness and is associated with body and strength of a coffee beverage. The authors also note that carboxylic acids primarily influence the sourness of the beverage, while chlorogenic acids and products of chlorogenic degradation are drivers of astringency.

Early correlation work was done by Farah et al. [2006] who investigated correlations in caffeine, chlorogenic acids, and trigonelline with cup quality in a variety of Brazilian coffees. The authors found that higher levels of 5-CQA was associated with an inferior cup quality, while trigonelline, 3,4-dicaffeoilquinic acid, and caffeine associated with better cup quality. It is important to keep in mind that the results presented were correlative and not causative. The study could be improved where known concentrations of these compounds could be added to beverages and evaluated for sensory. Contradictory results to Farah et al. [2006] were presented by Zanin et al. [2016] who reported a wide range of various chlorogenic acid contents, specifically 5-CQA, in various processed Brazilian coffees. The authors in that study concluded that brewed coffees with high chlorogenic acid contents could have good cup quality, and ultimately found no correlation of 5-CQA to coffee cup quality.

Section 2.4: Overview of Brewing Various Coffee Beverages

Section 2.4.1: Brewing Roasted and Ground Coffee

The general process of coffee extraction has been studied extensively over the past 50 years. There are numerous brewing techniques employed around the world to create the beverage consumer's demand. Coffee brewing technology has changed during the past three decades, especially as more literature was published about common preparation techniques. Moreover, it has permitted the comparison of several of the more common techniques, where often the authors conclude there is no one technique better than any other, even with marked differences in the end state beverage [Gloess et al. 2013, Angeloni et al. 2019].

Coffee brewing and the extraction of soluble coffee solids from roasted and ground coffee is a series of complicated, time dependent interactions to make a beverage. Voilley and Simatos [1980] provide an explanation of the general extraction process:

1) Introduction of water to the solids where the particles are surface wetted and imbibition of water into the particles occurs.
2) Concurrently during the imbibition process, the initial wetted surfaces of the coffee containing soluble solids begin to dissolve in the presence of the water.
3) Dissolution of soluble components continues to occur as the liquid-solid interface penetrates through the porous cellular matrix of the coffee particle, until reaching the core of the particle.
4) In parallel to the liquid-solid interface progressing through the particle, diffusion of the dissolved soluble solids is occurring at both the surface and throughout the matrix of the wetted portion of the coffee particle.
5) These processes, dissolution of soluble species and diffusion throughout the particle, occur until the bulk liquid and the bulk wetted solids are physically separated or until a state of equilibrium is achieved between the wetted solids and bulk liquid.

Section 2.4.2: Comparison of Common Brewing Methods

Common coffee brewing technologies include: French press, espresso, pour-over filtered coffee, percolator, moka, aeropress, espresso pods, gravimetric or low pressure filtered pods, and cold brew [Angeloni et al. 2019]. As mentioned in Section 2.2.3 and shown in Figure 2.4, the grind size distribution varies greatly amongst the various brewing technologies.

Many of the previous studies focused on comparing filtered coffee to espresso, as these two were the most widely consumed coffee beverages [Ludwig et al. 2012]. Ludwig et al. [2012] investigated the impact of brew time on espresso and filtered coffee brewed beverages by fractionating the beverage during the brewing process for both an arabica and robusta coffee. Concentrations of caffeine and antioxidant compounds, including chlorogenic acids were measured and compared between the two brewing methods as a whole, and on a fraction-by-fraction level. Table 2.4 shows the aggregate results from Ludwig et al. [2012] of the caffeine and 3-CQA concentrations for the espresso and filtered brew methods, and for both arabica and robusta coffees.

Table 2.4: Caffeine and 3-CQA concentrations per fraction for espresso and filter brewed coffee [Ludwig et al. 2012].

Brew Method	Origin-Species	Fraction ID	Extraction Time (s)	Fraction Brew Volume (mL)	Caffeine (mg/100mL)	3-CQA (mg/100mL)
Espresso	Guatemala Arabica	F1	0-8	16	297	91
		F2	8-16	14	83	26
		F3	16-24	17	40	15
Espresso	Vietnam Robusta	F1	0-8	17	575	49
		F2	8-16	14	159	16
		F3	16-24	15	75	9
Filter	Guatemala Arabica	F1	0-75	80	107	31
		F2	75-150	146	57	17
		F3	150-225	186	36	11
		F4	225-300	94	49	15
		F5	300-375	26	89	25
Filter	Vietnam Robusta	F1	0-75	74	66	11
		F2	75-150	120	158	19
		F3	150-225	160	113	15
		F4	225-300	112	104	15
		F5	300-375	54	118	15

The collected fractions of espresso showed pronounced differences in the antioxidant capacity with 70% of the overall concentration found in the first fraction of espresso; the brew was divided up into three equal sections by time. The third and last fraction of the espresso only accounted for 12% of the total antioxidant concentration. Filtered coffee showed very different behaviors for extraction than espresso, where only 30% of the overall antioxidant concentration was collected in the first fraction. Different behaviors among the two coffee types were also observed, where the caffeine concentration in the first fraction of the filter brew of robusta was nearly half the concentration in arabica, despite having 65% more total caffeine content. The authors reported that the robusta beverages had less chlorogenic acid content than arabica, which is a deviation from previously published results.

Comparisons of espresso to filtered coffee beverages continued with work by Gloess et al. [2013]. The authors studied nine different extraction methods, focusing on various espresso brewing methods and various filtered or lungo type methods. A lungo coffee is an espresso based extraction that is diluted down with additional water. The studied methods included semi-automatic machines for both espresso and lungo formats, automatic machines for both espresso and lungo formats, espresso capsules, a moka brew, pour-over, drip filtered, and a French press. The responses of the experiments in this study were sensory focused such that physiochemical properties could be related to sensory characteristics of each brew. Positive correlations were observed for total solids with beverage body or texture, attributing more coffee body with higher solids. Additionally, positive correlations were observed for the ratio of caffeine to chlorogenic acids or with bitterness to astringency. Higher sensory scores were noted for bitterness and astringency in flavor with increasing caffeine; these higher scores were more pronounced with increasing amounts of chlorogenic acid. It was also noted that there was no correlation between pH nor titratable acidity with sensory scores for coffee acidity; however, only one type of coffee was tested in the nine brewing methods.

In general, it was observed that the espresso beverages had a higher concentration of the compounds studied versus the filtered or lungo type beverages; however, the authors are quick to note that the total contents per cup are generally higher in filtered or lungo type coffee beverages. The consumer is unlikely able to discern total contents, and are more sensitive to

concentration differences, and associate coffee beverage strength with higher concentrations [Gloess et al. 2013].

Beverage technologies within a beverage type, specifically espresso coffee, were compared by preparing espressos made *via* commercial café equipment and two different espresso capsules manufactured by Illy Coffee Company [Parenti et al. 2014]. Each beverage produced was analyzed for physiochemical properties after brewing. These properties included percent extraction, caffeine, chlorogenic acid, trigonelline concentrations, foam generation and stability. Beverages produced by the two capsules were found to have less variation in nearly each of the 19 measured properties. The authors concluded that the reduced variation in beverage attributes is due to the control in manufacturing of capsules and the ease of use by the consumer. These two factors lead to more consistent beverages produced by brewing single serve capsules [Parenti et al. 2014].

As popularity of cold brew coffee grew in North America, more studies on the extraction process and physiochemical properties of cold brew versus filtered coffee surfaced, with the first being by Fuller and Rao [2017]. The authors used identical raw material to compare cold brew extraction events versus traditional French press extractions and beverages. The juxtaposition of these two beverages is very intriguing as the two methods of preparing a coffee beverage represent the two most extreme points on the spectrum of brew temperature and contact time, where the hot coffee was brewed in six minutes with a water temperature of 98^{o}C and the cold brew was brewed at 21 °C for 24 hours. Table 2.5 shows the 3-CQA and caffeine concentrations reported by Fuller and Rao [2017] of the final coffee beverage for various degrees of roast, particle sizes, brew times, and brew temperature.

Table 2.5: Caffeine and 3-CQA concentrations for cold brew and French press coffee brewed coffee [Fuller and Rao 2017].

		400 min Cold Extraction		1440 min Cold Extraction		6 min Hot Extraction	
Coffee Roast	Grind Size	3-CQA (mg/L)	Caffeine (mg/L)	3-CGA (mg/L)	Caffeine (mg/L)	3-CGA (mg/L)	Caffeine (mg/L)
Medium	Medium	480 ± 60	1060 ± 60	510 ± 20	1180 ± 90	510 ± 30	1040 ± 70
Medium	Coarse	490 ± 30	1130 ± 50	520 ± 40	1230 ± 60	460 ± 40	970 ± 70
Dark	Medium	380 ± 10	970 ± 60	390 ± 10	1080 ± 70	430 ± 30	1060 ± 70
Dark	Coarse	330 ± 50	930 ± 40	360 ± 20	990 ± 30	340 ± 10	840 ± 10

Fuller and Rao [2017] observed that 3-CQA followed first order kinetics as first published by Spiro and Selwood [1984]. Concentrations in 3-CQA rapidly increased in the first 180 minutes of cold brew but did not increase beyond 400 minutes of contact time, or approximately 6.7 hours; caffeine showed similar kinetic behavior achieving near steady state conditions at 400 minutes. The grind size of the coffee had no impact on the 3-CQA concentration in all cold brew beverages, suggesting that the rate limiting step in mass transfer is not related to available surface area or coffee structure. The authors reported higher concentrations of caffeine in both medium roast coffee and dark roast coffee via the cold brew method versus the hot brew counterparts. Interestingly, it was observed that the medium roast coffee had higher concentrations of caffeine and 3-CQA versus the dark roast in the cold brew beverages.

Fuller and Rao [2017] cited the multiscale model of coffee extraction kinetics presented by Moroney et al. [2015], as an accurate explanation of the cold brew extraction process. Evidence for the two-part extraction process proposed by Moroney et al. [2015] can be seen in the hot brewing of the coffee samples. After six minutes of contact time at 98 °C, caffeine did not fully extract from the inner cellular matrix; suggesting that caffeine is diffusion limited in a hot brewing extraction event like the French press method. The authors support the application of coffee extraction kinetic modeling from Moroney et al. [2015] and Spiro and Selwood [1984] to cold brew extraction events.

Jeon et al. [2017] measured the concentrations of caffeine and 3-CQA of brewed coffee, prepared by the pour-over method. Several coffee origins, particle sizes and two different roasts were tested. Table 2.6 shows the concentrations of caffeine and 3-CQA reported by Jeon et al. [2017]. The authors reported decreasing caffeine and 3-CQA content with decreasing particle size. The observed decrease was quite pronounced between the coarse particle size distribution and the fine particle size distribution, where in most cases the reported concentrations for both caffeine and 3-CQA were 35-45% lower. It was also reported that the medium-dark roast coffee had substantially less 3-CQA concentration versus the medium roast coffee, where the medium-dark roast coffee had 50-65% lower 3-CQA concentrations.

Table 2.6: Caffeine and 3-CQA concentrations in various brewed coffees prepared by the pour-over method [Jeon et al. 2017].

Origin or Type	Roast or % Wt Loss	Particle Size (µm)	Caffeine (mg/L)	3-CQA (mg/L)
Brazil	Medium	Coarse (≥1000µm)	703	336
Brazil	Medium	Medium (500 -700µm)	639	297
Brazil	Medium	Fine (≤300µm)	460	192
Brazil	Medium-Dark	Coarse (≥1000µm)	592	77
Brazil	Medium-Dark	Medium (500 -700µm)	591	74
Brazil	Medium-Dark	Fine (≤300µm)	396	47
Ethiopia	Medium	Coarse (≥1000µm)	665	426
Ethiopia	Medium	Medium (500 -700µm)	589	362
Ethiopia	Medium	Fine (≤300µm)	420	237
Ethiopia	Medium-Dark	Coarse (≥1000µm)	585	146
Ethiopia	Medium-Dark	Medium (500 -700µm)	600	145
Ethiopia	Medium-Dark	Fine (≤300µm)	402	92
Kenya	Medium	Coarse (≥1000µm)	715	390
Kenya	Medium	Medium (500 -700µm)	630	330
Kenya	Medium	Fine (≤300µm)	460	222
Kenya	Medium-Dark	Coarse (≥1000µm)	675	128
Kenya	Medium-Dark	Medium (500 -700µm)	657	123
Kenya	Medium-Dark	Fine (≤300µm)	461	83
Colombia	Medium	*	494	290
Colombia	Medium-Dark	*	523	100
Costa Rica	Medium	*	577	292
Costa Rica	Medium-Dark	*	567	109
Guatemala	Medium	*	553	288
Guatemala	Medium-Dark	*	524	103
Indonesia	Medium	*	509	290
Indonesia	Medium-Dark	*	555	125
Papua New Guinea	Medium	*	482	261
Papua New Guinea	Medium-Dark	*	537	109
Tanzania	Medium	*	534	294
Tanzania	Medium-Dark	*	537	95

Angeloni et al. [2019] studied the differences of eight extraction methods in terms of physiochemical differences observed in the end state beverage, all using the same raw material. Table 2.7 shows the caffeine and 3-CQA concentrations, total dissolved solids (TDS), and percent extraction for various coffee brewing methods.

Table 2.7: Caffeine, 3-CQA, total dissolved solids (TDS) and percent extraction for various coffee brewing methods [Angeloni et al. 2019].

Extraction Method	Grind Size	Coffee Mass (g)	Water Volume (mL)	Brew Temp (°C)	Brew Pressure (Bar)	Brew Time	TDS %	Extraction %	Caffeine (mg/mL)	3-CQA (mg/mL)
Espresso Classical Method (EC)	Fine	14	*	93	9	27 (s)	5.20	22.59	4.10	1.80
Espresso Caffe Firenze (ECF)	Fine	15	*	92	20	70 (s)	3.32	13.46	1.43	0.60
Espresso Specialty Methods (ECS)	Fine	18	*	93	9	26.5 (s)	8.44	17.54	4.20	1.86
Moka	Fine	15	150	100	1.5	2.13 (min)	3.40	28.60	1.28	0.45
V60 Pour-over Method	Coarse	15	250	93	1	2.3 (min)	1.55	22.14	0.74	0.31
Cold Brew	Coarse	25	250	20	1	4.7 (hr)	1.54	20.89	1.25	0.50
Aeropress	Coarse	16.5	250	93	1	1.35 (min)	1.52	20.56	0.78	0.27
French Press	Coarse	15	250	93	1	5 (min)	1.35	18.61	0.52	0.21

The authors found that there were significant differences among the eight brewing methods for percent extraction, total dissolved solids (TDS), and viscosity of the beverage. It was observed that brew methods with high pressure, specifically the three espresso preparation techniques, had higher concentrations in chlorogenic acids (in mg/mL) than those brewed at lower pressures. When comparing concentrations of chlorogenic acids on a mg/cup basis, it was cold brew that reported the highest values. The authors appropriately call out that all conclusions drawn from the data must be done so keeping in mind the differences in coffee to water ratios, brewing pressure, brewing temperature, brewing time, and particle size of the coffee, as these factors can impact extraction kinetics. Interestingly, the authors make no reference to Fuller and Rao [2017], who reported very different results in comparing French press to cold brew preparation methods.

Section 2.4.3: Analysis of Single Serve Coffee Pods & Brewing Systems

The popularity of single serve coffee pods in North America exploded in volume during the past 10 years, with many years demonstrating exponential growth in sales as seen in Figure 1.2 [Gonzalez 2014]. The pods, commonly referred to as K-Cups, are designed to be brewed by the Keurig single serve brewers that are commercially available. Given the popularity of K-Cups, Keurig brewers, and Keurig compatible pods in the market, it is astonishing how little literature exists on the Keurig brewing system and pods. A sole reference on the subject exists

which investigated the effects of capsule parameters on coffee extraction when brewed using a Keurig K-200 commercial brewer [Wang et al. 2016].

Wang et al. [2016] focused on the effects of particle size, packing volume or fill weight, and brew volume on the physiochemical properties of brewed coffee. The authors also measured various responses in the appliance, such as brew pressure, temperature, piston strokes, and air purge time. Table 2.8 shows the measured physiochemical properties of the brewed coffee for the various brew volumes produced with a Keurig K-200 appliance.

Table 2.8: Brewed coffee total dissolved solids, percent extraction, and caffeine concentration from a Keurig K-200 brewer, for pods at a 8.9 g coffee fill weight, with a volume mean particle diameter equal to 734 µm, brewed using the 4 oz., 6 oz. and 8 oz. settings [Wang et al. 2016].

Origin	Roast	Brew Volume (mL)	Brew Time (s)	TDS %	Extraction Yield (%)	Caffeine (mg/L)
Ethiopia	Medium	113	32	1.78	17.1	560
		170	42	1.28	19.5	420
		226	50	1.06	21.39	340
Colombia	Medium	113	31	1.76	16.81	590
		170	40	1.31	19.89	440
		226	48	1.07	21.83	370
Ethiopia	Dark	113	33	2.16	20.43	660
		170	38	1.49	22.49	470
		226	48	1.15	23.45	370
Colombia	Dark	113	29	2.16	20.12	670
		170	38	1.52	23.08	500
		226	47	1.22	24.34	410

It was found that reducing the particle size increased the extraction yield with a relative increase of approximately 65%. An increase of the fill weight in the pod did not change the percent extraction yield, but did change the ratio of chemical compounds, thus indicating a likely change in the flavor profile. Greater than 80% of the total solids were extracted from the pod in the first 113 mL with the remaining water flow merely diluting the beverage and introducing more astringent and bitter compounds.

Brew time was reported to significantly increase as particle volume mean diameter decreased. Moreover, the medium roast coffees reported longer brew times than the dark

roast equivalents. The latter observation went uncommented as this contradicts the former observation of brew time increasing with smaller particles; the medium roast coffee particles were coarser at each sieve cut versus the dark roast samples. The time for the air purge to complete, increased with decreasing particle size, doubling when particle volume mean diameter changed by a factor of five. The authors attribute this to the greater packing density as particle size decreases. A similar behavior was also observed with an increasing resistance to water flow as particle size decreased. Greater extraction yields were observed with decreasing particle size, and dark roast had greater extraction yields than medium roast, as dark roast has higher porosity values [Wang and Lim 2014]. A positive correlation between color and TDS was strong with a correlation coefficient value greater than 0.9.

The authors reported greater changes in acidic and phenolic compounds as particle size decreased, arguing most extraction occurs at surface and internal particle diffusion is limited due to the short brew time. The increase of fill weight had little to no change in extraction yield, but did increase chemical concentrations, as was seen with increasing TDS values. This reported work was done absent of consumer sensory evaluations and conclusions are solely based on ratios of the chemical analyses mentioned in the paper. An opportunity exists to study additional brewers in the Keurig appliance portfolio, as the company advertises differences in the appliance performances on Keurig.com.

Section 2.5: Factors Influencing Coffee Extraction & Early Models of Extraction Kinetics

Section 2.5.1: Extraction Process of Cellular Material at Particle Scale: Influences of Material

Several publications over the last five decades have studied effects of the solid physical properties or the liquid properties on coffee extraction. Examples of investigated properties include the effects of particle size, coffee origin, coffee type, coffee roasting, brew temperature, coffee to water ratio, brew volume, flow rates, brew water pressure, contact time, coffee swelling, and water quality.

Among the several studies, Nicoli et al. [1990] repeated the work of Voilley and Simatos [1980], using robusta coffee instead of arabica coffee, and studied coffee extraction in a well stirred batch reactor. The authors reported that as temperature substantially increases, the delta in solid yield values between one minute of extraction time and 30 minutes of extraction time narrows considerably. This was most evident as the temperature of the water approached boiling conditions; the solids yield values were within 10% relative difference between 30 minutes of extraction and one minute of extraction. After several minutes at the highest temperatures, further contact time becomes negligible in solid yield values. It is important to note the time scale reported, as all the data relating to contact time is after one minute, which is greater than most commercially available single-serve systems. Contact time likely has a large influence due to the short brew times in single-serve systems, not to mention the dynamics of a packed bed are different than a well stirred batch reactor.

It was found that pH remained a constant value regardless of grind size, and that the optimum situation for solids extraction was with particle sizes between a 40 and 45 US standard mesh, or between 350-425 μm. It was noted that as particle size decreases a reduction in solid content and optical density was observed, the authors suggested this was due to the agglomeration of fines creating a reduced surface contact area with water. The authors made no mention of the dispersion forces in well stirred batch reactor, as in most cases using a magnetic stir bar, the particles are coupled to the flow lines of the liquid and have no slip velocities.

Additional work was done by Oshita et al. [1994], who measured total dissolved solids (TDS) in coffee extract for various temperatures and particle sizes. It was found that decreasing grind size had an effective increase on the observed rate constant for TDS extraction, as did increasing brew temperature. Unlike others who previously reported first order steady state kinetics, the authors claim the extraction process was well represented by an equation of the second order to fit the data of TDS values.

Beyond studying total dissolved solids or total solids yield, Lee et al. [1992] completed early studies of 44 components extracted out of drip brewed coffee. The authors determined the maximum length of time for brewing coffee with this method, drip based, was 10-11

minutes. The data showed that anything less than seven minutes contributed to less than 80% of the maximum concentration in a coffee brew. The effects of flow rates were studied as well, with higher rates of extraction found with higher flow rates of water, 250 mL/min versus 50 mL/min; it was suggested that greater mixing of the coffee grounds and water occurs with higher flow rates. The authors were able to group compounds into fast and slow extractors, and noted in 22 of the 44 compounds, the extraction rates were agnostic of the flow rate utilized in brewing; of these 22 compounds, 16 were fast extractors, and the other 6 exhibited maxima.

Other factors studied on coffee espresso brewing included the effect of brew pressure and temperature. Masella et al. [2015] introduced a new patented Caffe Firenze Espresso brewing method. The authors compared beverage attributes against pre-manufactured capsules, as capsules were found to be more consistent from previous work [Parenti, A. et al. 2014]. Pressure and temperature significantly affected the espresso coffee quality. Increasing pressure was found to be beneficial in delivering an espresso with greater body and appearance, as demonstrated by higher observed values of density, viscosity, total solids and foam index [Masella et al. 2015].

A more recent study on brewing of espresso focused on the brew process with a temperature gradient. Salamanca et al. [2017] investigated three brewing scenarios, a ramp up in water temperature during brewing from 88 °C to 93 °C, a ramp down from 93 °C to 88 °C, and a fixed temperature of 90 °C during the entire brew process; the authors focused on different coffees. It was observed that the coffees all demonstrated different physiochemical properties measured because of the temperature gradients. Most importantly, the authors noted that the espressos brewed with the ramp up temperature gradient from 88 °C to 93 °C exhibited the most favorable sensory qualities across all coffees tested.

A missing component from many published studies on coffee extraction is the water used in preparing the beverage. Water quality recommendations have been established by the Specialty Coffee Association (SCA) for ensuring a better tasting coffee [Sage 2013]. Navarini and Rivetti [2010] studied how water quality affects espresso brewing, in particular foam generation and stability. No difference in brewing times was reported as a function of water

hardness, with a wide range tested. Water quality did show marked differences in foam generation, foam texture, and foam persistency. Water with no or near minimal solute generated less foam during brewing. Foam generated from no solute water (ultra-pure, reagent grade water), was solely because of the carbon dioxide from the coffee. The study was absent of mentioning sensory characteristics from the differences in the brewing using various waters.

Additional factors influencing the brewing process include particle swelling, a dynamic material property. Mateus et al. [2007] and others have observed that coffee particles swell during hydration. This swelling has been captured by observing changes in the volume mean diameter of the particles over a time of 10 minutes when placed in 90 °C water, where a relative increase of 20-23% has been observed. Mateus et al. [2007] proposes that the water absorption into the cellular matrix behaves like a plasticizer of the biopolymers, morphologically changing the cellular structure permitting greater effective diffusivity and access to the closed porosity. These observations were in support of the previously published data by Spiro and Chong who demonstrated that the extraction kinetics of caffeine were approximately double with pre-swollen or previously hydrated coffee versus regular roast and ground coffee. Similar results have been reported by Hartegan et al. [2020] who found that coffee particles swell by 15% by volume during brewing, and the observed swelling was independent of particle size.

In contrast to the studies concluding coffee particles swell during brewing, Corrochano [2017] found that particles did not swell and suggests water chemistry and degree of roast differences are the reason for obtaining conflicting results from Mateus et al. [2007]. Maille et al. [2021] found that particles do not swell within brew methods up to five minutes. The authors studied different coffee origins, roast levels, decaffeination, water chemistries, and water temperatures on coffee particle swelling. *In situ* digital microscopy and liquid dispersion laser diffraction measurements were used to evaluate changes in particle size due to particle swelling. Figure 2.5 presented by Maille et al. [2021] shows the *in situ,* digital microscopy time sequence images of a single, dark roast coffee particle submerged in deionized water at various

times. The black contour lines in (e)—(h) are the original contour of the particle in (a) which was taken after 18 s of being submerged, overlaid on the images (b), (c), and (d).

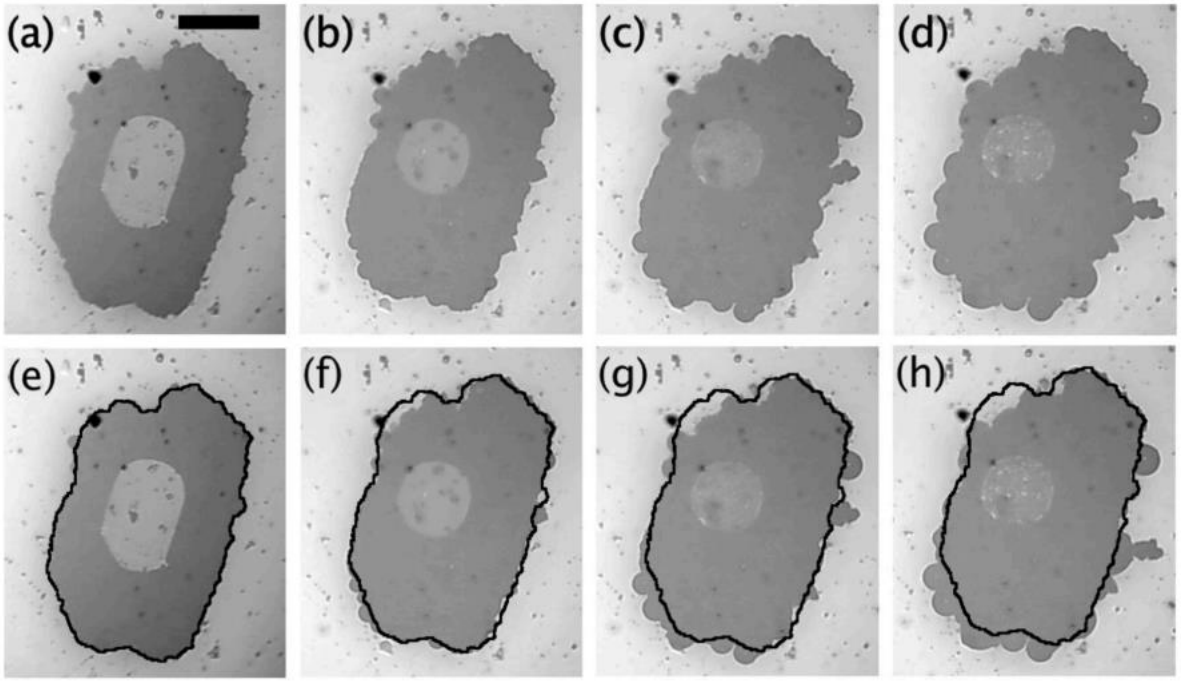

Figure 2.5: The time sequence images of a single coffee particle of a dark roast, Central American coffee, submerged in deionized water for: (a) 18 s, (b) 66 s, (c) 180 s, and (d) 283 s. In (e)–(h), the outline of the particle at 18 s is superimposed as a black line on the original images. All 8 images have the same magnification, and the black scale bar shown in (a) represents a length of 250 μm. [Maille et al. 2021].

The microscopy images show the evolution of gas bubbles growing on the surface of the coffee particles over time. It was hypothesized that these gas bubbles were formed from the remaining CO_2 leaving the coffee particle when brewed, as some CO_2 does not fully diffuse out of the coffee matrix after roasting and is trapped due to the closed cell porosity [Mateus et al. 2007, Corrochano, 2017]. The authors determined the buoyancy forces on the large particles at the start of the recurring laser diffraction measurements skewed the early, sequential particle size statistics, as the large particles were neither entrained in the flow nor measured until later in the sequence.

Section 2.5.2: Modeling Based on Fick's Second law of Diffusion

The start of modeling of coffee extraction started with modeling of the decaffeination process where the rate of extraction of caffeine from whole coffee beans was modeled using Fick's second law of diffusion [Bichsel 1979]. This work was extended to roast and ground coffee by Voilley and Simatos [1980]. Voilley and Simatos [1980] studied the brewing process and observed the influences of coffee to water ratios, particle sizes of coffee grounds, water temperature, and water-coffee contact time. The key findings from Voilley and Simatos [1980] included: nearly 90% of all solids content were extracted in the first minute, as particle size decreased the soluble solids concentration increased in all cases, rates of extraction increased with increasing water temperature, as ratio of coffee water increased the extraction yield decreased due to the gradient between the solid and the bulk liquid concentration being smaller, and that titratable acidity was directly proportional to total solids content in all cases.

Voilley and Simatos [1980] proposed describing the extraction rate of total solids by means of the diffusion equation in a sphere as provided by Crank [1975].

$$\frac{\partial c}{\partial t} = \frac{1}{r^2}\frac{\partial}{\partial r}\left(r^2 D \frac{\partial c}{\partial r}\right) \quad Eqn\ 2.1$$

This work was limited to a single effective diffusivity and rate constant, which described the extraction kinetics of the total soluble solids. The application of the analytical solution for diffusion from a sphere to roast and ground coffee was based on the following assumptions:

1) Particles were spherical.
2) The diffusion process was radial and isotropic, with the diffusion coefficient being constant or independent of the concentration.
3) All soluble substances are homogenously distributed within each particle.
4) There are no concentration gradients in the solvent (water).

These assumptions permit the application of a simple diffusion model, but it is known the coffee particles are not spherical, plant materials are often anisotropic, the diffusion coefficient is not likely constant and is dependent on the concentration in the solvent and the concentration remaining inside of the particle.

Section 2.5.3: Steady State First Order Extraction Modeling

A simpler approach than using the full analytical solution to Fick's second law is implementing a steady state, lumped parameter mass transfer model where the rate of water uptake is ignored, and the particles are assumed to be fully hydrated just after solid-liquid contact; this permits the sole observation of the rate of loss of soluble components from the particles [Spiro and Selwood 1984]. This approach tests whether the extraction process is limited by intra-bean diffusion, is limited through the coffee-water interface, or is limited through a Nernst layer. Secondly, Spiro and Selwood [1984] assume that the particles are spherical, monodisperse, and homogenous in extractable soluble components. Lastly, since the model is developed for steady state conditions, it is assumed that the concentrations vary linearly with distance in the particle and Nernst layer. The resulting model equation is:

$$\ln\left(\frac{C_\infty}{C_\infty - C}\right) = k_{obs}t + a \quad Eqn\ 2.2$$

where

$$\frac{1}{k_{obs}}\left(1 + \frac{m}{\rho KV}\right) = \frac{1}{k} = \frac{R_p^2}{12D_{eff}} + \frac{R_p}{3k_1} + \frac{R_p\delta}{3KD_{soln}} \quad Eqn\ 2.3$$

Spiro and Selwood [1984] determined that the rate limiting step of caffeine extraction was intra-bean diffusion. The authors calculated the diffusivity values of caffeine and found them to be relatively constant, within a factor of two, at isothermal conditions even for a range of particle sizes that span a factor of 40, or a particle radius squared factor of 2000. In comparison of these observed diffusivity values versus those of caffeine in water, the authors noticed that the diffusivity of caffeine in water was nearly 30 times greater, suggesting that there is a chemical association of caffeine, and the extraction process is not of pure caffeine but of a larger molecule, or that the extraction process is greatly hindered by the physical impediment of the cellular matrix, preventing diffusion of a species out of the particle. Table 2.9 shows the calculated diffusivities of caffeine, D_{eff}, from the observed rate constants as a function of particle size and temperature reported by Spiro and Selwood [1984].

Table 2.9: List of calculated effective diffusivities of caffeine for various coffees, roast levels, particle sizes, water temperatures and treatments.

Coffee Origin	Species	Roast (Sample ID)	Particle Diameter (μm)	Water Temperature (°C)	Calculated Diffusivity D_{eff} (10^{-11} m^2 s^{-1})	Source
Kenya	Arabica	Medium	190	25.8	1.60	Spiro and Selwood [1984]
Kenya	Arabica	Medium	256	25.8	2.30	Spiro and Selwood [1984]
Kenya	Arabica	Medium	354	25.8	3.00	Spiro and Selwood [1984]
Kenya	Arabica	Medium	494	25.8	2.20	Spiro and Selwood [1984]
Kenya	Arabica	Medium	726	25.8	2.70	Spiro and Selwood [1984]
Kenya	Arabica	Medium	976	25.8	2.00	Spiro and Selwood [1984]
Kenya	Arabica	Medium	1366	25.8	1.70	Spiro and Selwood [1984]
Kenya	Arabica	Medium	1976	25.8	1.60	Spiro and Selwood [1984]
Kenya	Arabica	Medium	8260	25.8	2.50	Spiro and Selwood [1984]
Kenya	Arabica	Medium	976	44.8	4.90	Spiro and Selwood [1984]
Kenya	Arabica	Medium	976	64.9	8.60	Spiro and Selwood [1984]
Kenya	Arabica	Medium	976	84.1	17.3	Spiro and Selwood [1984]
Kenya	Arabica	Green	980	80.0	17.0	Spiro and Hunter [1985]
Kenya	Arabica	Dark	980	80.0	24.0	Spiro and Hunter [1985]
Kenya	Arabica	Green-Dry	1072	80.0	23.0	Spiro et al. [1989]
Kenya	Arabica	Green-Water Swollen	1287	80.0	43.0	Spiro et al. [1989]
Kenya	Arabica	Green-(Swollen Solute Free)	1287	80.0	60.0	Spiro et al. [1989]
Kenya	Arabica	Medium-Dry	994	80.0	27.0	Spiro et al. [1989]
Kenya	Arabica	Medium-Water Swollen	1163	80.0	41.0	Spiro et al. [1989]
Kenya	Arabica	Medium-Swollen Solute Free	1163	80.0	59.0	Spiro et al. [1989]
Santos	Arabica	Roasted for 12 min at 230°C	≤600	90.0	0.11	Zanoni et al. [1992]
Santos	Arabica	Roasted for 12 min at 230°C	130-138	90.0	0.06	Zanoni et al. [1992]
Santos	Arabica	Roasted for 12 min at 230°C	247-255	90.0	0.02	Zanoni et al. [1992]
Santos	Arabica	Roasted for 12 min at 230°C	554-600	90.0	0.42	Zanoni et al. [1992]
Santos	Arabica	Roasted for 12 min at 230°C	130-138	90.0	0.06	Spiro [1993]
Santos	Arabica	Roasted for 12 min at 230°C	247-255	90.0	0.23	Spiro [1993]
Santos	Arabica	Roasted for 12 min at 230°C	554-600	90.0	0.57	Spiro [1993]
Kenya	Arabica	Medium-Dry	850-1000	25.5	2.45	Spiro and Chong [1997]
Kenya	Arabica	Medium-Water Filled	850-1000	25.5	5.90	Spiro and Chong [1997]
Kenya	Arabica	Medium-Solube Free (Caff 0.02M)	850-1000	25.5	6.15	Spiro and Chong [1997]
Kenya	Arabica	Medium-Solube Free (Caff 0.03M)	850-1000	25.5	7.15	Spiro and Chong [1997]
Kenya	Arabica	Medium-Solube Free (Caff 0.05M)	850-1000	25.5	5.60	Spiro and Chong [1997]
Kenya	Arabica	Medium-Solube Free (Caff 0.065M)	850-1000	25.5	8.35	Spiro and Chong [1997]
Kenya	Arabica	Green-Dry	850-1000	25.5	1.75	Spiro and Chong [1997]
Kenya	Arabica	Green-Water Filled	850-1000	25.5	5.25	Spiro and Chong [1997]
Kenya	Arabica	Green-Soluble Free (Caff 0.03M)	850-1000	25.5	8.35	Spiro and Chong [1997]
Kenya	Arabica	Green-Soluble Free (Caff 0.065M)	850-1000	25.5	8.80	Spiro and Chong [1997]
Kenya	Arabica	Medium	1700-2000	80.0	15.8	Jaganyi and Madlala [2000]
Santos	Arabica	Medium	1700-2000	80.0	20.5	Jaganyi and Madlala [2000]
Blue Mtn. Java	Arabica	Medium	1700-2000	80.0	19.6	Jaganyi and Madlala [2000]
Zimbabwe	Arabica	Medium	1700-2000	80.0	20.3	Jaganyi and Madlala [2000]
Mocha	Arabica	Medium	1700-2000	80.0	15.9	Jaganyi and Madlala [2000]
South Africa	Arabica	Medium	1700-2000	80.0	18.0	Jaganyi and Madlala [2000]

It is important to note the experimental setup designed and used by Spiro and Selwood [1984]. This method is often referred to a well stirred batch reactor, or slurry method. Sieved, ground coffee is placed in a stirred water bath at isothermal conditions, where aliquots during the extraction event are taken as function of time. This setup is important as it ensured the particles were instantly dispersed when added to the water and there was no residence time distribution of the particles in the solvent, unlike that of a coffee bed with a moving solid-liquid interface. This setup was later used by Corrochano [2017] and a modification of this setup is proposed in this thesis.

Spiro and Page [1984] repeated kinetics studies of caffeine extraction using a spinning disc with attached coffee to assess the effect of the diffusion through different Nernst layers. They concluded that at a constant rotational speed, the observed rate constant was inversely proportional to the particle radius squared. The observed rate constants were independent of the applied rotational speed, concluding that particle diffusion is the rate limiting step in caffeine extraction from roast and ground coffee particles.

Spiro and Hunter [1985] repeated the methodology of measuring kinetics of caffeine from the work of Spiro and Selwood [1984], but rather focused on the effects of roasting, comparing green coffee against five different roasted coffee samples. The authors reported that the rate constant, k_{obs}, was highly dependent on the roast level, as the physical changes in bean volume (measured as an ellipsoid) were large as roast level increased. Spiro and Hunter [1985] suggest the cellular structure and the coffee particle cellular matrix is the most influential piece to affecting the diffusion of caffeine from roasted coffee, in contrast to the near constant effective diffusivities for a broad range of particle size reported by Spiro and Selwood [1984]. The authors suggested that there is a tipping point in which the degree of roast is so extreme that the cellular structure is compromised and thus the rapid initial extraction of caffeine is captured by the large intercepts in the extraction versus time plots. The calculated effective diffusivities reported by Spiro and Hunter are listed in Table 2.9.

Spiro et al. [1989] investigated extraction kinetics of caffeine where an additional preparation step was involved for both roasted ground coffee and ground green coffee. The samples were prepared in a manner where they were “pre-swollen,” by placing roasted coffee

beans in a coffee extract equal in concentration to the soluble solids found in a coffee bean, or "solute free," where the coffee had been through a numerous series of extraction events such that no soluble solids remained in the matrix. The authors proposed six reasons for slow intra-bean diffusion including inward flow of water inhibiting the diffusion process, swelling of the bean increasing the length of the diffusion path, dissolution of the material before it can diffuse, molecular association with the matrix, molecular association with other molecules, and physical restraints by the matrix known as the bean tortuosity.

In this study, Spiro et al. [1989] provided data collected by scanning electron microscopy (SEM) on the swelling of coffee particles after several minutes submerged in 80°C distilled water. Values of swelling were reported to be approximately 20% and 17% for green coffee particle and roasted coffee particles, respectively. In well stirred batch reactor coffee extraction testing, the rate constants k_{obs} of pre-swollen and solute free beans were found to be double that of the control materials. The half-lives of caffeine infusion from the two treatments were found to be half that of the control. The authors concluded that the first four of six proposed reasons for slow intra-bean diffusion accounted for an observed hindrance factor of 3, while the last two comprise an additional hindrance factor of 4, thus giving further insight into specific events leading to observed, slow diffusion in coffee extraction processes.

While these observations of faster rate constants were enlightening, there was a missed opportunity to explore the physical changes due to the treatments to the coffee. A surface area and a pore size analysis of the ground green and roasted coffees post treatment could have ruled out faster rate constants as result of morphological changes due to the treatment process. Moreover, rather than only surface drying the coffee and measuring kinetics of extraction, a complete drying step could have been included to ensure that the slower rates were due to water intrusion and dissolution and again not morphological changes to due to the expanded matrix. Without a better control and additional data regarding the changes to morphology because of the treatment process, it is difficult to truly assign proportions of hindrance factor to the six proposed reasons stated by the authors.

Espinoza-Pérez et al. [2007] proposed a simplified and rigorous model for caffeine kinetics during the extraction process of decaffeinating green whole bean coffee. The model

developed was a non-steady state diffusion equation. In fitting this new, simple model to extraction data, the authors yielded a diffusivity of caffeine of 3.21×10^{-10} m^2 s^{-1} at 90 °C which was nearly double the value reported by Spiro and Selwood [1984]. The authors argue that the spherical assumption of coffee beans is invalid due to the shape of the particle being a semi-ellipsoid.

Zanoni et al. [1992] later repeated similar work performed previously by Spiro and others. The authors quickly point out that none of the previously reported models fit the experimental data well at early stages of extraction, stating that a simple diffusion model is insufficient to describe the brewing process of coffee. This lack of fit statement comes from non-zero intercept terms observed in all previously published models. It was proposed that there are two distinct phases to extraction: a wash phase and a diffusion phase. The authors observed that during the wash phase a linear relationship existed between the particle surface area and the extraction yield. It was observed that the overall composition of extract does not change with brew times beyond 1 minute to as long as 60 minutes, with the data showing 90% of soluble solids are extracted during the washing phase. Zanoni et al. [1992] reported caffeine diffusion values that were two orders of magnitude smaller than other publications, primarily those by Spiro and others.

Spiro [1993] re-evaluated and recalculated the published values from Zanoni et al. [1992] showing that the majority of extraction reported (85-90%), could be accounted for by a diffusion model and not a washing phase. Spiro went on to show mathematically that the two orders of magnitude discrepancy in diffusion values occurred only because the data from one minute onward was used in the calculation. Spiro [1993] suggested that the values published by Zanoni et al. were comprised of the diffusivities of larger molecules accounting for the remaining 10-15% of soluble solid content and not the smaller faster diffusing molecules as previously reported.

Spiro and Chong [1997] continued to explore various factors contributing to slow intra-bean diffusion. A focus on hindrance factor contributions was investigated for pre-swollen and solute free coffee particles at various temperatures. As part of the investigation, the authors calculated the partition coefficient of caffeine for the studied temperatures, finding that the

partition coefficient was lower at 25 °C versus 80 °C; 0.68 vs 0.87 respectively. Additionally, the hindrance factor at 25 °C was compared against the work previously done at 80 °C by Spiro et al. [1989]. It was observed that the value of the hindrance factor at 25 °C was more than 2.5 times the hindrance factor at 80 °C in roasted coffee. The authors suggested that differences in swelling behavior, especially with swelling being less at lower temperatures, coupled with a greater caffeine association with the cellular matrix at lower temperatures, explains the observed differences in the hindrance factors at different temperatures. Moreover, the fact that the partition coefficient was found to be lower at lower temperatures, was evidence supporting the assertion that there is a greater affinity between the extracting species and the cellular matrix.

Additional first order, steady state extraction studies were carried out by Jaganyi and Madlala [2000]. The authors studied rates of extraction and intra-bean diffusion of caffeine, phosphorous, potassium, magnesium, and manganese. The diffusion coefficients of each species were calculated using the observed rate constants and half-lives of infusion, similar to the work by Spiro and others. The authors calculated hindrance factors for each species, finding differences among the species. Values for hindrance factor were reported as low as 11 (caffeine) and as high as 48 (manganese). Data for caffeine when corrected for particle size and temperature using the Arrhenius equation, was in good agreement with Spiro and Selwood [1984]. In addition to citing the hindrance of the extraction process, the authors claim slower rates of diffusion are also due to mineral association with the matrix, and/or complex formation of minerals with other soluble compounds, creating a larger, slower moving molecular structure.

Analysis of the model proposed by Spiro and others and commonly referenced in additional work reveals one major weakness with the model, a non-zero intercept. In the real world, there is no solute in the solvent at time zero, thus a non-zero intercept cannot exist. Stapley [2002] investigated mathematically why a non-zero constant existed in the Spiro equation. It was shown that the long-term approximation proposed by Spiro and others is in fact the first term of the series solution to Fick's second law. The non-zero intercept was a result of using the long-term approximation and not calculating a large number of terms in the

series, which is often mathematically complex and tedious. Thus, to achieve accurate solutions at small values of time, the summation of a large number of terms in the series needs to be considered [Stapley 2002].

Section 2.5.4: Particle Scale Mathematical Models Developed in Supercritical Fluid Extraction

Oliveira et al. [2011] conducted a review of the development of mathematical models describing the mass transfer of plant-based materials during supercritical fluid extraction (SFE). The models in the review included: the linear driving force model (LDFM), the shrinking core model (SCM), the broken and intact cell model (BICM), and the broken and intact cell-shrinking core hybrid model (BIC-SCM). The application of these models is not limited to SFE of plant oils, but also to solvent based extraction of plant-based material [Kassing et al. 2010].

The common assumptions amongst these models are that the particles and respective cells within the particle are spherical, all cells contain solute, all particles and cells have uniform distributions of solute throughout the matrix, and that dissolved solute diffusing through the matrix cannot be reabsorbed. In the case of the SCM, the structure of the particle is assumed to be constant regardless of radial position, unlike the BICM or BCIM-SCM where a layer of particles could be broken [De Melo et al. 2014].

Section 2.5.4.1: Shrinking Core Model:

The shrinking core model assumes a sharp liquid-solid interface as it recedes within the particle. This interface defines wetted, extracted regions and non-wetted, non-extracted regions, until the core of the particle is reached, and the extractable volume is exhausted [De Melo et al. 2014]. Goto et al. [1996] applied the shrinking core model to leaching of solutes from a solid material in supercritical fluid extraction. The SCM was used to account for intraparticle diffusion and external fluid film mass transfer for oil extraction from seeds in flow through a column with axial dispersion. The authors noted that intraparticle diffusivity is the most important parameter in the extraction process from solid materials, as it has a large effect on the inverse of dimensionless residence time, noted as parameter a', in the model equations.

Additionally, intraparticle diffusivity has a large effect on the Biot Number, which is a relative comparison of internal versus external mass transfer resistances, or that of the intraparticle diffusivity and external fluid-solid mass transfer [Litster 2016]. The numerical solutions of the model were found to be in good agreement with experimental results; however, when comparing a simplified version of the model, such as a quasi-steady state assumption, the model did not fit as well due to small parameter *a'* values and large Biot numbers.

Section 2.5.4.2: Broken and Intact Cells Model:

The origin of the BICM was a result of an observation in mass transfer rates declining as a function of time, suggesting an increase in resistance. The BICM was an extension of Lack's model where a distinct, rapid transition is observed in the extraction kinetics, suggesting two phases in the mass transfer. The first phase of the extraction curve was typically represented by a straight line with a large positive slope, with the second extraction phase being much slower, with an extraction function converging to an asymptotic extraction yield. The physical explanation for two distinct phases, was attributed to open cells at the surface of particles with a limited mass transfer resistance (phase one), followed by a second phase where the mass transfer resistance was increased by the presence of intact cells with low permeability [Sovová 2017].

This work was extended by Reverchon and Marrone [2001] who introduced solute-matrix interactions, distinguishing broken cells containing unbound free solute and intact cells containing solute bound to the matrix, giving rise to two different mass transfer terms which occur in parallel.

Section 2.5.4.3: Hybrid of Broken and Intact Cells with Shrinking Core Model:

The ideas of the BICM and the SCM were merged by Fiori et al. [2009] where a particle of plant-based material can be discretized into N number of concentric layers, where N is the ratio of the particle radius to a single cell diameter [Oliveira et al. 2011]. This model permits multiple broken layers, with a broken layer always present at the surface, and possible hidden

broken layers inside of the particle. Like Reverchon and Marrone [2001], the authors propose two different mass transfer rates, one representing the broken cells on the surface of the particle and the other representing the internal, intact cells which have a higher mass transfer resistance due to the solute diffusing through intact cell walls. The authors make several assumptions in the hybrid broken and intact cells-shrinking core model (BIC-SCM). These assumptions include spherical particle geometries, each intact cellular layer within a particle has the same mass transfer coefficient k_c, and the total soluble content is homogenously distributed within the particle.

This new hybrid model, with its assumptions can describe the mechanisms of the coffee extraction process at the particle scale. The coffee extraction process begins with dry, ground particles mixing with water. The surface of the particle where broken, individual cells exist, is the first to hydrate. The hydration process is considered rapid [Spiro and Selwood 1984] and the soluble solids within this broken cellular layer begin to dissolve and diffuse directly into the bulk fluid. There is limited mass transfer resistance due to the absence of any particulate structure and the short diffusion distance to the bulk fluid [Zanoni et al. 1992]. This is also reflected in the mathematical models proposed by Fiori et al. [2009] where the first layer has a distinct mass transfer coefficient, k_1, and is independent of the other subsequent layers of the particle.

As the particle continues to hydrate beyond the first layer, the shrinking core model (SCM) describes a receding liquid-solid interface until the core of the particle is reached, and the particle is fully hydrated. As additional intact cellular layers are wetting, the soluble solids begin to dissolve and diffuse into the hydrated particle pore space. As the liquid-solid interface progresses through each concentric layer inside the particle, the mass transfer resistance increases as the dissolved solute must diffuse from the core through the exhausted layers to the surface of the particle and into the bulk solvent. The inner particle mass transfer coefficient is dependent upon the radial position within the particle. The diffusion of soluble solids from the particle continues until each layer is exhausted, and the particle has a coffee solids concentration equal to the concentration of the bulk liquid. Figure 2.6 shows the conceptual model of the hybrid BIC-SCM.

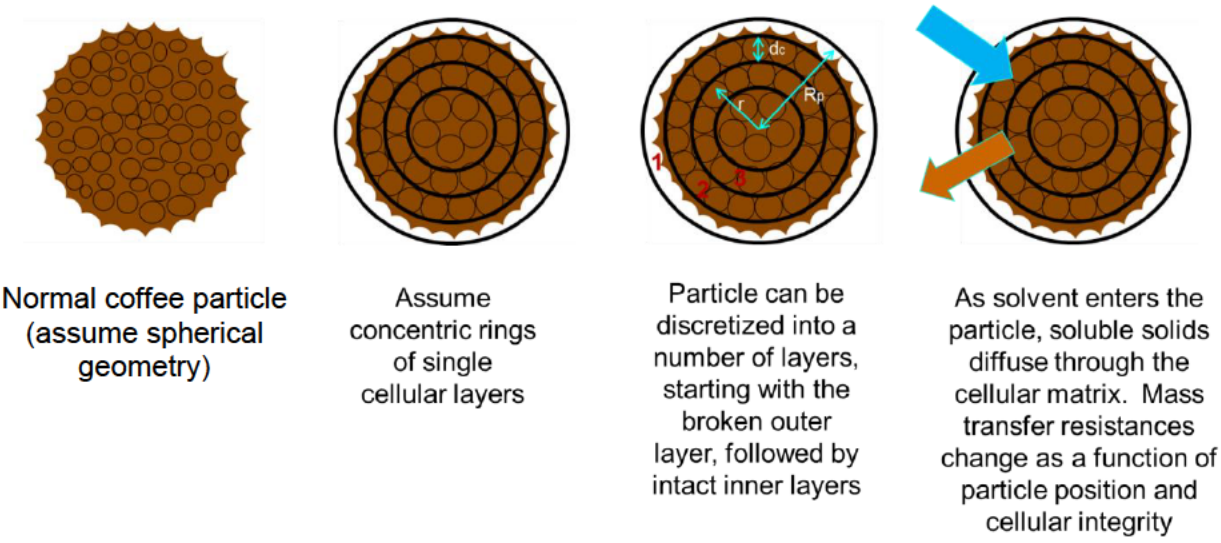

Figure 2.6: Setup of the hybrid BIC-SCM [Fiori et al. 2009].

Fiori et al. [2009] proposed three different mathematical descriptions of the mechanism of internal solute extraction from the inner portions of the particle to the external surface. These descriptions are the discrete model, the continuous model and the semi-continuous model for the overall mass transfer coefficient. In each set of mathematical equations, the overall mass transfer coefficient, k, is related to the exhaustion degree, x, of the particle, which is the ratio of exhausted particle volume to the total particle volume.

The authors establish the discrete model combining equations 2.4, 2.5 and 2.6 to find the overall mass transport coefficient, k, of the solute transferred from the inner portion of the particle to the outer shell.

The mass transfer resistance for any layer of the particle is:

$$\frac{1}{k_j} = \frac{1}{k_1} + \frac{1}{k_c}\sum_{n=1}^{j-1}\left[\frac{R_p}{R_p - nd_{cell}}\right]^2, \qquad j = 1, \ldots, \left[int\left(\frac{R_p}{d_{cell}}\right) + 1\right] \quad Eqn\ 2.4$$

Where k_j is the mass transfer coefficient of the j^{th} layer of the particle, k_1 is the mass transfer coefficient for the broken surface layer of the particle, k_c is the mass transfer coefficient for each individual, inner annular layer with a thickness of an individual plant cell with intact cell walls, R_p is the particle radius, and d_{cell} is the diameter of an individual plant cell. As described in equation 2.4, as additional layers of intact cells are considered, *i.e.* larger particles, the overall mass transfer resistance increases substantially, reflecting the increased diffusion distance and particle structure.

The overall mass transfer coefficient related to the amount of particle solute exhaustion, x is:

$$k = k_j, \qquad x_{j-1} \leq x < x_j \quad Eqn\ 2.5$$

$$x_j = 1 - \left[\frac{\frac{R_p}{d_{cell}} - j}{\frac{R_p}{d_{cell}}} \right]^3, \qquad x_0 = 0 \quad Eqn\ 2.6$$

Where k is the overall mass transfer coefficient of the solute being transferred from the inner portion of the particle to the outer shell, k_j is the mass transfer coefficient of the j^{th} layer of the particle, and x_j is the exhaustion degree of the particle at the j^{th} layer, and is defined as the ratio between the solute exhausted volume of the particle and the total volume of the particle. The overall mass transport coefficient as a function degree of solute exhaustion is evaluated as a step function in this model.

Similarly, the authors suggest a continuous model can be substituted for the discrete model where the ground plant particles are much larger than the size of an individual plant cell ($R_p \gg d_{cell}$).

The overall mass transfer resistance as related to the solute exhaustion of the particle is:

$$\frac{1}{k} = \frac{1}{k_1} + \frac{1}{k_c}\frac{R_p - r}{d_{cell}}\left(\frac{R_p}{r}\right), \qquad 0 \le r \le R_p \quad Eqn\ 2.7$$

$$x = 1 - \left[\frac{r}{R_p}\right]^3, \qquad 0 \le r \le R_p \quad Eqn\ 2.8$$

Where r is any specific radial position bounded between the surface and the absolute core of the particle.

Lastly, the authors proposed a combination of the discrete model and continuous model. This combination described as the semi-continuous model considers the overall mass transfer coefficient to be constant until the first, broken layer is completely exhausted, as seen in the discrete model, and then varies depending on the radial position within the remaining intact cellular layers, as shown in the continuous model.

The discrete portion of the overall mass transfer resistance is:

$$\frac{1}{k} = \frac{1}{k_1}, \qquad R_p - d_c < r \le R_p \quad Eqn\ 2.9$$

With the degree of exhaustion for the first shell, x_1 defined as:

$$x_1 = 1 - \left[\frac{\frac{R_p}{d_{cell}} - 1}{\frac{R_p}{d_{cell}}}\right]^3 \quad Eqn\ 2.10$$

The continuous portion of the overall mass transfer resistance is:

$$\frac{1}{k} = \frac{1}{k_1} + \frac{1}{k_c}\frac{R_p - r}{d_c}\left(\frac{R_p}{r}\right), \qquad 0 \le r \le R_p - d_c \quad Eqn\ 2.11$$

With the degree of solute exhaustion described by equation 2.8 above.

The authors noted that it is possible to describe the solute mass balance in terms of the particle exhaustion over time by:

$$\frac{dx}{dt} = 3\frac{k(x)\,\rho_f}{R_p}\left(\frac{C_{l,sat} - C_t}{C_{s,0}}\right) \quad Eqn\ 2.12$$

Where $C_{l,sat}$ is the saturation concentration of the solute in the solvent, C_t is the actual concentration of the solute in the solvent as a function of time, $C_{s,0}$ is the initial solid solute concentration in the particle, ρ_f is the fluid density, and $k(x)$ is the overall mass transfer coefficient for the solute exhaustion degree of the particle, x. The authors used each of the three models above to represent $k(x)$, with equations 2.4, 2.5, and 2.6 representing the discrete model for the overall mass transfer coefficient, equations 2.7 and 2.8 representing the continuous model, and equations 2.8, 2.9. 2.10, and 2.11 representing the semi-continuous model of $k(x)$.

In comparison of the three models describing the overall mass transport coefficient, Fiori et al. [2009] noted that k is consistently underestimated when using the continuous model, and that the continuous approximation exacerbates that error at smaller and smaller particle sizes. The discrete approximations provided the most accurate results, as the authors mention it represents the physical state of the particle best. The semi-continuous model was reported to be a good compromise between the continuous approximations and the discrete ones, providing near identical results of the discrete model.

The initial single broken shell models overall did not fit the data. The predicted mass transfer values seemed to underestimate the amount of free oil extracted in the system. Upon adding a factor of two to the broken layer, later referenced as the double broken shell model, the predicted values were in good agreement with experimental results. The authors

hypothesized that the necessity for the second layer of broken cells, likely comes from internal particle damage during the milling process that generates additional free oil. While this model was developed for supercritical CO_2 extraction from milled grape seeds, it can also be applied to other milled, plant-based particles with solvents, such as ground coffee and water [Fiori et al. 2009].

Section 2.6: Extraction Models of Well Stirred Batch Reactors and Packed Beds

Section 2.6.1: Multi-Scale Modeling of Coffee Extraction

Coffee bed extraction has been the recent focus of several investigators, most notably by Moroney et al. [2015], Corrochano et al. [2015], Melrose et al. [2018] and Kuhn et al. [2017]. The latter three research groups focused on modeling extraction of espresso based beverages, while the former, Moroney et al. [2015], developed a double porosity multiscale model that has been applied to both a stirred dilute system and a packed bed of coffee, with slight modifications adapting the model to various commercial brewing techniques including drip coffee machines.

The multiscale, double porosity model developed by Moroney et al. [2015] included: the dissolution of the soluble solids from the matrix, the transport of the solids through the individual particles, and the transport of the solids through the void fraction of the packed bed of coffee, or the space between the individual coffee particles. This required the authors to develop equations representing all three different time scales of diffusion and dissolution, represented by two regimes of extraction, a rapid regime where the surface of the particles undergo immediate extraction, and a second slower regime where soluble solids are extracted from within the particles. The authors provide similar arguments as presented in the BICM for the observation and necessity to have two different regimes of extraction; moreover, the authors expressly state that the mathematical models developed are along the premises of the BICM parallel model as described by Reverchon and Marrone [2001].

The authors fitted the mathematically derived model equations to empirical data for two brewing conditions, a well stirred batch reactor and a packed, cylindrical bed of coffee. Several assumptions were made, and were similar to those previously made by others, including: steady state extraction occurs, the wetting phase of the particle is ignored, there is no swelling of the particles, the density of the liquid during extraction is constant, the particle size distribution is comprised of spherical particles of two different size classes, the soluble content is homogenously distributed within the particle, and the soluble material within the particle is initially dissolved. These assumptions and embedded boundary conditions simplified the original system of equations into a smaller set of equations which were solved numerically.

The simplified equations contain primarily physical parameters of the particles or of the system that can be characterized directly, or values taken from previously published results. There are two fitting parameters, alpha and beta, which the authors used to account for error in estimations made for values of real physical characteristics and any invalid assumptions made to simplify the model.

Moroney et al. [2016] builds on the previous work of Moroney et al. [2015], where the authors focus on the well mixed batch reactor system, demonstrating model reduction and development of asymptotic solutions to the equations with a finite number of dimensionless parameters, providing quick analysis of factors influencing coffee extraction. It was found that the approximate solutions were in good agreement with the numerical solutions.

Complimentary to Moroney et al. [2015], Corrochano [2017] also proposed a multiscale modeling technique for the well stirred batch reactor and cylindrical brewing chamber for espresso extraction. Corrochano [2017] conducted extensive characterization work on the macrostructure and microstructure of roast and ground coffee, providing the foundation to the multiscale coffee extraction model presented. The kinetics of coffee extraction were studied under two conditions, the first was a well stirred batch reactor like that of Spiro and Selwood [1984], and the second was a packed coffee bed in espresso brewing conditions. The well stirred batch reactor was studied by Corrochano [2017] using both a numerical solution to Fick's Second Law of Diffusion for early time scale modeling, and by using the long term approximation and analytical solution provided by Stapely [2002].

In the extraction of the coffee bed, Corrochano [2017] used an *ad hoc* analytical equation with fitting parameters to describe the empirical data representing the non-steady state cumulative volume function of brewed coffee as a function of time; four parameters were solved for to fit the model to the empirical data. This equation was linked to the time dependent flow rate. Corrochano [2017] demonstrated that the time dependent flow rate function is the time derivative of the non-steady state cumulative brew volume function. The time dependent flow rate function coupled with the physical characteristics of the bed, such as bed porosity, permeability, and the chemical compound concentration of the bed as a function of the particle scale model, were combined to produce a multiscale model of coffee extraction. This multiscale model of coffee extraction modeled the total dissolved solids and included the bimodality of ground coffee and the tortuosity of the particle matrix as captured by mercury intrusion-extrusion hysteresis.

The results obtained for the experiments in the stirred batch reactor could not be described by a global effective diffusion coefficient. Corrochano [2017] hypothesized that at long extraction times, several hours in the experiments, the difference in molecular weights of soluble species prevented the applicability of a single effective diffusion coefficient. Corrochano [2017] demonstrated by implementing four effective diffusion coefficients, representing different species of soluble solids, that the maximum error between the model and the experimental data was halved, from 17% to 8%. Similar values in mean percentage errors between the model and empirical data were found for the extraction in packed coffee beds. Corrochano [2017] reported that particle size distribution and extraction time had greater levels of sensitivity versus brew temperature in the range tested 85+/-5 ^{o}C.

Suggested opportunities for further work included a deeper understanding of the non-steady state phenomena, with a kinetics model including the effects of gas escaping the coffee grounds, capturing the real world three phase system coffee extraction exhibits. Moreover, it was suggested a better understanding was necessary in the characterization of particle size measurements in using a liquid dispersion, laser diffraction system such as one provided by Malvern Instruments. There exists an opportunity to tease out coffee oil, soluble particles, insoluble particles and gas bubbles during a laser diffraction measurement. Additionally,

Corrochano [2017] also encouraged more exploration in methods to measure or estimate the microstructure of coffee particles, specifically, the particle porosity, tortuosity, and surface area measurements.

Corrochano et al. [2015] focused on modeling steady state permeability during espresso brewing. The authors observed error in the model predicted permeability values substantially decreased when a correction to the Carman-Kozeny equation via a tortuosity dependent power-law term was introduced. This tortuosity value was defined as the inverse of the bed porosity to the n^{th} power. The parameter n, the exponential term on the inverse of the bed porosity, was found to vary with particle size and increased as particle size increased. These factors were combined and included in the Carman-Kozeny equations for estimating permeability of the packed coffee bed under brewing conditions; the pre-factor value in the tortuosity corrected equation was approximately 196-1330 versus the traditional coefficient value of 180 in the Carman-Kozeny equation. The authors noted that these new, higher pre-factor values were commensurate with other published values for consolidated, non-spherical packed beds.

Previous investigators have traditionally used custom and ideal brewing situations where several factors are controlled during an experimental run, such as presented in a stirred batch reactor. Kuhn et al. [2017] studied the time resolved extraction of caffeine and trigonelline by incorporating a rotary sample splitter designed to capture aliquots of brewed espresso coffee from a commercial espresso machine. Figure 2.7 shows the setup used by the authors.

(a) **(b)**

Figure 2.7: (a) The rotary sample splitter setup underneath an espresso machine, (b) sampling an espresso brew [Kuhn et al. 2017].

This experimental setup permitted fractionated aliquots as a known function of time due to a fixed angular velocity of the sampling device. The experimental setup used by Kuhn et al. [2017] was adopted and modified for use in this thesis later presented in chapter 4. The authors studied the effect of particle size and tamping pressure on the extraction kinetics. It was reported particle size influenced extraction kinetics, with smaller particles leading to more extraction per collected aliquot of brewed espresso coffee. Particle size also influenced the liquid composition ratios of caffeine to trigonelline. Surprisingly, tamping pressure had no observed effect on extraction, flow rate, or composition of the coffee regarding caffeine to trigonelline ratios.

A simple, mechanistic model was developed and used to fit the data. The model included two averaging steps, one at the particle scale, the second on the bed scale. The first averaging step assumed that the coffee particle is homogenous in solute concentration. The second averaging step on the bed scale implied a linear profile in concentration across the bed. Other stated simplifications included assuming spherical particles, the coffee bed is homogeneous in structure and incompressible, the flow is stationary with initial wetting is not considered, and dispersion is ignored. The analytical solution to the model developed contains only physically meaningful parameters, such as initial solute concentration in the solid and liquid phases, a weighted mass transfer coefficient, height of the bed, superficial fluid velocity through the bed, porosity and the distribution coefficient between solid and liquid phase.

The model contains four constants, $C_{s,0}$, $C_{l,0}$, K, and k^* which were solved for in the fitting of the model to experimental data. The results of the initial solute concentration in the solid phase, one of the four fitted parameters, were comparable to previously published values. It was mentioned that the flow rate and the residence time of fluid in the coffee bed were dominant factors affecting the extraction process and concentration profiles. Commensurate to the data collected, larger particles permit a larger flow rate at given constant pressure according to the Carman-Kozeny model [Rhodes (Ed.) 2008], and therefore a greater decrease in the concentration curves was observed as particle size increases as a greater amount of fluid passes through the coffee bed per unit time at a fixed pressure.

One of the more recent publications on coffee extraction modeling is an effort to provide an engineering perspective and modeling approach to update the original brewing control chart proposed by Lockhart. Melrose et al. [2018] published a model in pursuit of updating a brewing control chart for espresso beverages where strength, yield and brew volume could be predicted based on flow rate, particle size, and brew time. The model proposed by the authors focuses on a discretized cylindrical brewing chamber where the length of the chamber is divided into a series of disks or layers, all are of equal volume and are axially symmetric. The model equations accounted for the concentration profile of the species of interest in each particle and for the moving liquid front in the void fraction of each layer in the bed. The authors simplified the particles to only two different particle size classes and three parameters, fine particle size, coarse particle size, and volume fraction of fines present, and like Corrochano [2017], ignored the multiphase effects of gas being released during brewing. Other assumptions in the presented model included: a constant flow rate, a constant partition coefficient equal to unity, spherical particles, homogeneous particle composition, and rigid particle geometry throughout the brewing process.

The authors presented a control chart for the espresso brewing regime for percent yield as function of time, extraction efficiencies, and strength contours. A typical espresso found at a cafe and a capsule based espresso beverage like that of Nespresso were predicted to have comparable extraction yields, but different strengths; the control chart presented was able to differentiate between the two brew methods. It was noted that an extension of this work could be done for a typical drip filter system with modifications to the model for differences in particle size, multiple diffusion constants, and brew time. Single serve pods producing drip like coffee beverages on similar time scales of espresso machines, were not mentioned as a possible extension to model; however, it is not an unreasonable idea.

Melrose et al. [2019] measured extraction kinetics of total dissolved solids in a well stirred batch reactor. The authors modeled the data with a parameterized, numerical solution to the diffusion equation within the particles. Two models were considered, one model was based on a mono-disperse particle size, and the second on a mono-disperse particle size coupled with a fast-release extraction contribution from the fines. The authors reported that

the model with the fast-release contribution and a separate slow-release extraction from the core of the coarse particles provided the best fits. The fast-release fraction of the total dissolved solids was estimated using:

$$\theta_{fs} = 1 - \left(1 - \frac{d_c/_2}{d_{3,2}(Co.)}\right)^3 \qquad Eqn\ 2.13$$

Where θ_{fs} is the fraction of the total dissolved solids released from the surfaces of coarse particles and the fine particles $\frac{d_c}{2}$ is half of an assumed diameter of a single coffee particle (25-35 µm), and $d_{3,2}(Co.)$ is the Sauter mean diameter for the coarse part (particles >100 µm) of the measured particle size distribution [Melrose et al. 2019].

Sano et al. [2019] presented lumped parameter analytical solutions obtained by integrating a general set of macroscopic governing equations for coffee extraction based on volume averaging theory. The authors solved these equations for three specific brewing methods including: espresso brewing, drip coffee brewing, and immersion brewing (well stirred batch reactor). The authors discovered that a dimensionless number, *Ca*, called the "café number" which is a combination of controllable brewing parameters. The café number, *Ca* is calculated by:

$$Ca = \frac{a_{sf} k V}{\varepsilon_v (1 - \varepsilon_v) Q} \qquad Eqn\ 2.14$$

Where a_{sf} is the volume specific surface area, k is the mass transfer coefficient, V is the volume of coffee grounds used in the brewing method, ε_v is the void fraction of the coffee beds, and Q is the flow rate of hot water [Sano et al. 2019].

The authors suggest that the value of the café number distinguishes brew methods where extraction is controlled by brewing parameters and coffee physical parameters versus brew methods where extraction is controlled by just brewing parameters. Low values of Ca are found in drip coffee brewing methods, where the authors suggest the value of Ca can be used to control coffee extraction. High values of Ca, found in brewing methods like espresso, are

brew methods the authors believe only brewing parameters can change the coffee extraction process, and specifically state only flow rate and the amount of coffee used in espresso affect the coffee extraction process. The latter statement by the authors is contradictory to previously published models [Moroney et al. 2015, Corrochano et al. 2015, Kuhn et al. 2017], and disregards the findings of Kuhn et al. [2017] who reported the important influence of particle size on espresso extraction kinetics.

Section 2.7: [redacted]

[redacted]

[redacted]

[redacted]

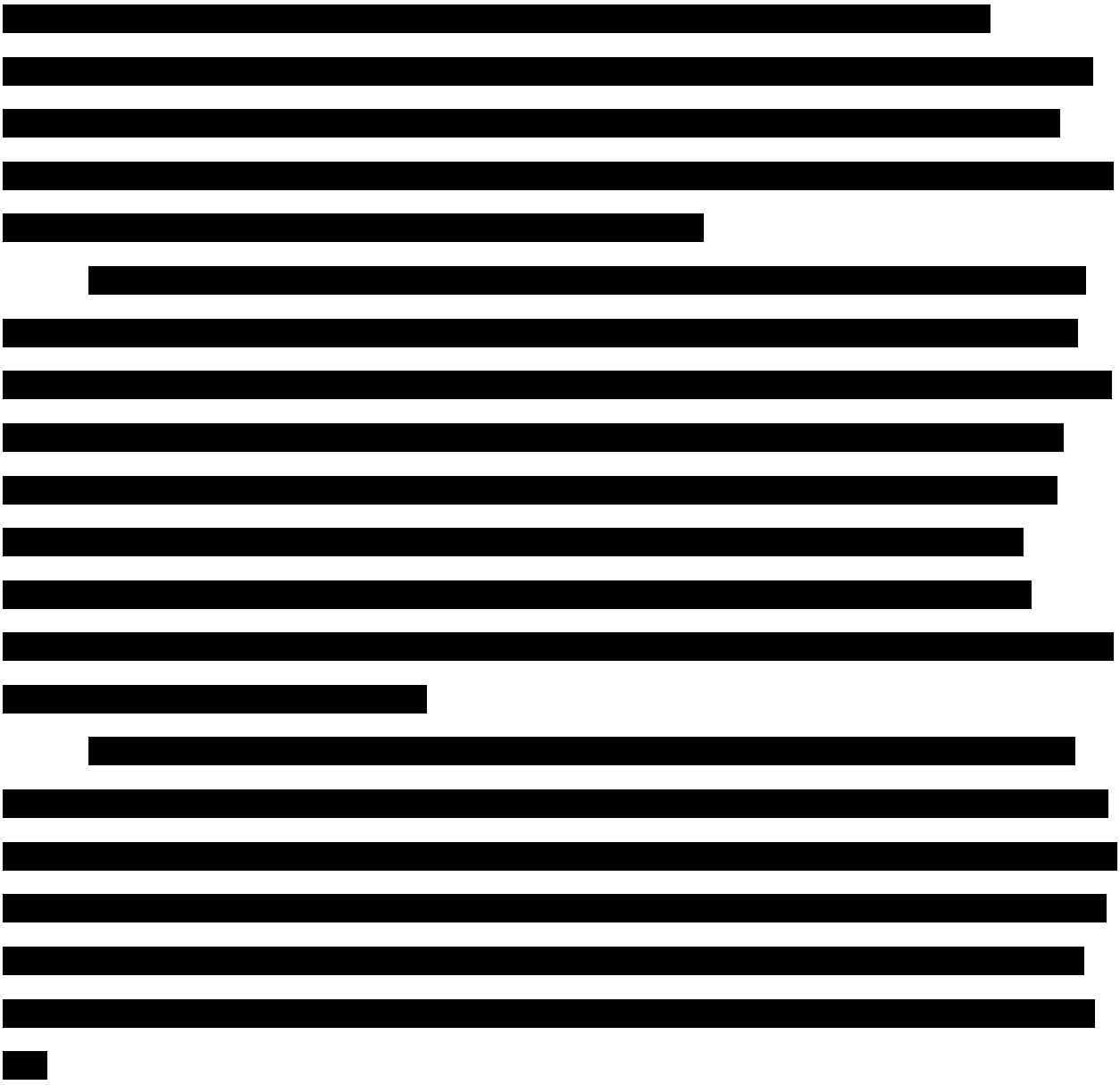

Section 2.8: Literature Review Summary and Knowledge Gaps

The first step in an engineering, quantitative approach to optimizing the quality of coffee produced for a given brew method is studying the extraction rates of soluble solids and organic compounds. The correlation of positive organoleptic ratings to coffee soluble solids and organic compounds such as chlorogenic acids, simple acids, proteins, and carbohydrates has been elusive to industry and academia. The work of Lockhart et al. [1955] is still widely

referenced and utilized nearly 70 years later but is limited and focuses on the lumped values of total dissolved coffee solids and percent extraction.

Over the last several decades researchers have investigated coffee extraction to identify optimal conditions for brewing a good tasting cup of coffee and to improve yields in commercial soluble coffee production. These collective efforts have overwhelmingly focused on coffee extraction kinetics beyond 60 s or on very long-time scales, as experienced in soluble coffee manufacturing. There are only a handful of published studies that contain extraction data under 60 s, and those that are available are with very few data points. Wang et al. [2016] demonstrated that single serve systems complete the entire brewing event in 30 s. Several models of coffee extraction kinetics have been developed over the last few decades with increasing complexity, but none have been fit to extraction data within a well-mixed batch reactor at short time scales (<30 s).

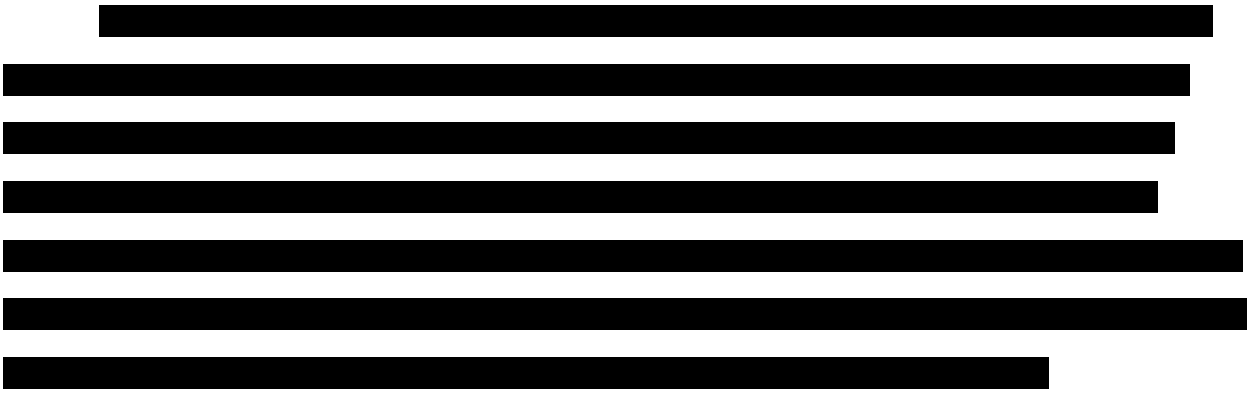

Section 2.9: Hypotheses and Thesis Objectives

There is an absence in literature of extraction kinetics of individual chemical compounds in brewed coffee. Furthermore, there is insufficient data on coffee extraction at early time scales even with the prevalence of single serve coffee systems. A new approach aimed at understanding the relationship of positive organoleptic properties of coffee to individual chemical compound starts with understanding the extraction kinetics of individual compounds for common brewing methods. A novel, robust measurement system is needed to capture individual chemical compound extraction kinetics over broad time scales of interest. The principal objective of this thesis is to develop a robust method for measuring coffee extraction

kinetics of individual chemical compounds at early time scales (<30 s) and at long time scales (≤10 min) using a well-mixed batch reactor.

[redacted]

Chapter 3: Materials and Methods

3.1: Introduction

This chapter gives a description of materials, equipment and methods for all experimental work in the thesis. Section 3.2 describes the green coffee, water, and coffee processing steps. Section 3.3 describes all physical characterization of the coffee in all roasted states, whole bean, ground, [redacted]. Section 3.4 describes the experimental setup of the Well-Mixed Batch Reactor (WMBR), while Section 3.5 presents the analytical techniques used in the measurement of extraction kinetics and the ensuing statistical analysis.

3.2: Coffee Materials and Coffee Processing

3.2.1: Coffee and Water

Natural materials, like green coffee, can impart variability on many aspects of the study. Therefore, it is imperative that the starting coffee material is as uniform as possible in all planned experimental testing. The green coffee used in all experiments consisted of a single 70 kg bag of a washed, green coffee from Antioquia, Colombia, grown between 1600-2200 m above sea level. The green coffee was provided exclusively by Keurig Dr Pepper Inc. (Frisco, Texas USA). The green coffee had a moisture content of 7.7% M_w measured by vacuum oven drying in accordance with ISO 6673 [2003].

Water quality recommendations have been established by the Specialty Coffee Association (SCA), with Navarini and Rivetti [2010] reporting water quality impacts on espresso brewing. To minimize variability during brewing, the water used in all experiments was Nestle Pure Life water (Nestle, USA). Nestle Pure Life was selected as an appropriate proxy for the SCA water quality recommendations for brewing coffee, given the commercial availability and quality consistency as found in their provided water quality reports. A comparison between the SCA recommendations [Sage 2013] and Keurig Dr Pepper internal water testing of Nestle Pure Life water quality can be seen in Table 3.1.

Table 3.1: Specialty Coffee Association (SCA) recommended water standards and measured values of Nestle Pure Life.

Water Characteristic	SCA Acceptable range	Nestle Pure Life
Chlorine Residual	None	None
Calicum Hardness	50-175 ppm	35.5 ppm
Alkalinity, as CaCO3	40-70 ppm	24.8 ppm
pH	6-8	7.3
TDS	75-250 ppm	90.4 ppm
Sodium (Na)	<30 ppm	6 ppm
Calcium (Ca)	N/A	8 ppm
Magnesium (Mg)	N/A	3.8 ppm
Potassium (K)	N/A	0

3.2.2: Roasting of Green Coffee

All green coffee was roasted in 1.8kg batches on a Diedrich IR-2.5 drum roaster (Diedrich Roaster, Ponderay, Idaho USA) using Profiling Dynamics software (Roaster Dynamics, Clearwater, Florida USA) to consistently control roasting curves and end points for each batch. The coffee was roasted to two different degrees of roast, light and dark. Figure 3.1 shows a typical roast curve obtained with Profiling Dynamics. The light roast batches were roasted for 9 minutes 50 seconds on average, to a final temperature of 225 °C, with an average roast loss of about 13.8 ± 0.6%. The light roast processing conditions consistently yielded Agtron commercial score values of 42.5 ± 1.2 as measured with an Agtron Spectrophotometer E20CP-III (Agtron Inc., Reno, Nevada USA).

The dark roast batches were roasted for 11 minutes 15 seconds on average, to a final temperature of 235 °C, with an average roast loss of 17.3 ± 0.3%. The dark roasting conditions consistently yielded Agtron commercial score values of 27.9 ± 0.5. Neither the light roast, nor the dark roast coffee batches were quenched with water upon discharge from the roaster. Table 3.2 contains the initial green coffee mass, roast time, final roast temperature, ending mass, percent loss, and Agtron color score for each batch roasted.

Table 3.2: Coffee Roasting batch data for Colombian green coffee.

Roast Batch #	Green Mass (g)	Roast Time (mm:ss)	Final Bean Temp (°C)	Roast Mass (g)	% Weight Loss	Agtron Color Score
1	1827	9:33	220	1599	12.5	45.2
2	1855	9:47	222	1609	13.3	43.3
3	1818	9:49	222	1578	13.2	45.5
4	1818	9:52	225	1570	13.6	41.9
5	1836	9:49	225	1588	13.5	42.6
6	1855	10:04	225	1568	15.5	39.9
7	1818	9:58	225	1596	12.2	42.8
8	1836	9:56	225	1578	14.1	42.0
9	1818	9:55	225	1571	13.6	42.2
10	1818	9:51	225	1575	13.4	42.3
11	1818	9:59	224	1565	13.9	40.8
12	1818	9:41	225	1569	13.7	43.0
13	1818	*	225	1565	13.9	41.6
14	1818	9:47	225	1572	13.5	43.3
15	1818	9:39	225	1574	13.4	42.7
16	1818	9:51	225	1578	13.2	42.4
17	1818	9:54	225	1564	14.0	40.9
18	1818	*	225	1566	13.9	42.3
19	1818	9:52	224	1572	13.5	43.3
20	1818	9:48	225	1567	13.8	42.4
21	1818	9:49	225	1569	13.7	44.0
22	1818	9:55	224	1568	13.8	42.8
23	1818	10:00	224	1555	14.5	41.3
24	1818	9:59	225	1560	14.2	41.9
25	1818	9:45	225	1562	14.1	43.5
26	1818	9:59	225	1562	14.1	43.0
27	1818	10:02	225	1564	14.0	42.5
28	1818	11:27	235	1495	17.8	27.5
29	1818	11:07	235	1502	17.4	27.7
30	1818	11:11	235	1501	17.4	27.4
31	1818	11:12	235	1503	17.3	28.4
32	1818	11:06	235	1513	16.8	28.7
33	1818	*	225	1546	15.0	40.4
34	1818	9:58	225	1559	14.2	41.6
35	1818	9:52	225	1559	14.2	42.4

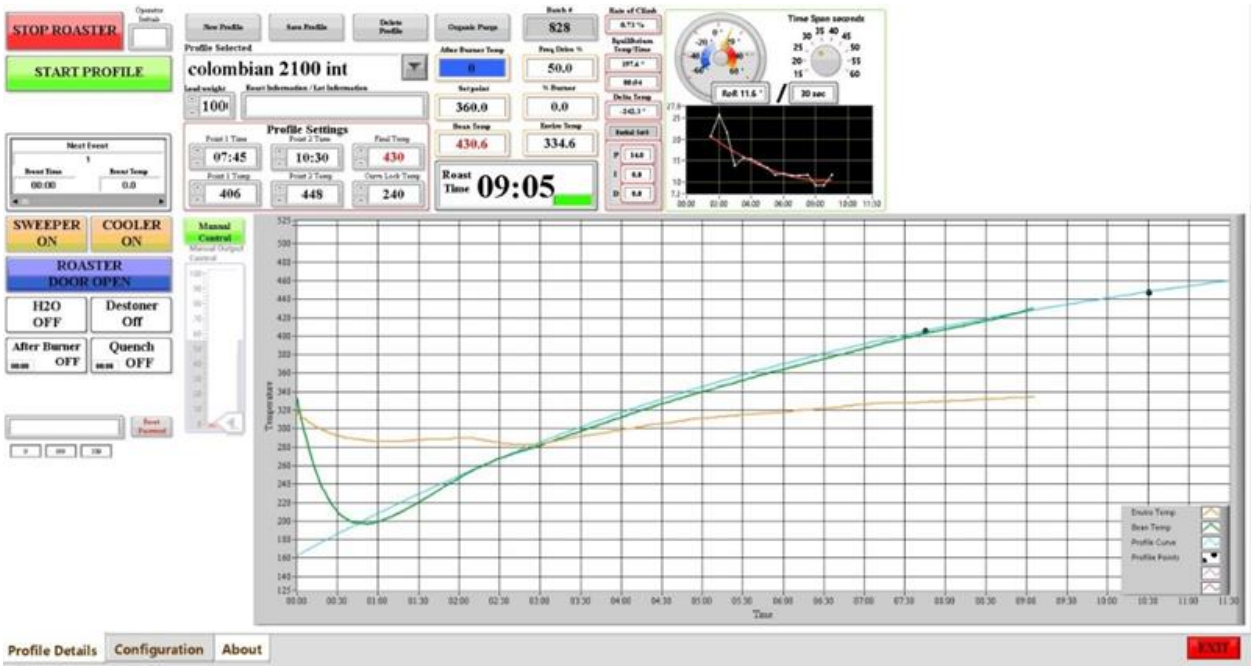

Figure 3.1: Typical roast curve for Colombian green coffee.

3.2.3: Roasted Whole Bean Blending and Storage

The light roast whole bean coffee batches were emptied into a large bin to create a homogeneous blend of roasted whole bean coffee. This was repeated independently for the dark roast whole bean coffee. After mixing the roasted beans, the whole bean roasted coffee was placed into five-pound coffee foil bags containing a one-way gas valve (Uline, Pleasant Prairie, Wisconsin USA). These bags were then placed under vacuum for six seconds and filled with pure nitrogen gas for two seconds and hermetically sealed using a Coffee Pac Vacuum Sealer (PAC Machinery, San Rafael, California USA). This method of sealing the freshly roasted coffee in foil bags prevented oxidation and moisture uptake of the freshly roasted coffee while permitting the coffee to degas over several weeks.

3.2.4: Coffee Grinding and Classification

All roasted whole bean coffee was ground using a Mahlkonig VTA-6-SW coffee burr grinder on a setting of 9 (Mahlkonig USA, Seattle, Washington USA). The resulting grind was classified using a RoTap RX-30 or RX-28 with 30cm or 20cm sieve screens, respectively (W.S.

Tyler, Mentor, Ohio USA). The sieves used included a 16, 18, 25, and 30 US Standard Mesh screens. The amount of ground coffee placed on the initial screen was either 200 g or 400 g for 20 cm or 30 cm diameter screens respectively. The RoTap was operated for three minutes and the ground coffee mass retained on each screen was individually collected in bulk, and sealed in a manner consistent with the freshly roasted whole bean coffee. The sieve screen stack was used only once for each classification step of ground coffee due to the oily nature of ground coffee creating a possible buildup over repeated uses and changing the screening efficiency and dimensions.

3.2.5: [redacted]

[redacted]

[redacted]

3.3: Physical Characterization of Coffee

3.3.1: Sample Preparation

Sample preparation and sample splitting are a critical step to reduce variability in any measurement [Allen 1997a]. Each characterization method used in this study has a unique sample mass requirement. These sample mass requirements range from several hundred milligrams to several hundred grams of sample material. A Gilson SP-230 rotary sample splitter with 16 positions (Lewis Center, Ohio USA) was used to divide large samples into equal, smaller representative samples of the original material. This instrument was used to prepare triplicate test samples of each treatment permutation and control in this study. These triplicate test samples were measured on all physical characterization methods, with only a single sample tested for mercury intrusion porosimetry and scanning electron microscopy.

3.3.2: Particle Size Distribution Measurements

The particle size distribution of all coffee samples was measured with a Malvern Instruments Mastersizer 3000SE (Malvern Panalytical, Westborough, Massachusetts USA). All samples were measured by both dry dispersion and wet dispersion methods. The dry dispersion method used the Mastersizer 3000SE with an Aero S dispersion unit. Approximately 9.0 +/- 0.5 g samples were loaded into the Aero S funnel, which was set to a height of 4mm above the vibratory feeder. A 25%-50% feed rate used to sustain an obscuration percentage of 0.5% to 5%. The air dispersion pressure was set to 100 kPa. The typical measurement period was approximately 60 s in duration; each sample was measured in its entirety. A new background measurement of 10 s preceded each measurement made on the Malvern. If the

background measurement failed to pass conditions set for a satisfactory background measurement, for example less than 100 units for any of the detectors, an intensive cleaning operation was performed in accordance with the original equipment manufacturers protocol.

In addition to the air dispersion measurements, particle size distribution measurements were taken using a wet dispersion system, specifically a Malvern Instruments Mastersizer 3000 attached with a Hydro MV. The dispersant used for the measurements was DI water. The coffee sample was pre-wetted with 10-15 mL of 99.5% isopropyl alcohol (IPA) obtained from Sigma Aldrich (Burlington, Massachusetts USA) to help reduce issues with particle entrainment.

Prior to each measurement, a 10 s background measurement was completed for both the red and blue lasers. If the background measurement failed, the system was cleaned, and the process repeated until passing. A coffee sample mass of 0.20 +/- 0.02 g was added to the Hyrdo MV with the assistance of a stainless-steel funnel. The Hydro MV contained approximately 125 mL of dispersant. Any remanence of sample on either the funnel or the original beaker containing the sample, was flushed with IPA and added to the Hydro MV.

The slurry was permitted to circulate with a stir speed of 3500 rpm to ensure all particles were entrained in the dispersant [Maille et al., 2021]. The sample was measured multiple times with a 10 s measurement time for each laser, and for each sequential repeat the system had a five second delay between each measurement. No sonication was used during any point in the measurement process. The Fraunhofer optical model was used in all data analysis, and results for each sample were averaged using the built-in averaging option in the software. After each sample, the system was flushed several times with DI water.

3.3.3: Loose Bulk Density

The loose bulk density was measured by using equipment from the Seedburo Company (Des Plaines, Illinois USA). The Model 29 Cox Funnel and Model 103 Seedburo metric cup, a 500mL volume cup with a one-to-one diameter to height ratio, were selected and used in each experiment. This equipment was selected because the sample dilates after flowing through the funnel and the 5 cm drop height is fixed as the funnel sits on top of the cup. The 500 mL cup is overflowed with sample and the top gently scraped flush with a 25 cm icing spatula. The mass of the cup and material was recorded, and then the sample discarded from the cup, but

retained for additional testing as the test is non-destructive. The weight of the cup was recorded and subtracted from the previous value to find the mass of the sample occupying the 500 mL volume cup.

3.3.4: Helium Pycnometry

The particle density of each sample was measured with an AccuPyc II 1340 Helium Pycnometer (Micromeritics, Norcross, Georgia USA). The three replicates of each permutation were measured at room temperature 20-23 °C with grade 5 helium gas. Each measurement consisted of 10-purge cycles to evacuate the air, followed by 10 measurements of the solid volume; the average of the 10 measurements was the reported final solid volume. The final density for each replicate was averaged and this was taken as the particle density value for the sample.

The particle density, ρ_s, of each coffee material was calculated by:

$$\rho_s = \frac{V_s}{m} \qquad Eqn\ 3.1$$

Where m is the weighed mass of the sample and V_s is the calculated sample volume. The sample volume, V_s is calculated by:

$$V_s = V_c + \frac{V_r}{1 - {P_1}/{P_2}} \qquad Eqn\ 3.2$$

Where V_c is the calibrated sample cell volume, V_r is the reference cell volume within the instrument, P_1 is the pressure of helium filled into the sample cell and P_2 is the measured pressure of the filled helium when expanded into the reference volume.

3.3.5: Surface Area

The surface area of roast and ground coffee was measured by gas adsorption using a Micromeritics TriStar II Plus krypton gas adsorption analyzer, coupled with a Micromeritics FlowPrep 060. All samples were degassed using grade 5 nitrogen gas, at 20-22 °C for six hours. In all measurements, the free space was measured by the instrument using grade 5 helium gas,

the evacuation rates were set to 0.13 kPa/s, and a leak test for a duration of 60 s was performed on each sample. The isotherm was measured between 0.05 and 0.30 relative pressures at 0.025 relative pressure increments. The adsorptive was grade 5 krypton gas, at liquid nitrogen bath temperatures of approximately 77.35 K.

A BET analysis of the isotherm data was conducted for each experiment. The BET equation can be used to describe Type I, II, and III isotherms, but for Type II isotherms is it most applicable between relative pressures of 0.05 and 0.35 [Allen 1997b]. The BET equation, which relates the quantity of gas absorbed to the relative pressure is:

$$\frac{P}{V(P^o - P)} = \frac{1}{cV_m} + \frac{c-1}{cV_m}\frac{P}{P^o} \qquad Eqn\ 3.3$$

Where P is the pressure during the measurement, P^o is the saturation pressure of the adsorptive gas, V is the volume of the adsorptive gas adsorbed at pressure P during the measurement, V_m is the monolayer volume, and c is a constant. Figure 3.4 provides a typical plot and linear regression line for the Kr gas adsorption BET analysis on coffee. A plot of $1/[V(P^o/P-1)]$ versus P/P^o generated a straight line with the slope equal to $[(c-1)/cV_m]$ and an intercept of $[1/cV_m]$.

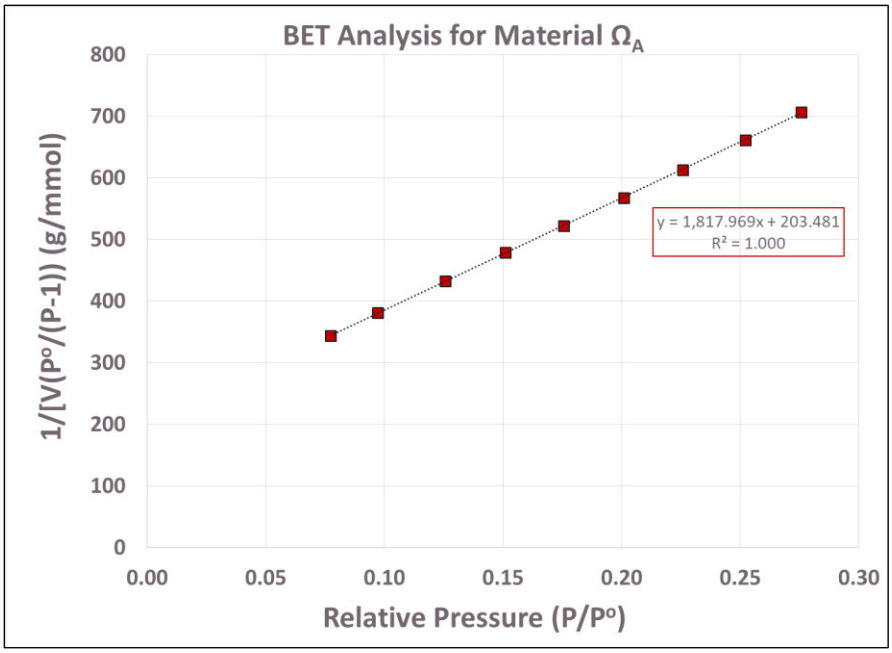

Figure 3.4: BET analysis on a krypton gas adsorption measurement for material Ω_A.

The value for the mono-layer volume, V_m, is used to find the specific surface area A_{sp}:

$$A_{sp} = \frac{V_m N_A \sigma^2}{22{,}414} \qquad Eqn\ 3.4$$

Where N_A is Avogadro's number and σ^2 is the cross-sectional area of the adsorptive molecule [Rajagopalan and Hiemenz 1997].

3.3.6: Mercury Intrusion and Extrusion Porosimetry

Mercury porosimetry testing was commissioned at Micromeritics Testing Laboratory (Norcross, Georgia USA) using an AutoPore IV 9500 version 2.03.00 Mercury Porosimeter. A 3 ml or 5 ml penetrometer volume was used, with approximately 0.15-0.50 g of sample depending on the material. Roasted whole bean coffee, roast and ground [redacted] were among the sample materials tested. The test included measurements of both intrusion and extrusion cycles up to pressures of 415 MPa.

Mercury intrusion can be used to find the envelope density, ρ_e, of particles as it is a non-wetting fluid when the contact angle between the mercury and the solid is greater than 90° [Litster 2016]. The particle porosity, ε_p, can calculated by:

$$\varepsilon_p = 1 - \frac{\rho_e}{\rho_t} \qquad Eqn\ 3.5$$

Where ρ_e is the envelope density and ρ_t is the true density of the solid [Litster 2016].

The envelope density is often reported automatically by a third party testing service as the mass of the test sample divided by the volume of mercury entering the bulb portion of the penetrometer at 3.4 kPa, or extremely low absolute pressure. The diameter of a pore filled with mercury as a function of increasing pressure can be calculated with the Laplace-Young equation:

$$\Delta P = \frac{4\gamma^{lv}\cos\theta}{d_{pore}} \qquad Eqn\ 3.6$$

Where γ^{lv} is the surface tension of mercury at 25 °C (0.4855 Nm^{-1}), θ is the contact angle of mercury and the solid (130°), and ΔP is the required increase in pressure to fill the pore [Litster 2016]. At an absolute pressure of 3.4 kPa, mercury will fill cylindrical pore diameters greater than 360 µm. It is important to note that mercury intrusion measurements are initiated under vacuum conditions, and ΔP is often referred to as P, for absolute pressure.

The envelope density values reported at this low pressure overestimate the volume of the particle, as small intergranular voids, particle surface features (not pores), and depressions of a length scale of 360 µm are not filled with mercury. It is well established in literature to identify the envelope density of coffee particles, as the sample mass divided by the volume of mercury added to the penetrometer bulb at a pressure sufficient to fill pores as small as 40 µm [Schenker et al. 2000, Mateus et al. 2007, Corrochano 2017]. Thus, a correction to the software reported envelope density values is required for each material tested.

The corrected envelope density, $\rho_{e,corrected}$ can be calculated by:

$$\rho_{e,corrected} = \frac{\rho_{e,reported}}{(1 - (\rho_{e,reported})(V_{pore,P=27.4kPa}))} \qquad Eqn\ 3.7$$

Where $\rho_{e,reported}$ (g cm^{-3}) is the reported value by the software, and $V_{pore,P=27.4\ kPa}$ is the cumulative pore volume (cm^3 g^{-1}) at an absolute pressure of 27.4 kPa.

The total particle porosity, ε_p, was calculated for each coffee material with the corrected envelope density, $\rho_{e,corrected}$, using equation 3.5, with the true density, ρ_t, assumed to be equal to the measured particle density value obtained for coffee materials Ω_W and Ω_X, which is considered to be the intrinsic true density of coffee. The total particle porosity was used to calculate the open pore porosity, ε_{open}, and closed pore porosity, ε_{closed}, of each coffee material. These two specific porosities were determined by equation 3.8 and equation 3.9, respectively.

$$\varepsilon_{open} = \varepsilon_p \left(\frac{\rho_s}{\rho_t}\right) \qquad Eqn\ 3.8$$

$$\varepsilon_{closed} = \varepsilon_p - \varepsilon_{open} \qquad Eqn\ 3.9$$

3.3.7: Scanning Electron Microscopy and Digital Microscopy

Regular roast and ground [redacted] were imaged using either a JEOL 6060 scanning electron microscope (commissioned at the Medical Imaging Center at the University of Vermont, Burlington, Vermont USA), or a Phantom XL desktop SEM (Nanoscience instruments, Pheonix, Arizona USA). In all cases, samples were sputter coated with gold powder, and adhered to mounting stems for imaging. Additional images of coffee were captured by a Keyence VHX-2000 digital microscope, equipped with a 20-200x lens (Keyence Corporation of America, Woburn, Massachusetts USA).

3.4: Coffee Extraction Chemical Testing and Analysis

3.4.1: HPLC Testing for Caffeine and 3-CQA

The HPLC system was comprised of an Agilent 1260 with a UV Diode Array Detector with two variable detection wavelengths. The column configuration was contained an Ascentis C18 column guard (4 mm x 20 mm, 100 Å, particle size 3 µm) with a 0.5 µm pre-column filter, and a Poroshell 120 EC-C18 column (4.6 mm x 50 mm, 120 Å, particle size 4 µm) (Agilent, USA). The column temperature was set to 50 °C for all measurements. A flow rate was 0.5 mL min^{-1} was used with an injection volume of 10 µL. A mobile phase comprised of methanol (Sigma Aldrich, USA) and 0.1% aqueous acetic acid, was used in a gradient elution to resolve caffeine and 3-CQA from the coffee brew samples. The method contained the following gradient conditions: 15% methanol for 0 to 5 min, 20% methanol from 5 min to 20 min, 100% methanol from 20 min to 25 min. A 10-minute column reconditioning step to 15% methanol followed every measurement. Caffeine was detected at a wavelength of 272 nm, while 3-CQA was detected at a wavelength of 325 nm.

3.4.2: LC-MS Testing for Organic Acids

The LC-MS system was comprised of an Agilent 1260 with a UV Diode Array Detector and a single quadrupole electrospray ionization mass spectrometer. The column configuration contained an Acclaim organic acid column guard (4 mm x 10 mm, 120 Å, particle size 5 µm) with a 0.5 µm pre-column filter, and a ThermoAcclaim Organic Acid column (4.0 mm x 150 mm, 120 Å, particle size 5 µm) (ThermoFisher Scientific, USA). The column temperature was set to 25 °C for all measurements. A flow rate was 0.3 mL min^{-1} was used with an injection volume of 15 µL. A mobile phase of 0.1% aqueous formic acid (Sigma Aldrich, USA) was used in an isocratic elution to resolve citric, malic, and quinic acid from the coffee brew samples. The selective ion mode was employed on the mass spectrometer with a value of 191 for citric and quinic acid, and value of 133 for malic acid.

3.4.3: Calibration Curves for Each Chemical Compound

Analytical standards of caffeine, chlorogenic acid, citric acid, malic acid and quinic acid were obtained from Sigma Aldrich, USA. A linear calibration curve was established for caffeine in the range of 10-1000 mg/L and for 3-CQA in the range of 15-750 mg/L. A logarithmic calibration curve was established for citric acid in the range of 78-1040 mg/L, for malic acid in the range of 22-300 mg/L, and for quinic acid in the range of 29-387 mg/L. All standards were measured daily, and calibration curves were created on a weekly basis.

It was observed that low concentrations of the 3-CQA standards, specifically the 15mg/L and 60 mg/L degraded within a few hours at ambient temperature. Repeated measurements over several hours showed a significant and rapid degradation for the 15 mg/L and 60 mg/L standards. These low concentration standards were prepared and subsequently kept frozen up until the point of measurement to minimize any concentration degradation. No other standards exhibited this behavior and were stored in refrigerated temperatures until point of measurement.

3.4.4: Correction of Sample Concentrations

All HPLC and LC-MS data was processed with Agilent Technologies ChemStation 7.1 software and exported to Microsoft Excel for analysis. The corrected system concentration $C_{sys,j}$, at time t_j, was calculated by:

$$C_{sys,j} = \left((C_{aliquot,j})(V_{sys,j}) + \sum_{i=1}^{j-1} (C_{aliquot,i} * V_{aliquot,i}) \right) \Big/ V_{sys,0} \quad for\ 1 \leq j \leq 20 \quad Eqn\ 3.10$$

Where $C_{aliquot,j}$ is the aliquot concentration at time t_j, $V_{sys,j}$ is the system volume at time t_j, $C_{aliquot,i}$ is the aliquot concentration at interval i, $V_{aliquot,i}$ is the volume of the aliquot removed at interval i, and $V_{sys,0}$ is the initial system volume. The system volume $V_{sys,j}$ at time t_j was calculated by:

$$V_{sys,j} = V_{sys,0} - \sum_{i=1}^{j-1} V_{aliquot,i} \qquad Eqn\ 3.11$$

Time t_j was calculated by:

$$t_j = \begin{cases} t_{exp,0} + (1.88 * j) & for\ 1 \leq j \leq 16 \\ 60\ s & for\ j = 17 \\ 180\ s & for\ j = 18 \\ 300\ s & for\ j = 19 \\ 600\ s & for\ j = 20 \end{cases} \qquad Eqn\ 3.12$$

Where $t_{exp,0}$ is the measured time from the addition of coffee to the well-mixed batch reactor to when liquid extract begins flowing out of the system, and j represents the number of the aliquot with the total number of aliquots removed from the system being 20 aliquots in total.

Equation 3.10 uses the measured aliquot concentrations ($C_{aliquot,i}$) multiplied by the volumes of the aliquots ($V_{aliquot,i}$) to find the cumulative absolute mass of the chemical compound previously removed. This cumulative absolute mass removed was added to the absolute mass of the chemical compound in the system at sample time t_j, and dividing the sum of these two masses by the initial system volume ($V_{sys,0}$). This correction accounts for all removed aliquots volumes prior to time t_j during the experimental procedure. A detailed example of the data reduction process can be found in Appendix A.

3.5: Statistical Analysis

All statistical analyses, including analysis of variance (ANOVA), model fitting, parameter estimation, and confidence intervals, were conducted with JMP® Pro 17.2 (SAS Institute, USA). The model regression and parameter estimation were done by a nonlinear least squares analysis.

Chapter 4: Development of a New Method for Measuring Short Time Extraction Kinetics

4.1: Introduction

This chapter will describe a new method for measuring early time-scale coffee extraction kinetics, specifically within 30 s of extraction, the validation of the measurement methodology and new discoveries in coffee extraction kinetics of specific chemical species as a result of this new method.

4.2: Well-Mixed Batch Reactor (WMBR) Experimental Setup and Execution

4.2.1: WMBR Components

The custom WMBR was comprised of a four-liter stainless steel beaker (SI-07205-90, Cole Parmer, USA) fitted with a custom lid milled from Delrin® stock, containing a large diameter O-ring or gasket to sustain low headspace pressures of 7-30 kPa. The custom lid incorporated a latching mechanism, to properly secure the lid to the stainless-steel beaker under low pressure. The lid also contained a sealed slide gate with a 5 cm diameter plastic tube as the hopper (McMaster Carr, USA), a type-k temperature probe with handheld digital analyzer (Fluke, USA), a pressure on/off switch, a 35 kPa safety relief valve, and a stainless-steel coffee extraction sampling tube.

The end of the sampling tube was fitted with a custom, spherical, double-layered filter screen comprised of a 100 US Std Mesh and a 400 US Std Mesh preventing the uptake of individual coffee particles greater than 40 μm into the fluid samples. A drawing of the custom WMBR can be seen in Figure 4.1.

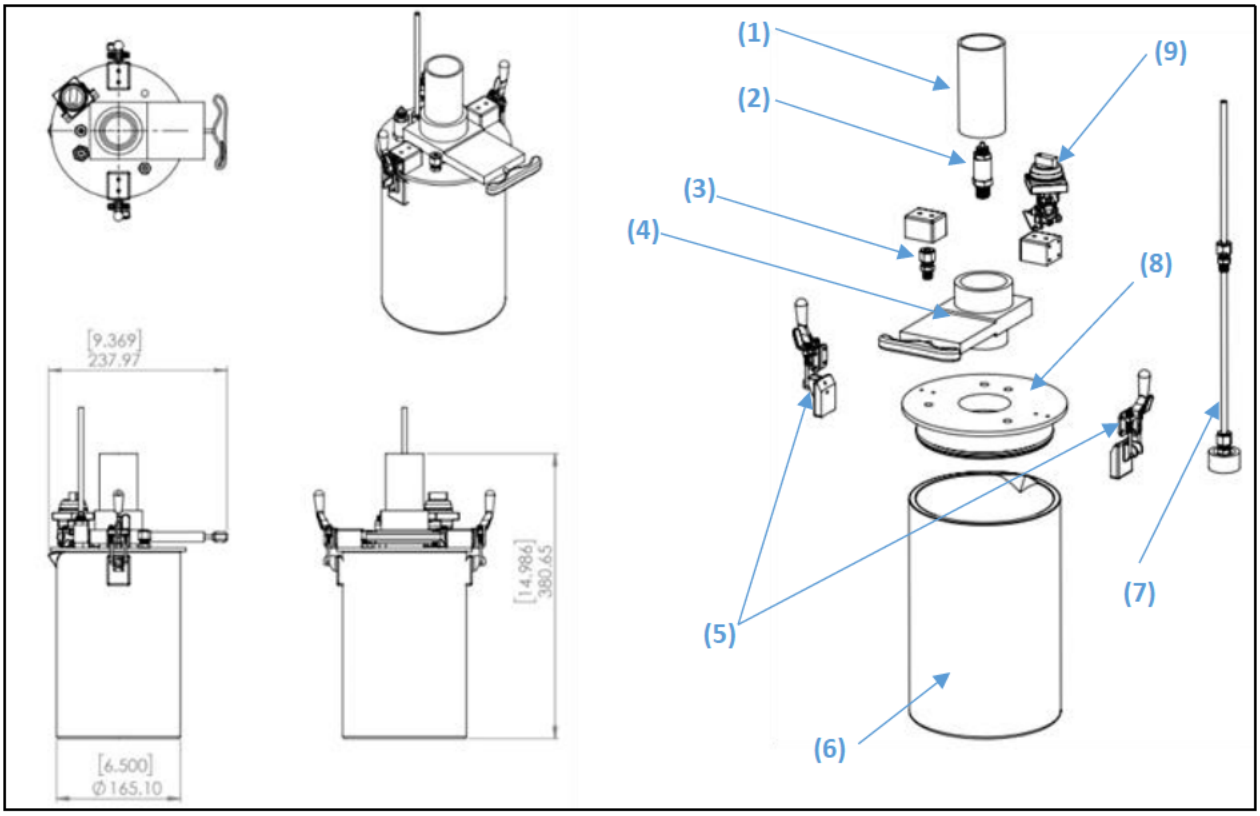

Figure 4.1: Assembly drawing of custom WMBR with exploded view. Key components are (1) 5 cm plastic tube hopper, (2) 35 kPa safety relief valve, (3) temperature probe port, (4) coffee slide gate, (5) custom latches to secure lid during extraction testing, (6) 4000 mL stainless steel beaker, (7) metal liquid sample tube with custom mesh filter on bottom, (8) custom milled Delrin lid, and (9) air supply on/off switch. Note: Dimensions within brackets are in inches, other dimensions are in millimeters.

4.2.2: WMBR System Setup

The WMBR was placed on a magnetic stirring hot plate (IKA C-Mag HS7, Cole Parmer, USA) and connected to a compressed air source with two inline air pressure regulators. The first regulator stepped down the 1 MPa compressed air source to approximately 0.3 MPa, and the second regulator stepped down the 0.3 MPa to as low as 3 kPa. The other end of the sampling tube contained a flexible plastic hose, which was positioned to deliver the brewed coffee to a Gilson SP-230 rotary sample splitter (Gilson, USA). The sample splitter contained 16 identical sized, glass test tubes for collecting aliquots of brewed coffee as a function of time.

The rotational rate of the sample splitter was set to 2 rpm, which collected 35 ± 5 mL of brewed coffee per test tube. The complete setup of the WMBR system can be seen in Figure 4.2.

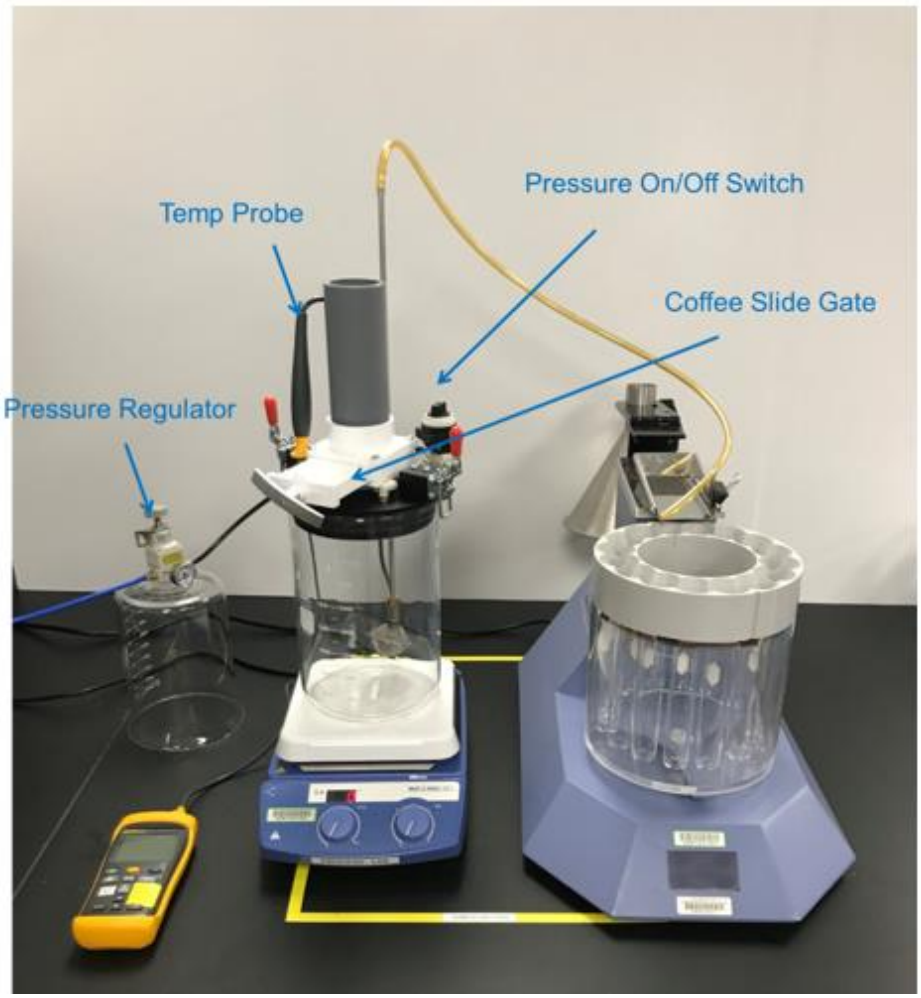

Figure 4.2: Complete custom extraction system setup. Note: The glass beaker was used only for visual purposes and never used for extraction experiments.

4.2.3: WMBR Experiment Execution

The well-mixed batch reactor was filled with 3625 +/- 50 mL of Nestle Pure Life Water (Nestle USA) that was preheated to 95 °C using electric kettles. The WMBR was placed on the hotplate, set to 100 °C, and the stir bar agitation set to a speed of five. These steps helped

maintain a near constant temperature of the water and ensured that the water was continuously stirred prior to the addition of coffee.

The unit was connected to the air supply regulated to 10 +/- 1 kPa and with the pressure on/off switch set to off. A sample mass of 100 +/- 0.5 g was loaded into the hopper attached to the slide gate. At a water temperature of 91.5 +/- 1 °C, the slide gate valve was opened, the coffee dropped into the WMBR, the gate was closed, and the pressure switch and Gilson sample splitter were turned on.

The time between opening the slide gate and collecting the very first aliquot in the Gilson was measured with a stopwatch and recorded for each experiment. The rotary sample splitter captured 16 evenly spaced samples when held at a constant rotational rate. Additional samples were collected 60 s, 180 s, 300 s, and 600 s for all experiments.

4.2.4: Effects of Stirring Speed in the WMBR

The effects of stirring speed were investigated early in the method development to determine if the agitation decreased a portion of the mass transfer resistance in the system. The particle relaxation time, τ_p was calculated using:

$$\tau_p = \frac{(\rho_t - \rho_f){d_p}^2}{18\mu_f} \quad Eqn\ 4.1$$

Where ρ_t is the true density of the particle, ρ_f is the density of the fluid, d_p is the diameter of the particle, and μ_f is the kinematic viscosity of the fluid. This was calculated for the largest particle size measured in all experiments as τ_p is directly proportional to the particle diameter squared. A very short particle relaxation time, O(0.05 s) indicated the particle, relative to the fluid, was in a stagnant medium [Litster 2016], and therefore it was assumed stirring speed had a negligible effect on the observed mass transfer rate.

Two experiments were conducted with different stirring speeds to confirm the assumption based on the calculation of the particle relaxation time. Figure 4.3 shows no

significant difference between the two stir speeds investigated. These results were consistent with the results previously reported by Spiro and Page [1984] where agitation speed was found to have no impact on the extraction kinetics of coffee particles. All future experiments had the stir speed fixed to the highest stir speed possible to promote the wetting and entrainment of the coffee particles during the start of the extraction event.

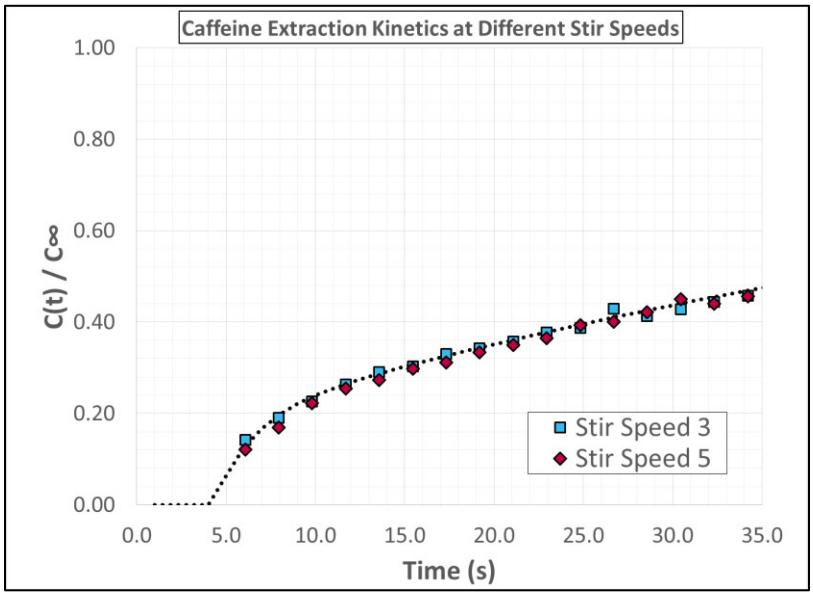

Figure 4.3: Caffeine extraction kinetics at two different stir speeds in the WMBR.

4.2.5: WMBR Design

The custom WMBR coffee extraction system described in section 4.2.1 was designed and built to facilitate the exploration of early time-scale coffee extraction kinetics. The inspiration for this custom extraction system was a result of coupling the two experimental setups described by Corrochano [2017] and Kuhn et al. [2017], with adding an air-over-water pump within the WMBR.

The deliberate addition of an air-over-water pump provided several benefits and improved the experimental setups previously presented by others. Initially, the system was designed with a peristaltic pump; however, back mixing of the coffee extract was observed within the sampling tube due to the inherent oscillatory nature of a peristaltic pump [Reis et al.

2010]. This was not observed with an air-over-water pump. Moreover, the air-over-water pump resolved issues with discrete sampling frequency by removing a continuous stream of coffee extract from the system. The volumetric flow rate of the continuous stream of coffee extract was a function of the air pressure within the sealed batch reactor.

The use of a rotary sample splitter, as presented by Kuhn et al. [2017], facilitated the fractionation of the continuous stream of coffee extract into an equal number of aliquots. The frequency of fractionation was a function of the rotational rate of the sample splitter. This piece of equipment enabled control of the sampling or fractionation frequency, unlocking high resolution, time resolved coffee extraction analysis at the time scale of interest.

Another key consideration was the total volume of the well mixed batch reactor. The removal of liquid extract during the experiment artificially increased the concentration of the system over time. A large vessel reduced the impact of aliquot removal on the system during an experiment. It was necessary to maintain very dilute bulk concentrations to minimize external mass transfer resistance during the experiment [Stapley 2002].

The controlled additional of coffee into the WMBR was an important design consideration as a critical assumption to the WMBR experiment was all particles wet simultaneously such that no residence time distribution exists. The design of the custom lid containing the slide gate and hopper, as mentioned in section 4.2.1, centered the ground coffee over the vortex inside of the beaker containing hot water. The addition of coffee directly into the liquid vortex promoted rapid particle wetting and dispersion. Moreover, the use of the slide gate ensured a well-defined start to the experiment, and the ability to quickly seal and pressurize the WMBR.

4.3: Selection of Specific Chemical Compounds to Measure Extraction Kinetics

The concentration of five chemical compounds of interest were measured in each extraction experiment. The specific compounds are listed in Table 4.1. These compounds were selected for a variety of reasons, but primarily because of well-established testing

capabilities and measurement methods readily available at Keurig Dr Pepper, and the prolific body of literature on extraction of some of these compounds from coffee, specifically caffeine and 3-CQA [Ludwig et al. 2012, Wang et al. 2016, Fuller and Rao 2017, Jeon et al. 2017, Angeloni et al. 2019]. Additionally, as discussed in section 2.3.3, organoleptic properties in coffee have been linked to these compounds [Buffo and Cardelli-Freire 2004, Farah et al. 2006]. Keurig Dr Pepper has also established proprietary relationships of favorable organoleptic properties to organic acid concentrations and desired ratios in coffee.

Table 4.1: Chemical compounds of interest during coffee extraction [PubChem CID 2519, PubChem CID 1794427, PubChem CID 311, PubChem CID 525, PubChem CID 6508].

Compound	Molecular Formula	Molecular Weight (g/mol)	Solubility in Water at 25°C (g/L)	Functional Groups
Caffeine	$C_8H_{10}N_4O_2$	194.19	21.7	(3) Methyl, (2) Carbonyl
Chlorogenic Acid (3-CQA)	$C_{16}H_{18}O_9$	354.31	40.0	(1) Carboxylic, (5) Hydroxyl
Citric Acid	$C_6H_8O_7$	192.12	1750	(3) Carboxylic, (1) Hyrdoxyl
Malic Acid	$C_4H_6O_5$	134.09	592	(2) Carboxylic, (1) Hyrdoxyl
Quinic Acid	$C_7H_{12}O_6$	192.17	400	(1) Carboxylic, (4) Hydroxyl

The chemical structures of the five compounds of interest are shown in Figure 4.4. Each compound contains functional groups of which are either polar or non-polar. The carboxyl and hydroxyl functional groups are polar, whereas methyl functional groups are non-polar. Polar functional groups are hydrophilic as these groups readily form hydrogen bonds with water, and the non-polar methyl groups are hydrophobic [McMurry 2008]. These structures and functional groups give insight into their extraction kinetics from coffee.

The three simple organic acids, citric, malic and quinic acids, contain several H-bond donor locations and are very soluble in water. Carboxyl groups dissociate more readily than hydroxyl groups due to resultant carboxylate ion being stabilized by resonance of two similar forms; however as the number of carbons in a carboxylic acid chain increase, or as the molecular weight increases, solubility in water will decrease [McMurry 2008]. Caffeine is mostly non-poplar due to the three methyl groups and its molecular structure, a flat heteroatomic bicyclic ring, promoting hydrophobic faces, which limit its solubility in water

[Tavagnacco et al. 2011]. Due to the chemical structures and molecular weights, it was expected that the three simple organic acids would extract faster than the larger molecular weight chlorogenic acid 3-CQA, followed by caffeine with the slowest kinetics.

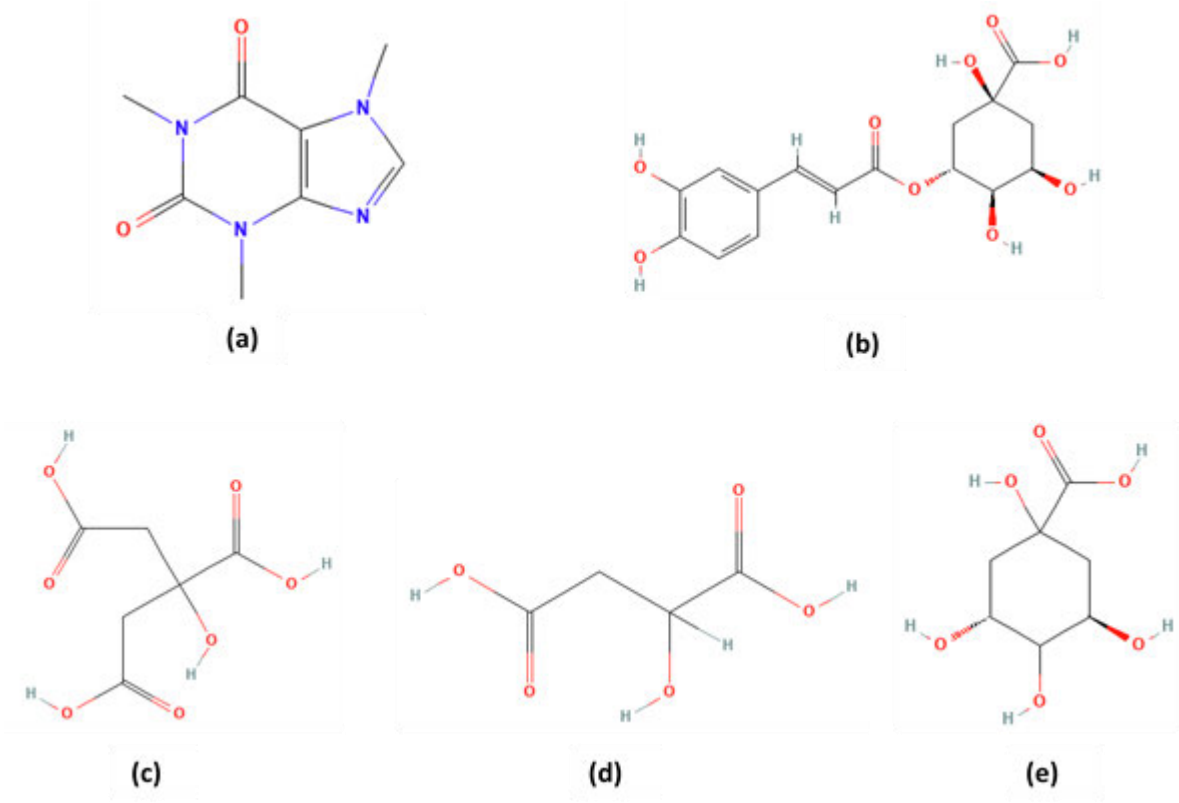

Figure 4.4: Chemical structures of (a) Caffeine [PubChem CID 2519], (b) 3-CQA [PubChem CID 1794427], (c) Citric Acid [PubChem CID 311], (d) Malic Acid [PubChem CID 525], and (e) Quinic Acid [PubChem CID 6508].

4.4: Aliquot Sample Preparation for Analysis

The caffeine and chlorogenic acid concentrations (3-CQA) of each sample were measured by HPLC, whereas organic acid concentrations of citric, malic, and quinic acid were measured by LC-MS (see section 3.4). Sample preparation for the chromatography required two separate 5 mL samples of each collected aliquot placed into 10 mL capped vials. The 5 mL samples collected for caffeine and chlorogenic acid analysis were pretreated with 5 µL of glacial acetic acid (Fisher Scientific, USA), recapped, swirled, and were permitted to rest for 30 minutes. After 30 minutes, 2 mL test aliquots from the samples were transferred using a

syringe and filter (13 mm, 0.22 µm, PP) into test vials and capped. The 5 mL samples collected for organic acid analysis did not require pretreatment and after 30 minutes 2 mL test aliquots were transferred with a syringe and filter (13 mm, 0.22 µm, PP) into test vials and capped.

4.5: Well-Mixed Batch Reactor Experimental Results

4.5.1: Absolute Concentrations at Equilibrium

Initial extraction experiments were conducted with regular, classified, roast and ground coffee prepared as described in section 3.2.4 above. The specific material used in these first experiments was a light roast (42 Agtron), burr ground coffee, classified between 1180 µm and 1000 µm; this material will be referred to as Ω_A.

The maximum absolute concentrations for each chemical compound were frequently observed at 300 s and 600 s (see Table 4.2 and Table 4.3). It was assumed that the system achieved a state equilibrium and the extraction process was complete for the compound of interest at 600 s, which is much shorter time scale than work previously reported by others [Corrochano 2017, Spiro and Selwood 1984].

This was a valid assumption as this body of work investigated the kinetics of individual chemical species and not a global concentration value such as total dissolved solids, which can be comprised of dozens of specific molecules which affect the measured TDS value [Povey et al. 2020]. Moreover, as reported by Angeloni et al. [2019] and Jeon et al. [2017], most hot brewing methods conclude well under 300 s, with only cold brew extraction methods exceeding the experimental time scale of interest [Fuller and Rao, 2017], and therefore extraction times beyond 600 s are out scope for this thesis.

Table 4.2: Absolute concentrations of caffeine and 3-CQA at times of 180 s, 300 s, and 600 s for material Ω_A.

		Caffeine (mg/L)			3-CQA (mg/L)		
Sample ID	**Replicate #**	**t=180 (s)**	**t=300 (s)**	**t=600 (s)**	**t=180 (s)**	**t=300 (s)**	**t=600 (s)**
Ω_A	1	361	388	398	167	189	206
	2	335	380	372	158	180	197
	3	343	381	382	166	199	209
Mean		**346**	**383**	**384**	**164**	**189**	**204**
Standard Deviation		**13**	**4**	**13**	**5**	**10**	**6**

Table 4.3: Absolute concentrations of citric acid, malic acid, and quinic acid at times of 180 s, 300 s, and 600 s for material Ω_A.

		Citric Acid (mg/L)			Malic Acid (mg/L)			Quinic Acid (mg/L)		
Sample ID	**Replicate #**	**t=180 (s)**	**t=300 (s)**	**t=600 (s)**	**t=180 (s)**	**t=300 (s)**	**t=600 (s)**	**t=180 (s)**	**t=300 (s)**	**t=600 (s)**
Ω_A	1	189	202	225	56	57	63	210	220	277
	2	178	188	194	54	57	55	196	207	202
	3	172	178	187	52	53	54	179	176	188
Mean		**180**	**189**	**202**	**54**	**56**	**57**	**195**	**201**	**222**
Standard Deviation		**9**	**12**	**20**	**2**	**2**	**5**	**16**	**23**	**48**

The values of absolute concentration at various times obtained from the initial WMBR experiments are within the range of values work previously reported in the work by Fuller and Rao [2017], Jeon et al. [2017] and Angeloni et al. [2019]. The comparison of extraction data requires normalization across multiple factors that would impact absolute concentration in coffee extraction. These factors include time, water temperature, coffee to water ratio, grind size, and degree of roast. Table 4.4 lists the average absolute concentrations of caffeine and 3-CQA obtained in the WMBR to the absolute concentrations obtained by others with various brew methods under similar conditions. The reported concentrations by each author, including the values from this body of work, were adjusted to an equivalent coffee to water ratio of 100 g/L.

Table 4.4: Comparison of caffeine and 3-CQA concentrations from extracted coffee by various methods. Note: Reported concentrations were normalized to an equivalent coffee to water ratio of 100 g/L.

Brew Method	**Origin**	**Roast**	**Grind Size (µm)**	**Brew Temp (ºC)**	**Brew Time (s)**	**Caffeine (mg/L)**	**3-CQA (mg/L)**	**Source**
WMBR	Colombia	Light	1180-1000	91.5	180	1255	595	This work
WMBR	Colombia	Light	1180-1000	91.5	300	1390	685	This work
V60 Pour-Over	Ethiopia	*	"Coarse"	93	170	1235	520	Angeloni et al. 2019
French Press	Hawaii (Kona)	Medium	"Coarse"	98	360	970	460	Fuller and Rao 2017
Pour-over	Brazil	*	Coarse (>1000)	100	120	1406	672	Jeon et al. 2017
Pour-over	Kenyan	*	Coarse (>1000)	100	120	1430	780	Jeon et al. 2017
Pour-over	Ethiopia	*	Coarse (>1000)	100	120	1330	852	Jeon et al. 2017

4.5.2: Normalizing Absolute Concentrations

The absolute concentrations of the extraction kinetics for each chemical compound need to be normalized as the range in values between compounds is large and necessary for comparative purposes. The maximum observed absolute concentrations for each chemical compound, at the longest time scales, were used to normalize the extraction data in each experiment. Table 4.5 and Table 4.6 show the relative percent difference between the maximum measured concentration of a given chemical compound, within a single experiment, and each of the last data points at 180, 300, and 600 s. In most cases the average percent relative difference between the last two data points, 300 and 600 s, was 5% or less.

Table 4.5: Percent relative difference of the maximum observed concentration and the 180, 300, and 600 s data points for caffeine and 3-CQA for material Ω_A.

	Caffeine			3-CQA		
Replicate #	**t=180 (s)**	**t=300 (s)**	**t=600 (s)**	**t=180 (s)**	**t=300 (s)**	**t=600 (s)**
1	9.3	2.5	0.0	18.9	8.3	0.0
2	11.8	0.0	2.1	19.8	8.6	0.0
3	10.2	0.3	0.0	20.6	4.8	0.0
Mean	**10.4**	**0.9**	**0.7**	**19.8**	**7.2**	**0.0**

Table 4.6: Percent relative difference of the maximum observed concentration and the 180, 300, and 600 s data points for citric acid, malic acid, and quinic acid for material Ω_A.

	Citric Acid			Malic Acid			Quinic Acid		
Replicate #	**t=180 (s)**	**t=300 (s)**	**t=600 (s)**	**t=180 (s)**	**t=300 (s)**	**t=600 (s)**	**t=180 (s)**	**t=300 (s)**	**t=600 (s)**
1	16.0	10.2	0.0	11.1	9.5	0.0	24.2	20.6	0.0
2	8.2	3.1	0.0	5.3	0.0	3.5	5.3	0.0	2.4
3	8.0	4.8	0.0	3.7	1.9	0.0	4.8	6.4	0.0
Mean	**10.8**	**6.0**	**0.0**	**6.7**	**3.8**	**1.2**	**11.4**	**9.0**	**0.8**

4.5.3: Aliquot Sample Time Corrections

The concentration of each individual species was plotted as a function of time up to 600 seconds. As described in section 4.2.2, the first 16 data points were sampled with the rotary sample splitter at 1.88 s intervals, and the remaining four data points were collected at the exact time of interest. This broad spectrum of sampling over time covers nearly all beverage brewing applications, with the exception of cold brew coffee beverages, which can have extraction events on the order of hours [Fuller and Rao 2017]. Only the final four extraction data points can be averaged for the three replicates as the samples were taken at exactly the desired time, whereas the first 16 extraction data points are unique to each experiment as the start time varied experiment to experiment.

The sample times for the first 16 samples were corrected based on the ratio of the volume of the first aliquot removed and the volume of aliquots at steady state condition. This ratio was multiplied by the 1.88 s time interval between samples obtained with the rotary sample splitter. Additionally, the last aliquot removed with the sample splitter was time corrected again based on the same process. These corrections account for any partial or excessive sample volume collection on the first and last aliquots removed. A detailed example of the data reduction process can be found in Appendix B. Figure 4.5 shows a comparison of time corrected data to uncorrected data; the most notable shift occurred on replicates 2 and 3.

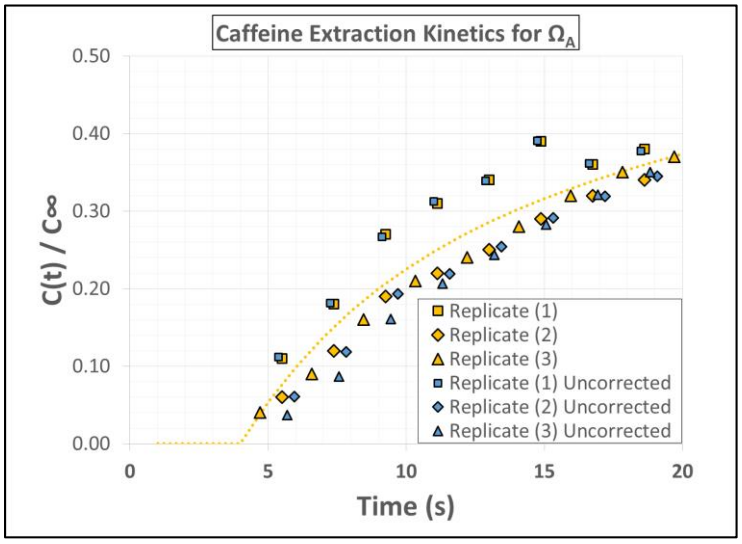

Figure 4.5: Comparison of time corrected data versus uncorrected data for caffeine extraction kinetics in material Ω_A.

4.5.4: Normalized Extraction Kinetic Curves

The normalized concentration C_t/C_∞ plotted versus time for each chemical compound in material Ω_A can be found in Figures 4.6 – 4.10. All graphs of extraction data use the same data shapes to distinguish which experiment the data originates, e.g. the square data points are from the first experiment, the diamond data points from the second replicate, and the triangle data points from the third replicate for any given material. The colored dotted lines are added to guide the eye for the extraction curves. Two graphs are needed to identify any trends in the kinetics data with the broad time scale of the extraction experiments, especially with three quarters of the data below 35 seconds. Moreover, while helpful in comparing extraction kinetics of different chemical compounds for a single material, such as citric acid to caffeine, a majority of the data is overlaid, and the results will generally be presented with only one chemical compound displayed.

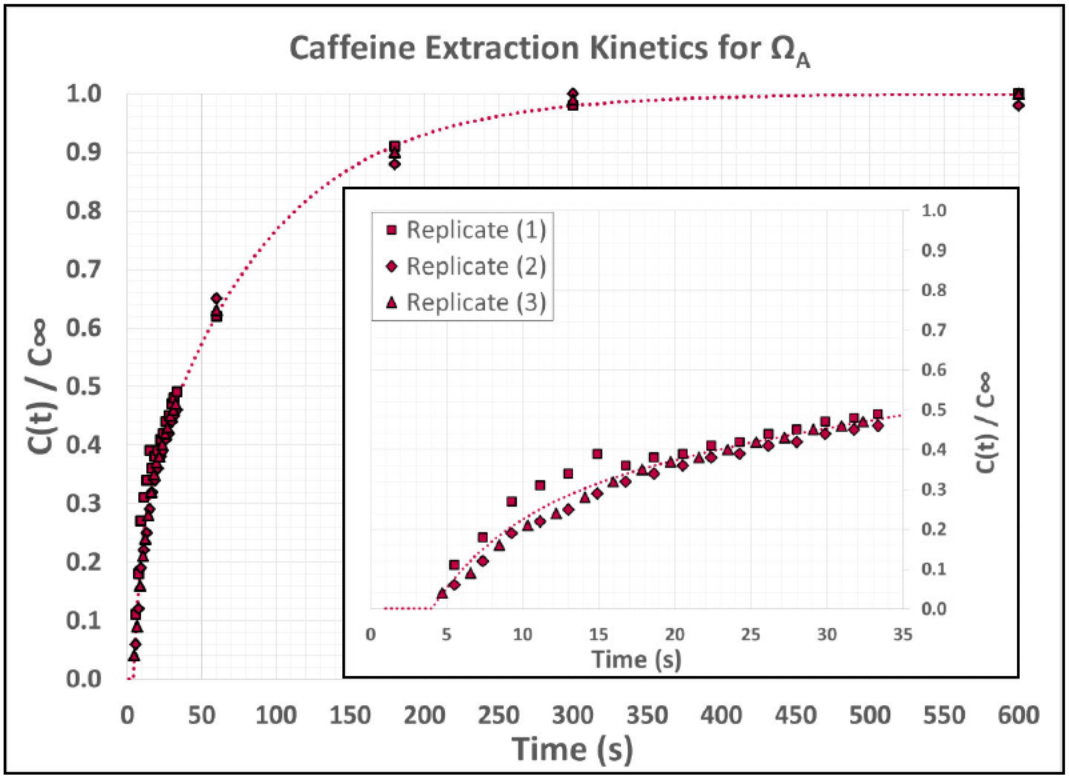

Figure 4.6: Caffeine extraction kinetics for material Ω_A.

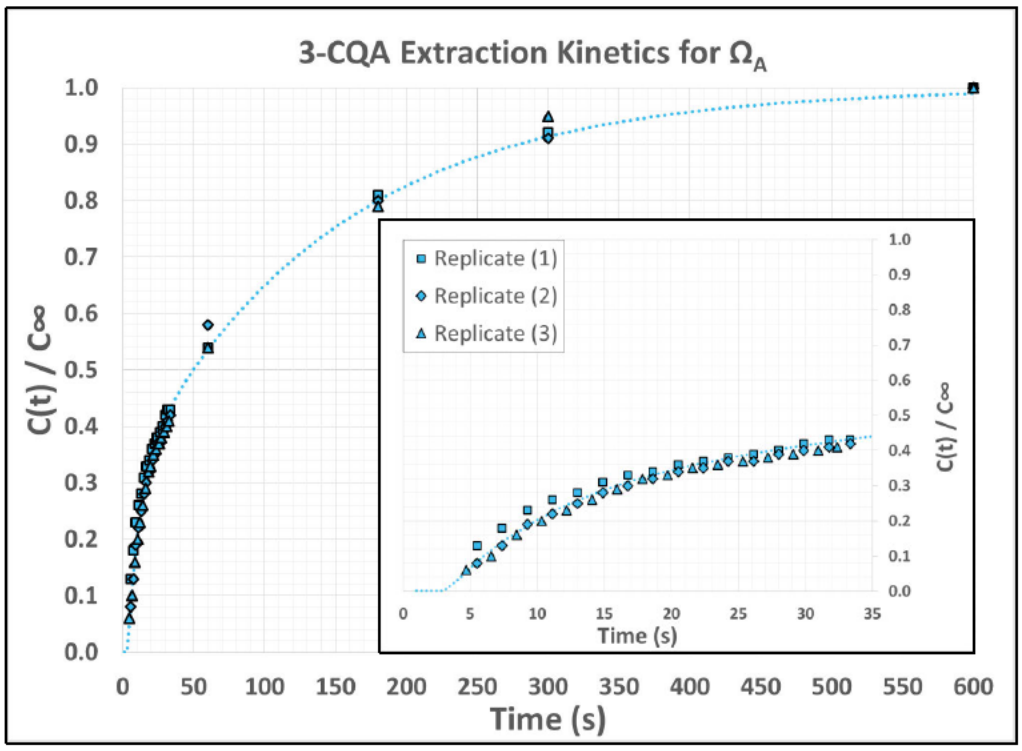

Figure 4.7: 3-CQA extraction kinetics for material Ω_A.

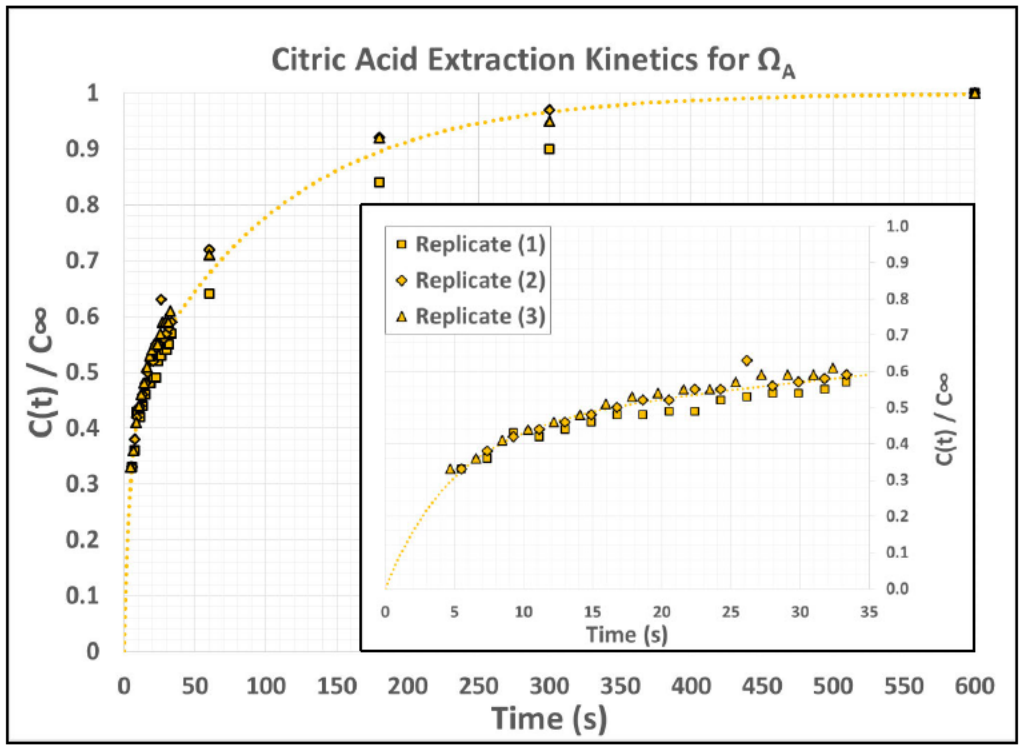

Figure 4.8: Citric acid extraction kinetics for material Ω_A.

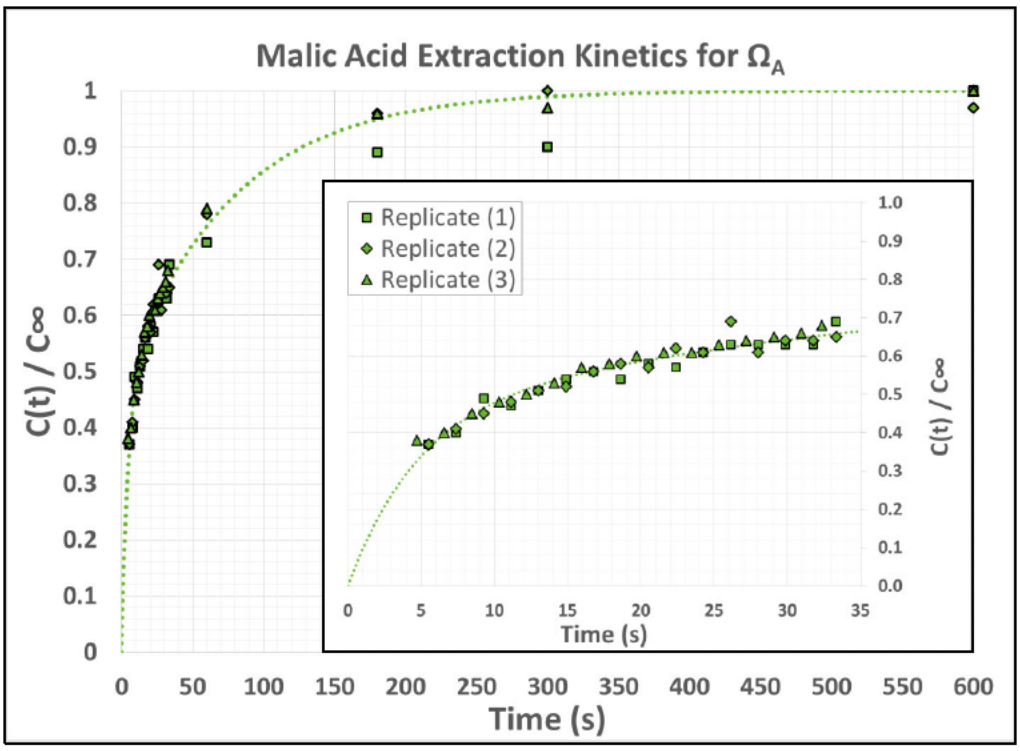

Figure 4.9: Malic acid extraction kinetics for material Ω_A.

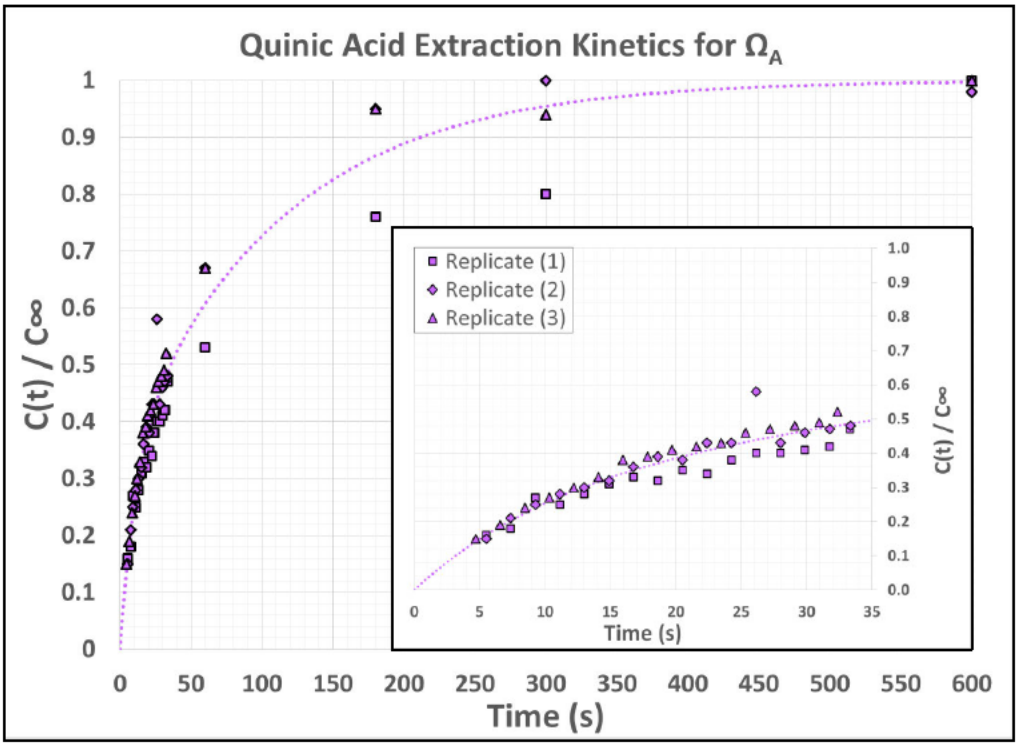

Figure 4.10: Quinic acid extraction kinetics for material Ω_A.

The data of the three extraction replicates plotted in each graph (Figures 4.6 — 4.10) are consistent for each of the five chemical compounds. As described in section 4.2.3 the first 16 data points of each experiment are collected with the rotary sampler. The data from these 16 samples of the three experiments for material Ω_A can be organized into 16 clusters of three data points each, one from each replicate experiment. A closer view of the extraction data of caffeine and malic acid at the earliest time scales can be seen in Figure 4.11. This figure provides a visual of the spread of the data over short units of time.

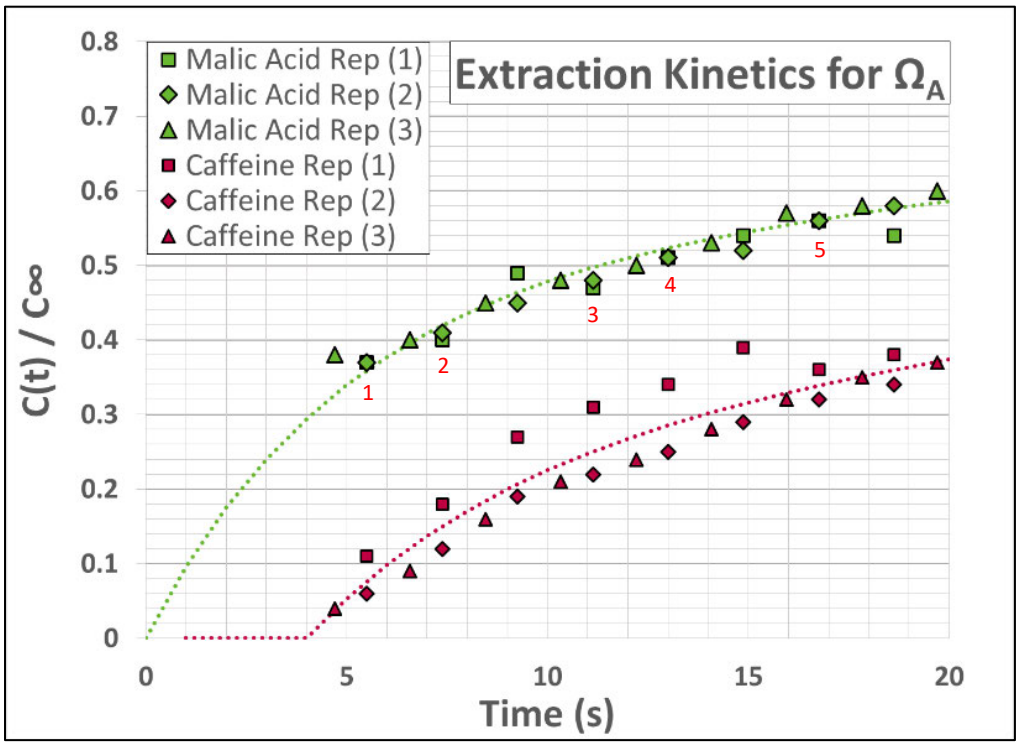

Figure 4.11: A visual evaluation of the reproducibility of replicate extraction data for malic acid and caffeine in material Ω_A at the earliest sample times.

The data set for material Ω_A is unique as the time differential between replicates 1 and 2 is on the order of a thousandths of a second, and a direct comparison between the concentrations at each time point is possible. A careful examination of the malic acid data set under 20 s reveals that there are five out of the first eight clusters where the measured concentration was either identical or within 0.01 normalized concentration of each other; these five points are numbered 1-5 in Figure 4.11 to aid the eye. This trend continues and can be

observed in 9 of the 16 clusters (see Figure 4.9). The third replicate for malic acid, which lags the first two replicates by three quarters of a second, is consistently within 0.01 normalized concentration of the other data points in each cluster, with the exception of the third and ninth cluster, where the spread in the normalized concentration is about 0.04. The caffeine data set has more variation between replicates 1 and 2 than the malic acid; however, the greatest difference in the data is within 0.10 normalized concentration occurring in cluster six at a time of about 15 s. These small spreads in measured, normalized concentration data over time is only possible with a robust system demonstrating excellent reproducibility.

In each experiment the sampling times are unique except for the last four samples as those samples were removed at a specific time. Therefore, these 16 clusters of extraction data cannot be averaged as each data point from each replicate experiment is tied to a unique time. An analysis of the experimental error and the sources of variation will be presented in chapter 6 where the data will be fit with an empirical model.

4.5.5: Observations from Extraction Kinetic Curves

There are significant differences in extraction kinetics for the different compounds, both qualitatively and quantitatively. The extraction kinetics for caffeine and 3-CQA exhibit a delay in extraction (see Figure 4.6 and Figure 4.7 respectively). By visual inspection of the caffeine data (Figure 4.6), nearly 4 s elapsed prior to observing any measurable concentration in bulk fluid. Similarly, 3-CQA has an approximate a 3 s delay. While the data suggests delays in extraction of for these two compounds, without data during the first five seconds of extraction in the WMBR, it is possible that these compounds are extracting at very low concentrations.

These observations were in stark contrast to the citric, malic, and quinic acid extraction profiles, which reasonably pass through the origin. Citric and malic acid also demonstrated a remarkable 42% and 46% extraction of the total citric and malic acid concentrations, respectively, in under 10 s.

These unexpected observations have never been previously reported in literature and were only captured due to this unique extraction system. It is postulated that the rapid extraction kinetics for citric and malic acids are a result of their respective chemical structures, being water soluble, polyprotic acids, with relatively low molecular weights. These

observations in aggregate are due to the chemical structure of these compounds and the hydrophobic or hydrophilic interactions with the coffee matrix itself. It is not solely molecular weight driven as citric acid, quinic acid and caffeine have nearly identical molecular weights but have vastly different extraction behavior.

[redacted]

4.5.6: Steady State First Order Extraction Model

A simple first order diffusion model for coffee extraction was developed by Spiro and Selwood [1984] (equation 2.2 presented in section 2.5.2). The data from the extraction experiments obtained for material Ω_A were plotted on a semi log plot for each of the five chemical compounds. Figure 4.12 shows the extraction data for 3-CQA fit with a simple linear trend line. The linear trend line is the Spiro and Selwood [1984] long term approximation model where the slope is equal to k_{obs} the observed mass transfer rate constant.

$$\ln\left(\frac{C_\infty}{C_\infty - C}\right) = k_{obs}t + a \quad Eqn\ 2.2$$

It is clear from Figure 4.12 that the simple long term approximation model does not properly fit the data especially at the earliest time scales. Moreover, it is clear from the plot that there is curvature in the data which shows there are two different extraction regimes occurring during the extraction event in the WMBR. The semi-log plots for the other four chemical compounds exhibited curvature in the data as well.

It is hypothesized that the custom extraction system has captured a rapid extraction regime where the chemical compounds are being extracted predominately from the surface of the coffee particles, and a slower extraction regime where the diffusion process is slowed or hindered by the complex internal particle structure of coffee; this added resistance to the mass transfer is commonly referred to as a hindrance factor [Spiro and Selwood 1984, Corrochano 2017, Melrose et al. 2019]. Therefore, an empirical model containing the sum of two first order exponentials, which captures both the fast and slow extraction regimes will be introduced in chapter 6.

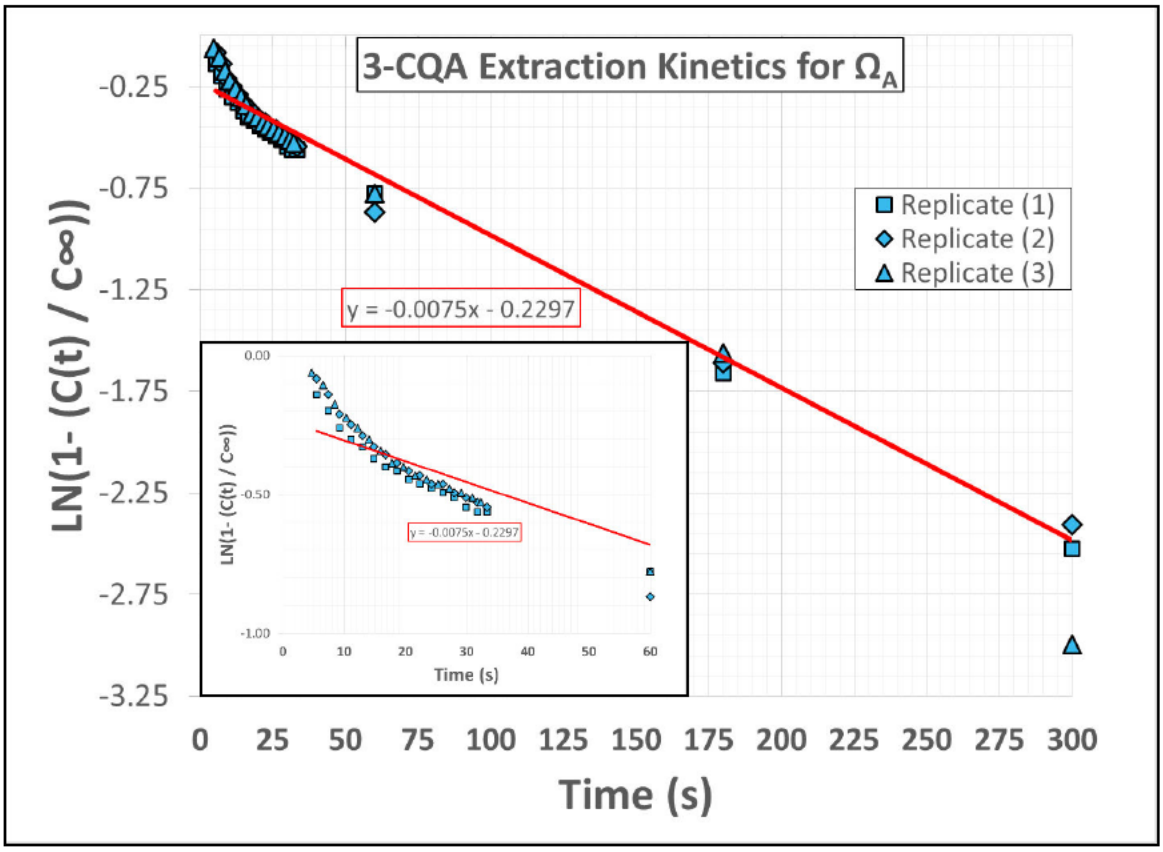

Figure 4.12: Semi-log plot of 3-QCA extraction data for material Ω_A.

4.6: Conclusions

A custom coffee extraction system was developed by creating a WMBR with an air over water pump and coupling that to a rotary sample splitter for continuous sampling of early time scale coffee extract. The ability to measure extraction kinetics on a short time scale is critical given the prevalence of single serve coffee products in North American and around the world. Despite the popularity of the single serve coffee market, very little literature has reported more than a few data points of coffee extraction under 30 s, whereas this custom system can measure over a dozen, which has not been previously done before.

The custom extraction system demonstrated it was robust and capable of measuring coffee extraction kinetics of five different chemical compounds with very repeatable results. The system captured the vastly different extraction kinetics for the five chemical compounds measured. The data from this method showed caffeine and 3-CQA had a delay in extraction, which has never been reported in literature. The system also captured the impressive speed of extraction for both citric and malic acid, where more than 40% of the total concentration of each compound extracted within the first 10 s of contact with water.

As the first of its kind to measure multiple data points at early time scales, the data collected demonstrated two distinct stages in extraction kinetics, a faster extraction followed by a slower extraction.

Chapter 5: Effect of Processing on Coffee Structure and Extraction Kinetics

5.1: Introduction

This chapter will present all coffee physical characterization results for all materials to understand how coffee extraction kinetics are affected by these properties. The extraction kinetics will be presented for regular roast and ground coffee for various particle sizes as well as for different degrees of roast. [redacted]

5.2: Physical Characterization of Roast, Ground [redacted] Coffee Materials

5.2.1: List of Coffee Materials

In total, 60 extraction events were completed for 21 different materials. In chapter 4, material Ω_A was described in detail and Table 5.1 below summarizes the key material differences, degree of roast, sieve fraction, and [redacted] treatment, for the other 20 materials evaluated.

Two materials, Ω_T and Ω_U, were the same roasted whole beans (see section 3.2.2) ground to different particle size distributions with the Mahlkonig VTA-6-SW disc burr grinder. [redacted] Additional coffee materials not tested for extraction, but for physical characterization are Ω_V, Ω_W, and Ω_X. Material Ω_V was light roast, ground coffee, sieved between 500-600 µm. Materials Ω_W and Ω_X were micro ground light roast beans and dark roast beans, respectively.

Table 5.1: List of coffee materials for extraction testing.

Sample ID	Roast Degree	Sieve class (µm)
Ω_A	Light	1000-1180
Ω_B	Light	710-1000
Ω_C	Light	600-710
Ω_D	Dark	710-1000
Ω_E	Light	1000-1180
Ω_F	Light	710-1000
Ω_G	Light	600-710
Ω_H	Light	1000-1180
Ω_I	Light	710-1000
Ω_J	Light	600-710
Ω_K	Light	1000-1180
Ω_L	Light	710-1000
Ω_M	Light	600-710
Ω_N	Dark	710-1000
Ω_O	Dark	710-1000
Ω_P	Dark	710-1000
Ω_Q	Light	Full Partice Size Dist.
Ω_R	Light	Full Partice Size Dist.
Ω_S	Light	Full Partice Size Dist.
Ω_T	Light	Full Partice Size Dist.
Ω_U	Light	Full Partice Size Dist.

5.2.2: SEM Imaging of Coffee Particles

Figure 5.1 shows SEM images that compares regular roast and ground coffee [redacted] across various magnifications. Distinct differences in particulate structure can be seen between the treated particles and the control particles. Regular roast and ground coffee particles show an ordered cellular matrix, and resemble a structure of a sponge; a very

porous open structure at the surface of the particles. Moreover, the control particles show the numerous tiny particles adhering to the surface and within the surface of cleaved coffee cells.

[redacted]

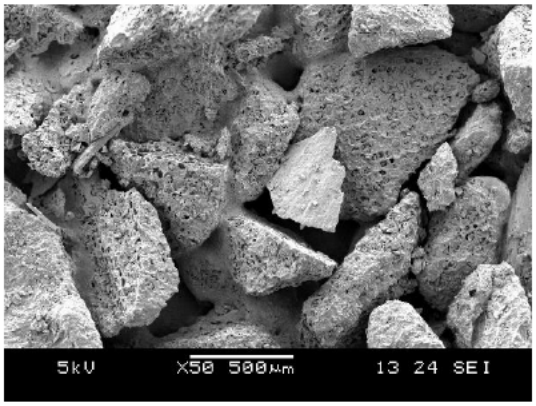

(a)

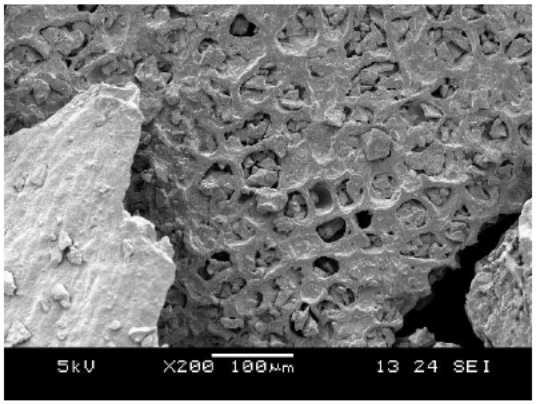

(b)

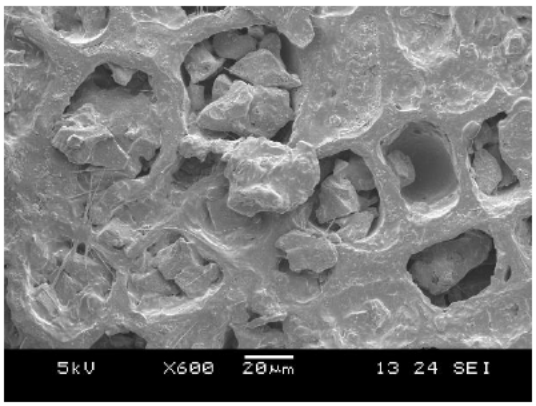

(c)

[redacted]

Figure 5.1: (a), (b), and (c) Roast and ground coffee; [redacted].

The coffee particle structure has a distribution of cleaved cell diameters and pores. Figure 5.2 shows a range of cleaved cell diameters (20-60 µm) and smaller pores (0.3-8 µm) within the individual coffee cell. The various cell diameters observed could both be of the true structure, but also due to the plane of the milled interface randomly bisecting the cells. The possible value of these diameters would be equivalent to any chord length of a circle, where it is known that all chord lengths will be smaller or equal to the diameter of that circle.

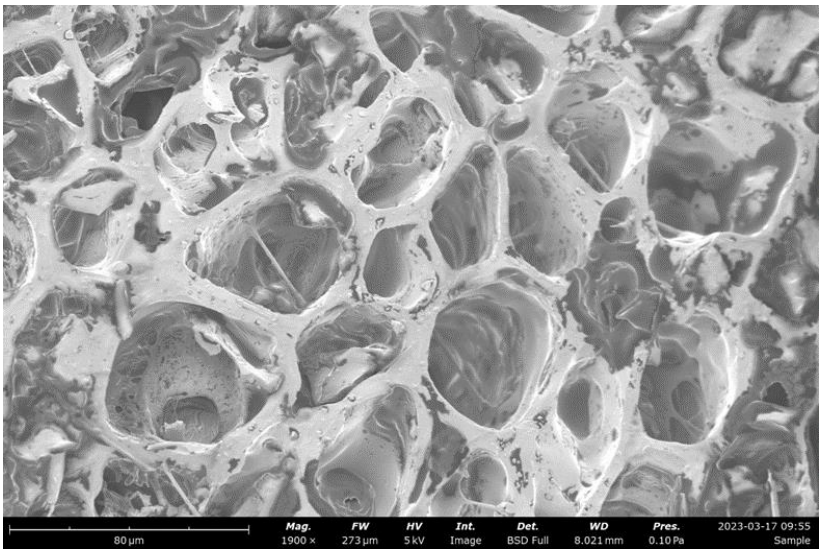

(a)

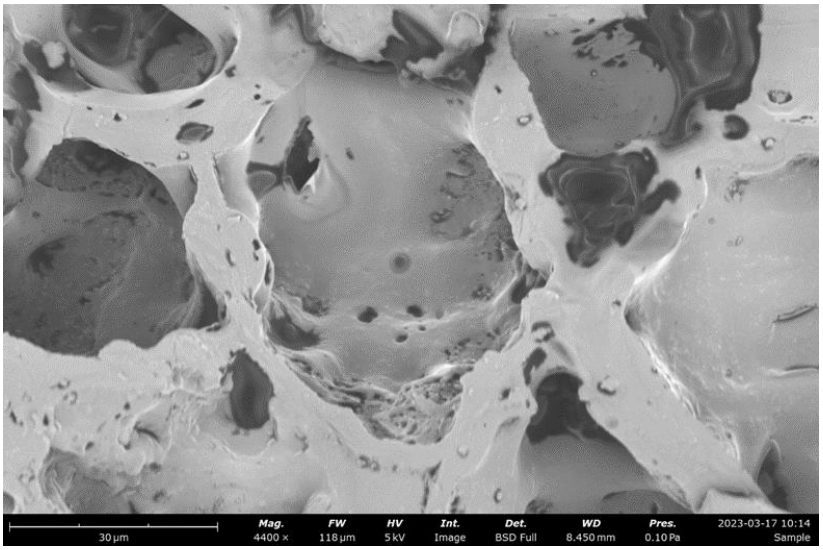

(b)

Figure 5.2: SEM image of a particle from material Ω_B. (a) Coffee cell diameters vary between 20-60 µm; (b) pores within a single cell wall vary in size of 3 µm to 300 nm.

Figure 5.3:

5.2.3: Particle Size Distributions—Impact of Measurement Technique

The particle size distributions were measured for all materials using two different dispersants and methods as described in section 3.3.2. The particle size distributions of additional roast and ground coffee reference samples were measured to elucidate coffee processing effects on particle structure and morphology. A complete list of all materials characterized and important particle size distribution statistics for both liquid and air dispersion methods can be found in Table 5.2.

Table 5.2: Comparison of particle size distribution statistics and results for all coffee materials measured with laser diffraction by liquid and air dispersion methods.

Sample ID	Dx50 [Median] (µm)		D[4,3] [Vol. Mean] (µm)		D[3,2] [Surface Mean] (µm)		Volume Fraction < 186µm	
Dispersant	Air	Liquid	Air	Liquid	Air	Liquid	Air	Liquid
Ω_A	1455	1818	1575	1849	1355	495	0.00	0.02
Ω_B	1023	1318	1117	1435	966	427	0.00	0.04
Ω_C	777	852	823	919	739	270	0.00	0.05
Ω_D	1015	1224	1113	1351	962	338	0.00	0.04
Ω_E	1187	1371	1297	1391	723	271	0.03	0.06
Ω_F	877	966	929	1086	533	252	0.04	0.11
Ω_G	719	685	745	725	460	175	0.04	0.15
Ω_H	1110	1262	1212	1420	569	275	0.04	0.09
Ω_I	884	925	942	1190	518	262	0.05	0.09
Ω_J	669	641	690	701	395	201	0.05	0.06
Ω_K	1093	1318	1197	1422	565	262	0.04	0.10
Ω_L	883	990	943	1077	498	210	0.05	0.10
Ω_M	691	676	717	670	399	188	0.06	0.11
Ω_N	874	1035	922	1205	512	279	0.05	0.06
Ω_O	863	1051	913	1192	439	232	0.06	0.09
Ω_P	801	1056	844	1195	381	236	0.07	0.11
Ω_Q	628	508	677	656	212	50	0.17	0.31
Ω_R	633	503	695	689	210	48	0.16	0.33
Ω_S	638	472	684	640	211	44	0.16	0.34
Ω_T	892	1151	979	1245	370	221	0.09	0.11
Ω_U	694	762	731	875	309	98	0.10	0.15
Ω_V	648	681	686	683	615	224	0.00	0.08
Ω_W	*	40	*	97	*	16	*	0.82
Ω_X	*	34	*	68	*	15	*	0.91

Figure 5.4 shows the particle size volume frequency distributions for materials Ω_A through Ω_D. The fines tail of the distribution is enlarged to show the overall particle size distribution for ground coffee was bimodal, which is consistent with the work reported by others [Uman et al. 2016, von Blittersdorff and Klatt 2017].

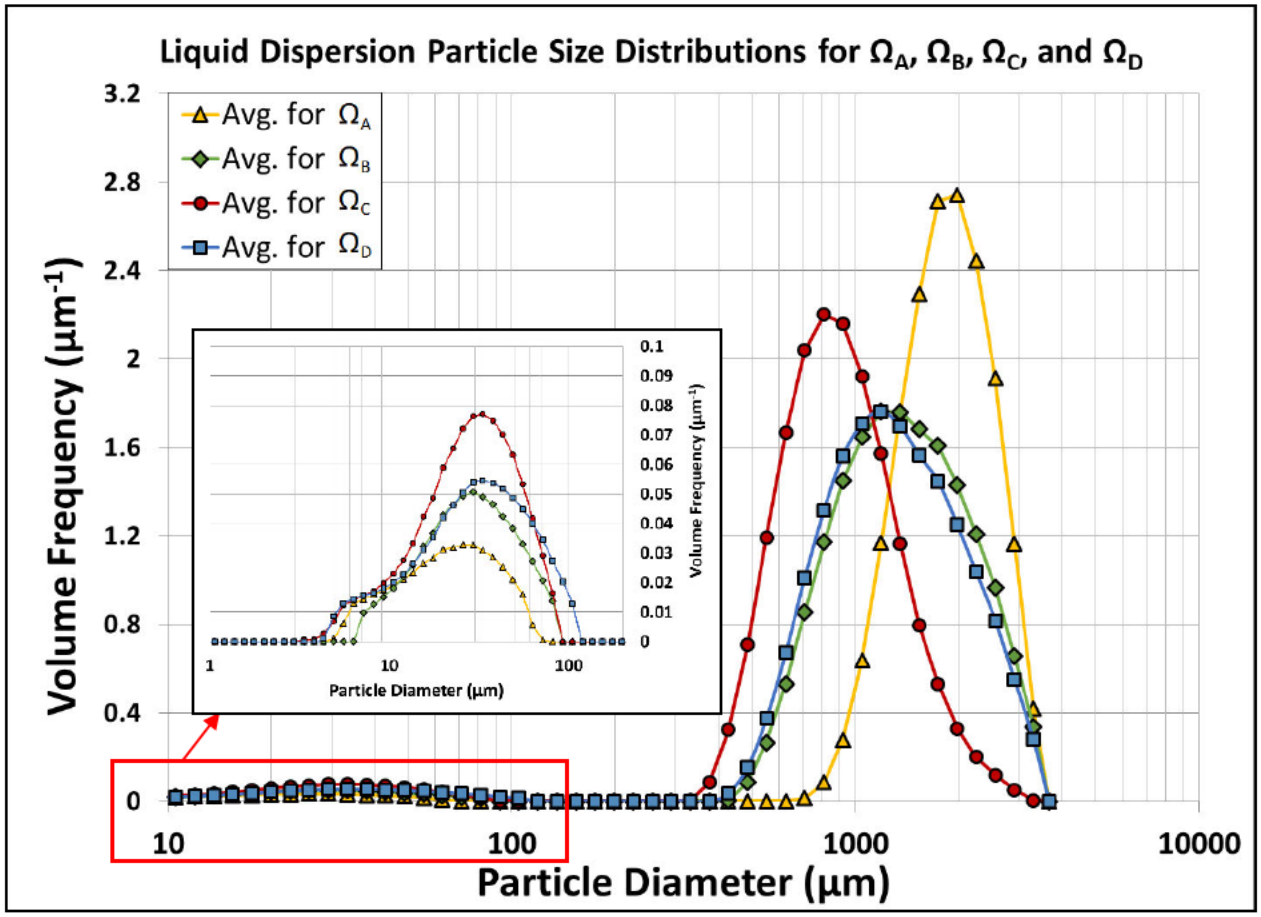

Figure 5.4: Particle size distributions for materials Ω_A through Ω_D measured with laser diffraction (liquid dispersion method).

It is noticeable that the two laser diffraction data sets do not generate similar results, as the measurement methods are different. This is consistent with the work of others [Melrose et al. 2019, Hartegan et al. 2020, Corrochano 2017]. In many cases the liquid dispersion method has higher values for the median particle diameter and the volume mean particle diameter than the air dispersion data set. This observation is counterintuitive and is inconsistent with other reported work [Melrose et al. 2019, Hartegan et al. 2020, Corrochano 2017].

It is clear in Table 5.2 the liquid dispersion method measures more of the fine particles than the dry dispersion method. This is due to the reduction of van der Waals and electrostatic forces by the liquid dispersant, thus removing the fines from the surface of larger particles [Litster 2016]. Therefore, the measurement of more fine particles should shift the overall statistics of the distribution to a smaller particle size. The data in Table 5.2 shows that the delta between the two dispersion method statistics narrows as the material particle size decreases. Figure 5.5 compares the two data sets with the greatest delta between the dispersion method particle size statistics.

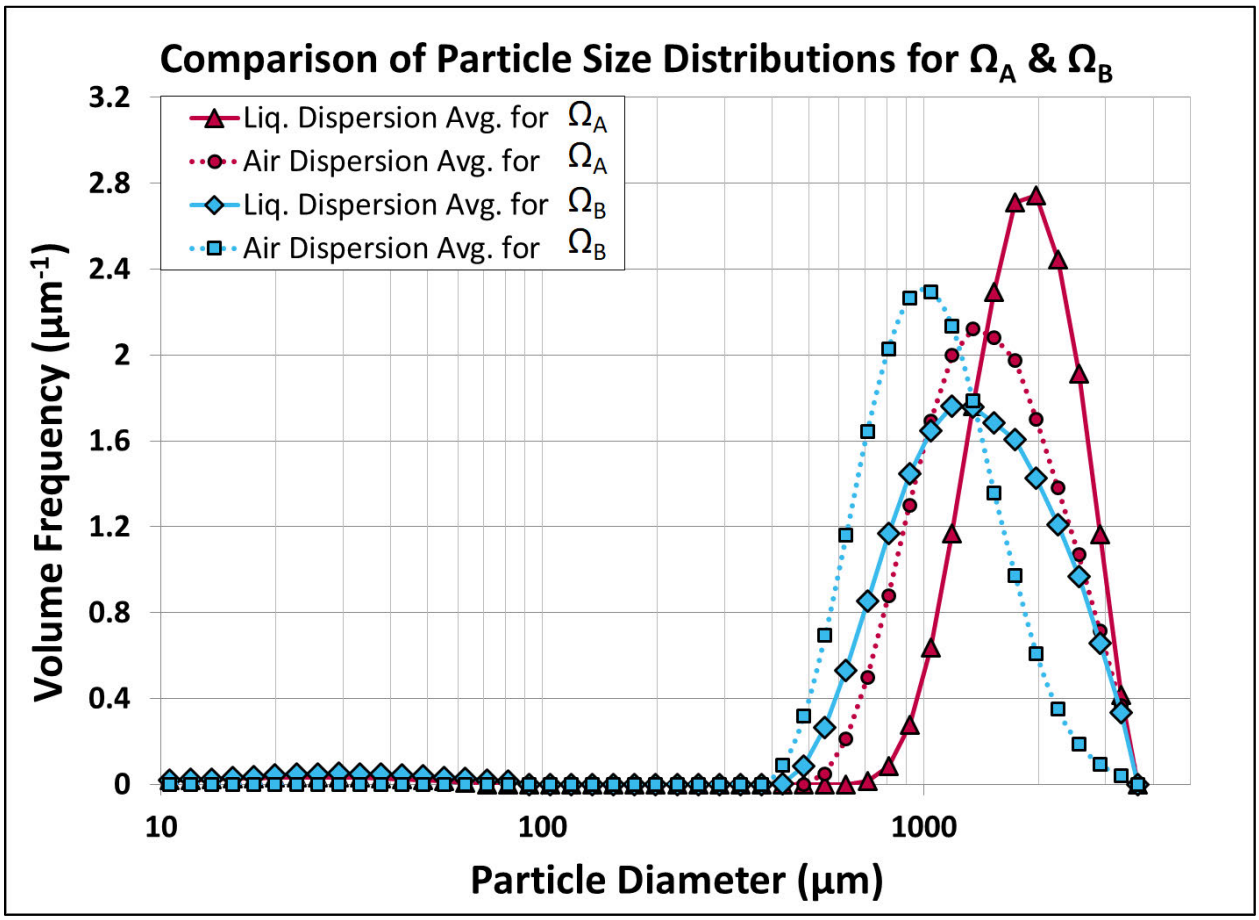

Figure 5.5: Comparison of particle size distributions from both dispersion methods for materials Ω_A and Ω_B.

A possible explanation for this observation could be the orientation of the particles in the respective dispersants when measured by the laser beam and detector in each of the

different methods. In the liquid dispersion method, where the particles are coupled with the dispersant, particles with a known shape factor, such as an ellipsoid, are consistently oriented perpendicular to the laser beam due to the velocity profile of the fluid flow in a laminar regime [Scott 2019]. In contrast, particles with a shape factor in a turbulent flow regime, such as the one created by the Aero S air dispersion unit on the Malvern, will have a random orientation when passed by the laser beam. Thus, depending on the internal calculations and averaging by the instrument, it is possible the reported particle size for the material could be smaller than that of one measured in a laminar flow regime.

Figure 5.6 shows particle images of material Ω_A taken with a Keyence VHX2000 digital microscope. Table 5.3 lists the approximate particle lengths and widths measured within the Keyence software. While not exhaustive, these few particles measured individually do show that all particles in material Ω_A have aspect ratios greater than one.

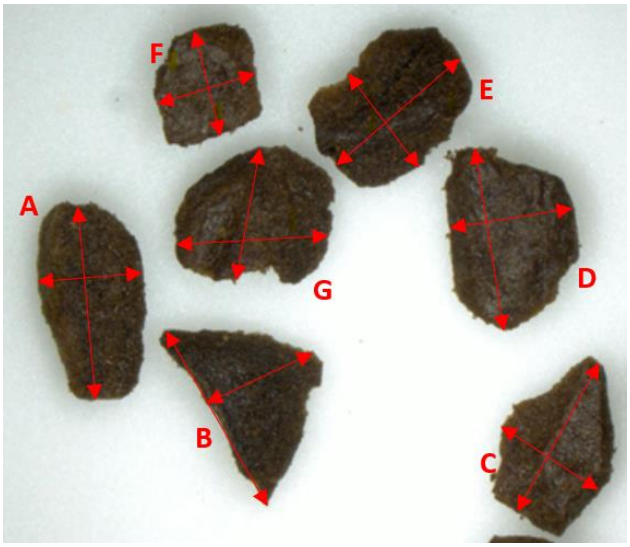

Figure 5.6: Particles from material Ω_A.

Table 5.3: Measurement of particles in Figure 5.6.

Particle	Length (µm)	Width (µm)	Estimated Aspect Ratio
A	2253	1216	1.85
B	2310	1368	1.69
C	1952	1324	1.47
D	2116	1437	1.47
E	1933	1311	1.47
F	1236	1209	1.02
G	1749	1572	1.11

It is also important to remember that the particle size results listed in Table 5.2 are almost exclusively from tightly sieved coffee fractions. In the case where the particle shape and

the orientation affects the measurement due to the flow regime, this effect would be amplified with very coarse, tightly sieved coffee versus coffee with a full particle size distribution. This conclusion is supported by the particle sphericity data reported by Corrochano [2017] where the smallest measured particle sphericity values, i.e. large shape factors, were found with the largest particle sizes.

[redacted]

[redacted]

[redacted]

[redacted]

[redacted]

[redacted]

[redacted]

5.2.4: The Creation of a Hybrid Particle Size Distribution

The issues from each of the two particle size measurement dispersion methods necessitated the creation of a hybrid particle size data set which combines data from both the liquid dispersion and air dispersion methods. This was necessary as the air dispersion method does not sufficiently measure the true fine particle volume fraction. The liquid dispersion data for the sieved, coarse particles is biased due to the aspect ratio of those particles causing longitudinal alignment in laminar flow during the measurement. [redacted]

[redacted]

The fine particle size data from the liquid dispersion method and the coarse particle size data from the air dispersion method were combined and appropriately weighted to create a hybrid distribution. It is important to note, the Malvern software uses 100 native particle size class bins to calculate particle size distributions.

The cumulative volume fraction of the hybrid particle size distribution is:

$$\theta_{hybrid,j} = \begin{cases} \sum_{i=1}^{j} v_{i,liquid} & for\ j \leq 75 \\ \theta_{fines\ (liquid)} + \sum_{i=76}^{j} v_{i,air}\left(1 - \theta_{fines\ (liquid)}\right) & for\ 76 \leq j < 100 \\ \theta_{fines\ (liquid)} + \theta_{coarse\ (air)} = 1 & for\ j = 100 \end{cases} \quad Eqn\ 5.1$$

Where $\theta_{hybrid,j}$ is the combination of the fines volume fraction from the liquid dispersion and the coarse volume fraction from the air dispersion particle size distributions.

The total fines volume fraction is:

$$\theta_{fines\ (liquid)} = \sum_{i=1}^{75} v_{i,liquid} \quad Eqn\ 5.2$$

Where $\theta_{fines\ (liquid)}$ is the total volume fraction of all particles below 186 µm, and $v_{i,liquid}$ is the measured particle size distribution volume fraction in each class bin for the liquid dispersion data set, where the 75th class bin has a mean particle diameter of 186 µm.

The total coarse volume fraction is:

$$\theta_{coarse\ (air)} = \sum_{i=76}^{100} v_{i,air}\left(1 - \theta_{fines\ (liquid)}\right) \quad Eqn\ 5.3$$

Where $\theta_{coarse\ (air)}$ is the total volume fraction of all particles above 186 µm, and $v_{i,air}$ is the measured particle size distribution volume fraction in each class bin for the air dispersion data set.

Table 5.4 lists the key particle size values for the hybrid particle size distribution for each coffee material. These values will be used in all analyses from this point forward, except where specifically noted.

Table 5.4: Key particle size values for hybrid particle size distribution for all coffee materials.

Sample ID	D[4,3] [Vol. Mean] (µm)	D[3,2] [Surface Mean] (µm)	Volume Fraction < 186µm
Ω_A	1540	460	0.02
Ω_B	1080	392	0.04
Ω_C	782	260	0.05
Ω_D	1068	321	0.04
Ω_E	1249	399	0.06
Ω_F	866	244	0.11
Ω_G	669	172	0.15
Ω_H	1155	306	0.09
Ω_I	899	286	0.09
Ω_J	687	340	0.06
Ω_K	1120	256	0.10
Ω_L	889	244	0.10
Ω_M	680	232	0.11
Ω_N	909	307	0.06
Ω_O	877	283	0.09
Ω_P	809	253	0.11
Ω_Q	558	50	0.31
Ω_R	556	48	0.33
Ω_S	537	44	0.34
Ω_T	951	211	0.11
Ω_U	685	97	0.15

5.2.5: Loose Bulk Density and Particle Density

The loose bulk density, ρ_b and the particle density, ρ_s for each material was measured as described in section 3.3.3 and 3.3.4 respectively and the results are compiled in Table 5.5. Figure 5.9 shows the loose bulk density versus particle size for [redacted] sieved materials. Figure 5.10 shows the measured particle density for [redacted] sieved coffee materials versus particle size.

Table 5.5: Loose bulk and measured particle density of each coffee material.

[redacted]

Figure 5.9:

The loose bulk density decreased as particle size decreased in coffee materials Ω_A through Ω_D, with the dark roast control, Ω_D, being slight lower in loose bulk density than its equivalent light roast control Ω_B.

Figure 5.10:

The values obtained in the helium pycnometry measurements for [redacted] sieved, roast and ground coffee were particle size dependent (Figure 5.10), which is evidence that the coffee particles have closed cell porosity, or pockets of volume inaccessible by helium or any other gas [Mateus et al. 2007]. Materials Ω_W and Ω_X measured particle density values of 1.27 g/cm^3 were well within the range of previously reported values [Singh et al. 1997, Bustos-Vanegas et al. 2018]. Ground coffee samples that are only comprised of particles less than 100 µm diameter (Ω_W and Ω_X), and are at most two coffee cells in diameter, should not have any closed cell porosity.

[redacted]

5.2.6: Surface Area

The measured specific surface area for each material was measured as described in section 3.3.5 and the results are compiled in Table 5.6. Figure 5.11 shows the measured specific surface area versus particle size for [redacted] sieved coffee materials.

Table 5.6: Specific surface area for all coffee materials measured by krypton gas adsorption. Specific surface area values are reported as average ± standard deviation.

Sample ID	Roast Degree	Sieve class (µm)	[redacted]	Specific Surface Area (cm^2/g)
Ω_A	Light	1000-1180		61 ± 1.5
Ω_B	Light	710-1000		84 ± 3.3
Ω_C	Light	600-710		98 ± 1.9
Ω_D	Dark	710-1000		85 ± 1.9

[redacted]

The measured surface area for the [redacted] sieved coffee materials (Ω_A - Ω_D, and Ω_V) followed the trend that surface area increased as particle size decreased. [redacted]

[redacted]

The specific surface area (SSA) ($m^2\ g^{-1}$) for a particulate material can be theoretically calculated based on the measured particle size distribution, the measured particle density, and assuming the particulate material is comprised of spheres. The theoretical specific surface area was calculated by:

$$SSA = \frac{6}{\rho_s\ D[3,2]_{dry}} \qquad Eqn\ 5.4$$

Where ρ_s is the measured particle density of that material, and the D[3,2] is the measured Sauter mean diameter from the Malvern dry dispersion method [Rhodes (Ed.) 2008, Litster 2016]. Table 5.7 is the comparison of the theoretically calculated values to the measured values for [redacted] sieved coffee.

Table 5.7: Comparison of measured and calculated specific surface areas for [redacted] sieved coffee materials.

Sample ID	SSA (cm^2/g) (Measured)	SSA (cm^2/g) (Calculated)	% Difference
Ω_A	61	57	6.37
Ω_B	82	77	6.45
Ω_C	98	98	0.44
Ω_D	85	84	1.1
Ω_V	116	113	2.73

The specific surface area values obtained from using equation 5.4 are remarkably similar to the measured values from the Tristar II Plus for sieved [redacted] coffee materials. The values derived from the equation slightly under predict the measured values. This slight difference is reasonable given the particles are not spheres, which have the minimum specific surface area of any comparable sized shape, and coffee particles have a textured surface whereas the theoretical calculation assumes a smooth surface.

[redacted]

Table 5.8: [redacted]

[redacted]

[redacted]

Nonetheless, this comparison gives a high degree of confidence in the measurement data obtained for all coffee samples, as no published literature was found on measurements of specific surface area of roast and ground coffee particles for comparative purposes.

5.2.7: Mercury Intrusion Porosimetry

Mercury intrusion and extrusion testing was performed on a select number of the materials presented in this chapter. Replicate testing was not done in triplicate due to the costs of third party lab services, and reported values are from a single characterization event. Materials Ω_A - Ω_C, Ω_H - Ω_J, and Ω_K - Ω_M were tested in addition to roasted whole beans from both the light roast and the dark roast batches; the whole bean samples were used as a reference. Figure 5.12 shows the cumulative and frequency pore size distributions for both light and dark roast whole beans.

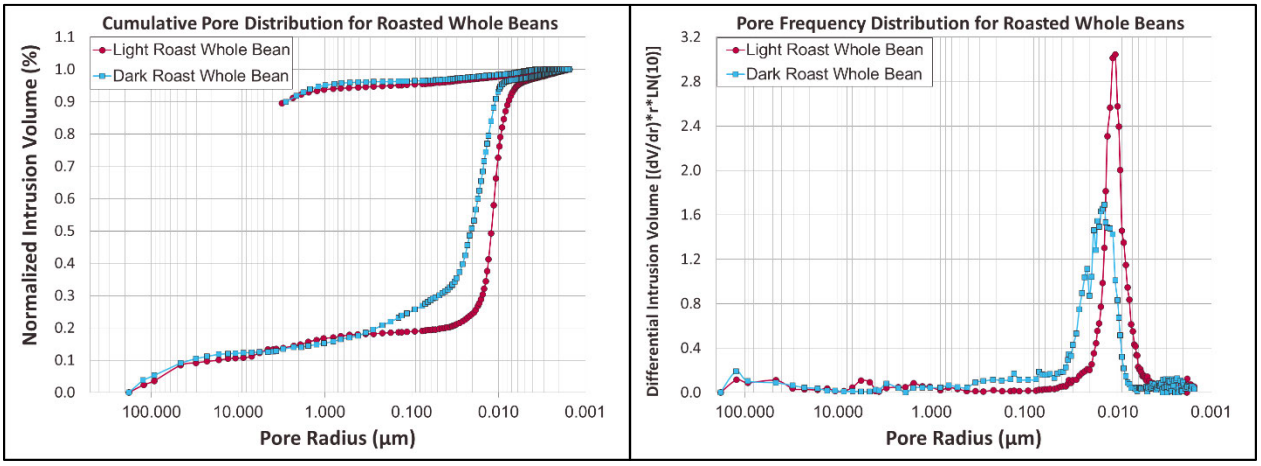

(a) **(b)**

Figure 5.12: (a) Cumulative and (b) frequency pore size distributions for light roast and dark roast whole bean coffee.

The data shows the most significant portion of pore sizes are between 35 and 20 nm in diameter, for dark and light roast respectively. The slight shift to the left in both distribution curves for the dark roast whole bean data set was expected as bean expansion during roasting occurs at higher temperatures [Geiger et al. 2004, Bustos-Vanegas et al. 2018]. The values for the pore size distribution are also consistent with the findings and structural analysis by Schenker et al. [2000] who investigated roasting speed impact on the coffee microstructure, with fast roast coffees having average pore diameters of 27 nm and slow roasted coffees having average pore diameters of 22 nm.

The mercury intrusion measurements of the whole bean samples provide a robust baseline of coffees internal structure to compare with regular roast and ground coffee [redacted]. It is important to recall that coffee is a plant-based material with an ordered cellular structure where large pockets of empty volume exist within each cell, which are remnants of the vacuole and that cells are primarily connected *via* plasmodesmata. [Robards and Lucas 1990].

Adjacent coffee cells connected *via* plasmodesmata present as an hourglass like structure. This structure must be taken into consideration when analyzing pore size distribution data. Without context, the pore size distribution data suggests that coffee is a highly mesoporous material. Particles with pore structures like an hourglass, or where a constricted neck opens to large voids, will assign all intrusion volume to the neck diameter [Allen 1997b]. The only indication of any underlying structure from these plots is the large hysteresis between the intrusion and extrusion curves, as other purely mesoporous materials, like alumina silicate, do not demonstrate such large hysteretic behavior [Matthews 2010]. A network of interconnected, complex pore shapes, such as an hourglass like network, would describe the hysteresis observed [Allen 1997b, Litster 2016] in Figure 5.12a.

Figure 5.13 shows the cumulative pore size distributions for light roast coffee materials Ω_A - Ω_C. The figure is broken down into three distinct regions to describe the portion of the structure of the coffee filled during the intrusion process.

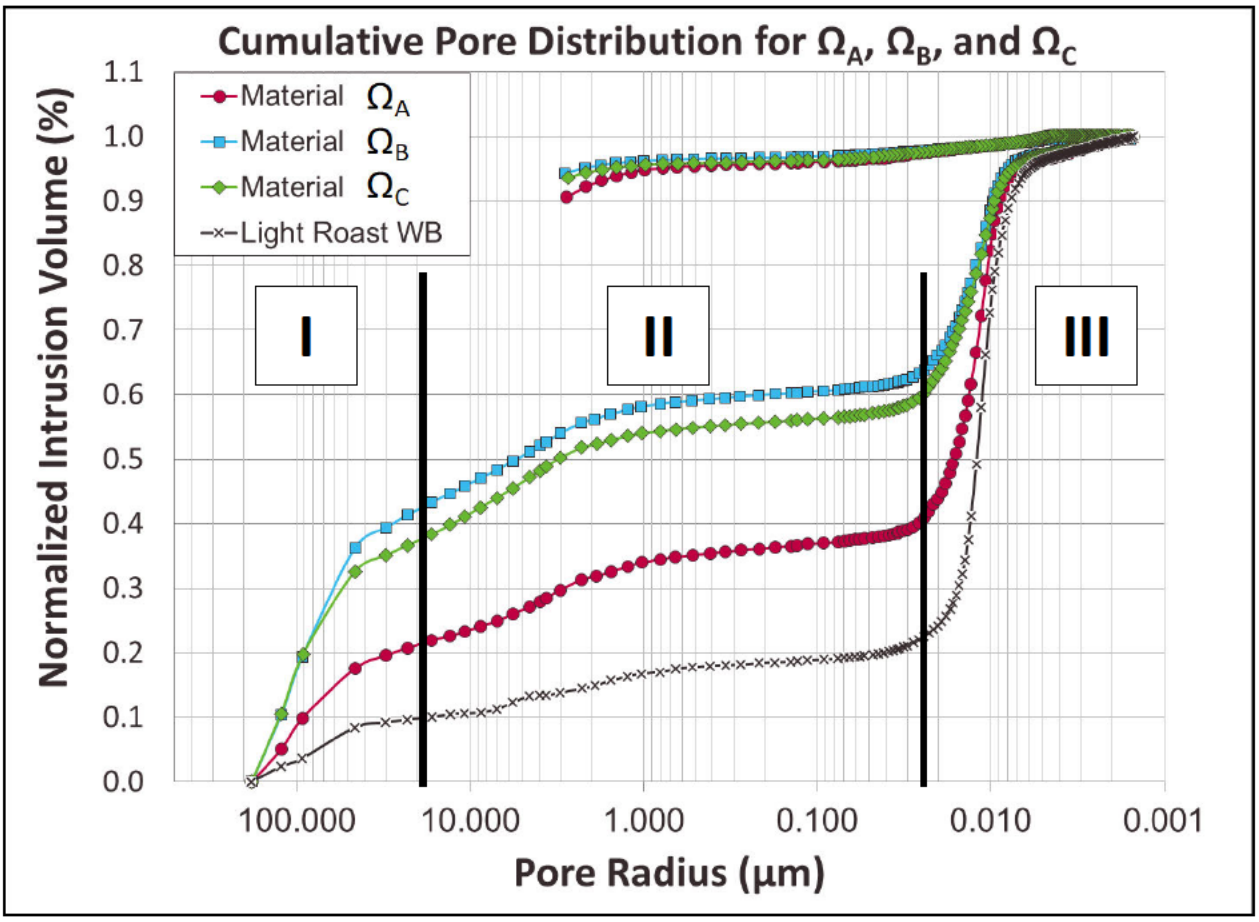

Figure 5.13: Cumulative pore size distributions for light roast coffee materials Ω_A - Ω_C and light roast whole bean.

In the first region, I, the void fraction of the coffee is being filled; this region stops up to the point of a single coffee cell, which was assumed to be 45 µm in diameter for consistency purposes. However, the size of individual coffee cells has been reported to vary between 10-70 µm within a single bean [Pittia et al. 2011]. In the second region, II, pores smaller than a single cell within the coffee particle are being filled. This small increase in volume within the region II could also be the onset of material compression due to the increasing pressure during the measurement [Johnston et al. 1990]. In the third region, at approximately 50 nm, is where the plasmodesmata within the first cellular layer are being filled with mercury [Schenker et al. 2000, Wang and Lim 2014]. This large spike in mercury intrusion volume is due to the empty

space of the adjacent, connected cells being filled, and this process repeats until the core of the particle is reached.

In region I in Figure 5.13, as particle size decreases, a greater volume of mercury is needed to fill to void fraction of the material in the penetrometer bulb. This difference in initial intrusion volume, for each material, needs to be subtracted from the measured cumulative intrusion and extrusion values to compare the pore size distributions across the materials.

Figure 5.14 shows the corrected cumulative pore size distributions for light roast coffee materials Ω_A - Ω_C and light roast whole bean.

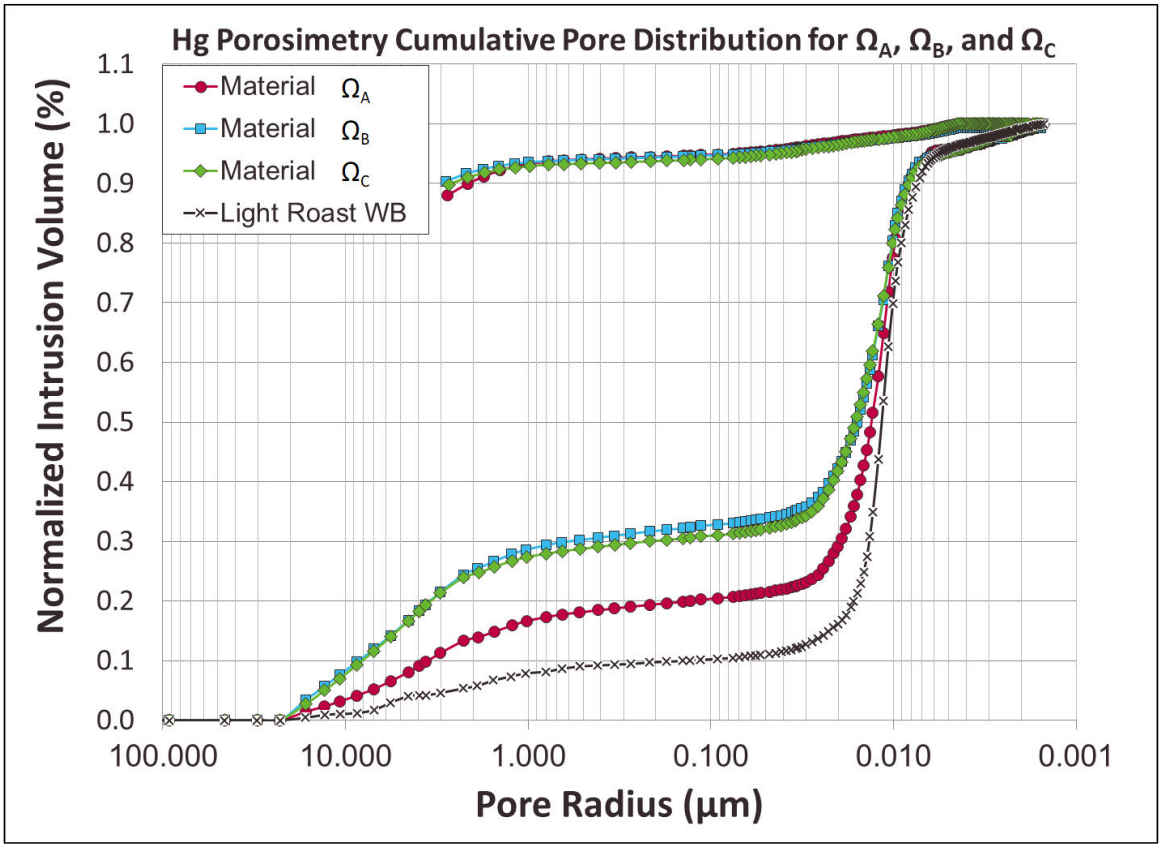

Figure 5.14: Corrected cumulative pore size distributions for materials Ω_A - Ω_C with intrusion volume filling the void fraction removed.

The general trend is still the same compared to the uncorrected graph in Figure 5.13; however, the differences in the hysteresis are less pronounced. Figure 5.15 shows the pore frequency distribution for the corrected mercury intrusion data set for materials Ω_A - Ω_C.

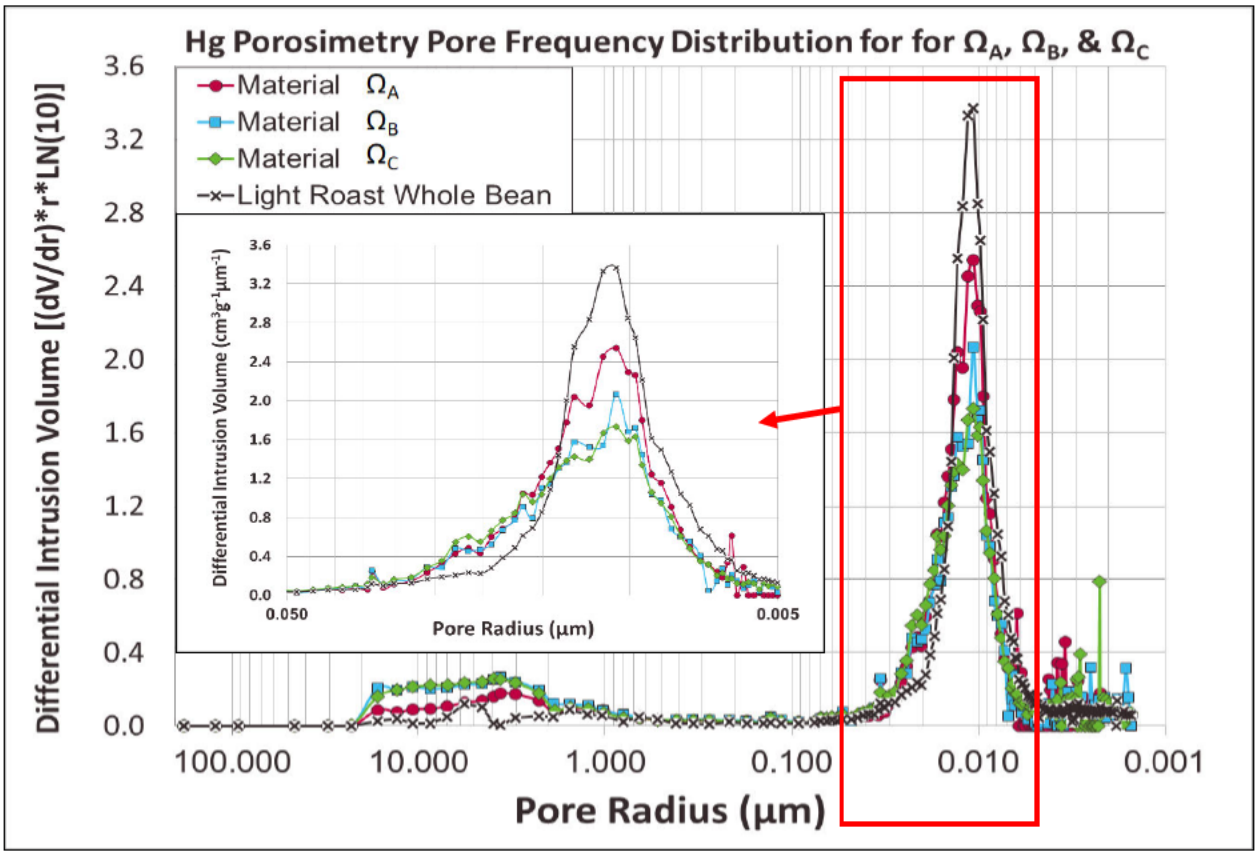

Figure 5.15: Pore size frequency distribution for materials Ω_A - Ω_C.

As the particle size decreases the primary peak centered at 25 nm decreases (see Figure 5.15 above), and the small secondary peak occurring in between 1-15 µm is increasing minimally. The data below 10 nm in diameter is quite noisy across all pore size plots as this portion of the data approaches the detection limits of the method and will be subsequently ignored in the analysis going forward. The linear increase in intrusion volume versus pore size at the end of the measurement (see Figure 5.14), occurring between 300 to 415 MPa, is indicative of material compression [Johnston et al. 1990].

[redacted]

[redacted]

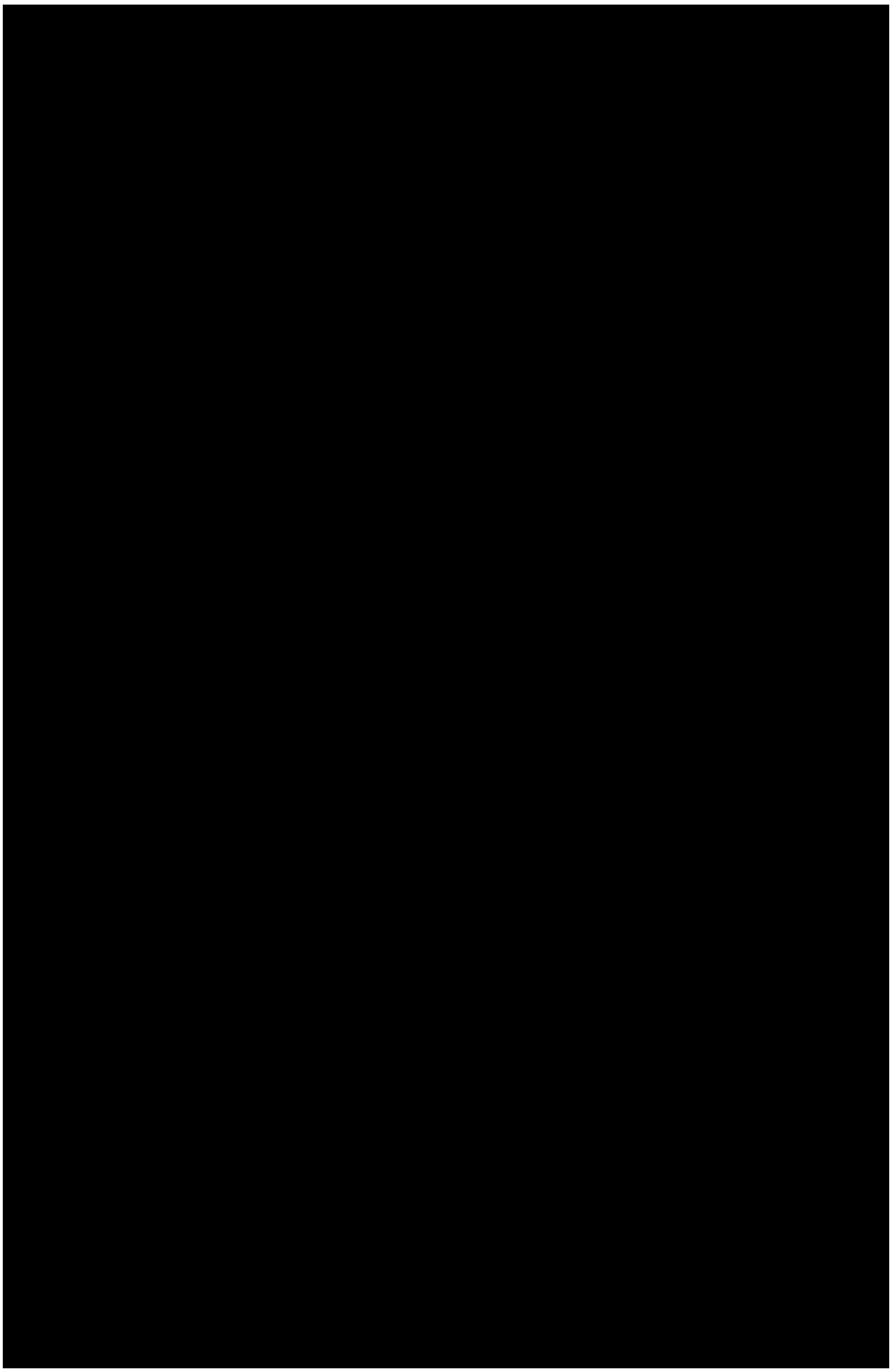

Figure 5.16: [redacted]

[redacted]

Figure 5.17: [redacted]

The corrected envelope density, $\rho_{e,corrected}$, the total particle porosity, ε_p, and both the open and closed porosity for each material were calculated as described in section 3.3.6 and the results are compiled in Table 5.9.

Table 5.9: Particle porosity values calculated from mercury intrusion data.

Sample ID	Roast	[redacted]	Sieve class (µm)	Corrected Envelope Density (g/cm^3)	Particle Density (ρ_s) (g/cm^3)	Total Particle Porosity (ε_p)	Closed Particle Porosity (ε_{closed})	Open Particle Porosity (ε_{open})
Ω_A	Light		1000-1180	0.702	0.78	0.447	0.176	0.271
Ω_B	Light		710-1000	0.709	0.81	0.442	0.162	0.279
Ω_C	Light		600-710	0.634	0.83	0.501	0.176	0.325
[redacted]								
Whole Bean	Light		*	0.708	*	0.443	*	*
Whole Bean	Dark		*	0.549	*	0.568	*	*

[redacted]

5.2.8: Summary of the Coffee Particle Morphology

The results for the physical characterization of all coffee materials demonstrated that coffee processing strongly affects the particle structure. There were strong relationships of particle density and surface area with particle size in the [redacted] sieved, roast and ground coffee materials. As particle size decreased both specific surface area and measured particle density increased.

[redacted]

[redacted] light and dark roast coffee materials had distinct structural differences. The roasted whole bean mesopore diameters for the dark roast coffee were about 40% larger than the light roast coffee at 32 nm versus 23 nm, respectively. The measured particle density and the loose bulk density for the [redacted] dark roast coffee were 9% and 21% lower respectively, than the light roast material, despite both materials having nearly identical particles sizes. [redacted] These differences are consistent with previously reported data, which has directly linked the dissimilarities of coffee structure to the thermal treatment of the coffee beans in the roasting process [Schenker et al. 2000, Geiger et al. 2004, Bustos-Vanegas et al. 2018]. [redacted]

[redacted]

5.3: Extraction Kinetics [redacted] and Influence of Particle Size

The extraction kinetics of the five chemical compounds for each sieve fraction of the light roast, [redacted] coffee materials (Ω_A - Ω_C) were compared. Figures 5.18 to 5.22 are the normalized extraction kinetic curves for materials Ω_A - Ω_C for each of the chemical compounds measured.

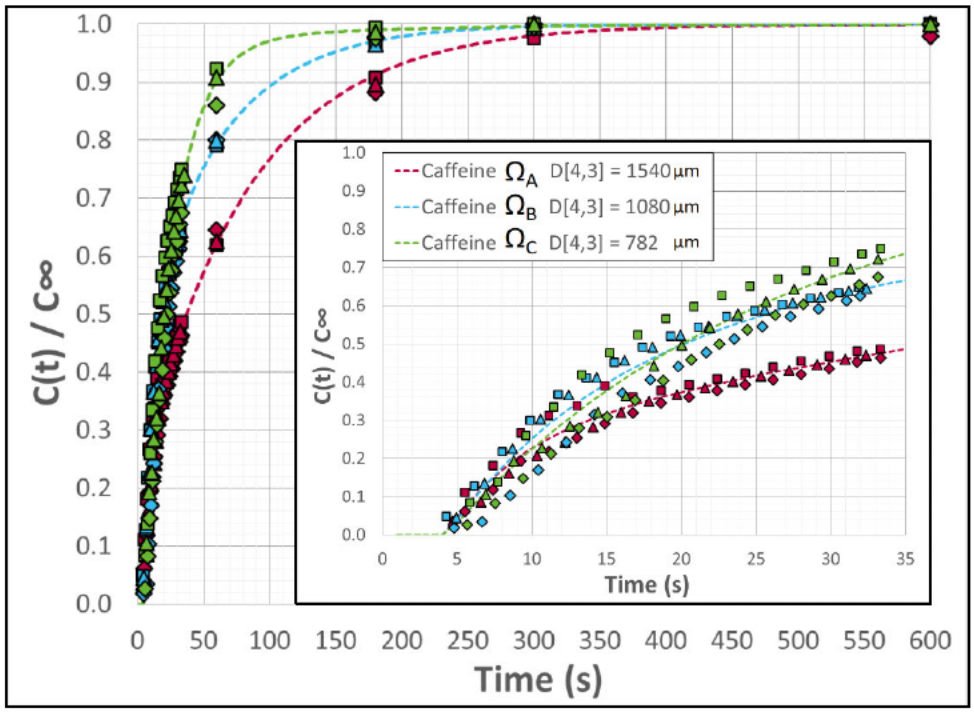

Figure 5.18: Caffeine extraction kinetics for light roast materials Ω_A, Ω_B, and Ω_C.

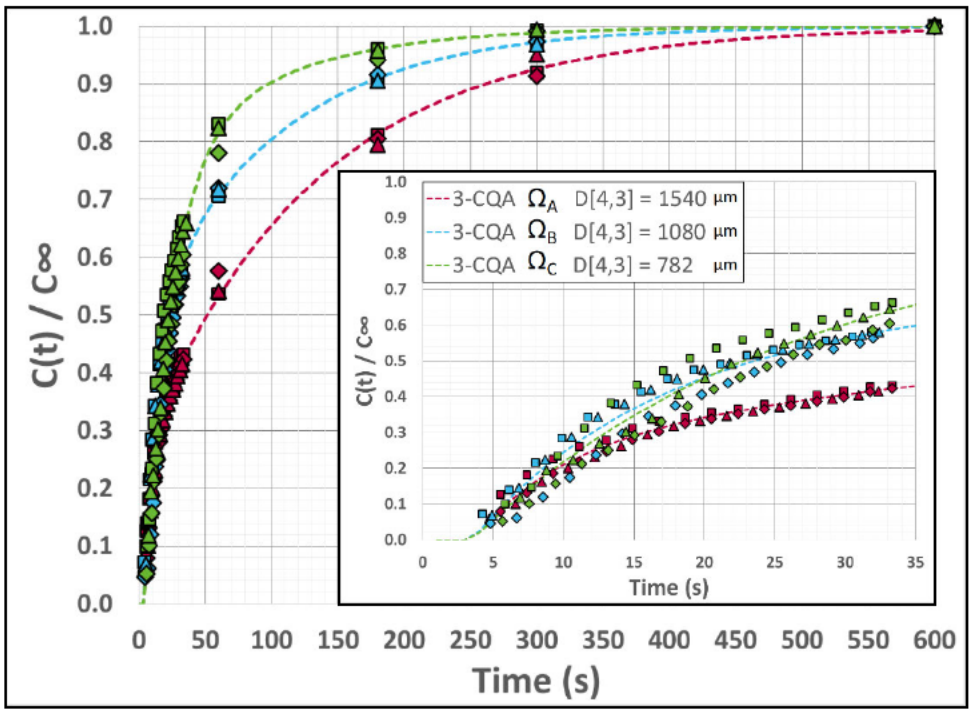

Figure 5.19: 3-CQA extraction kinetics for light roast materials Ω_A, Ω_B, and Ω_C.

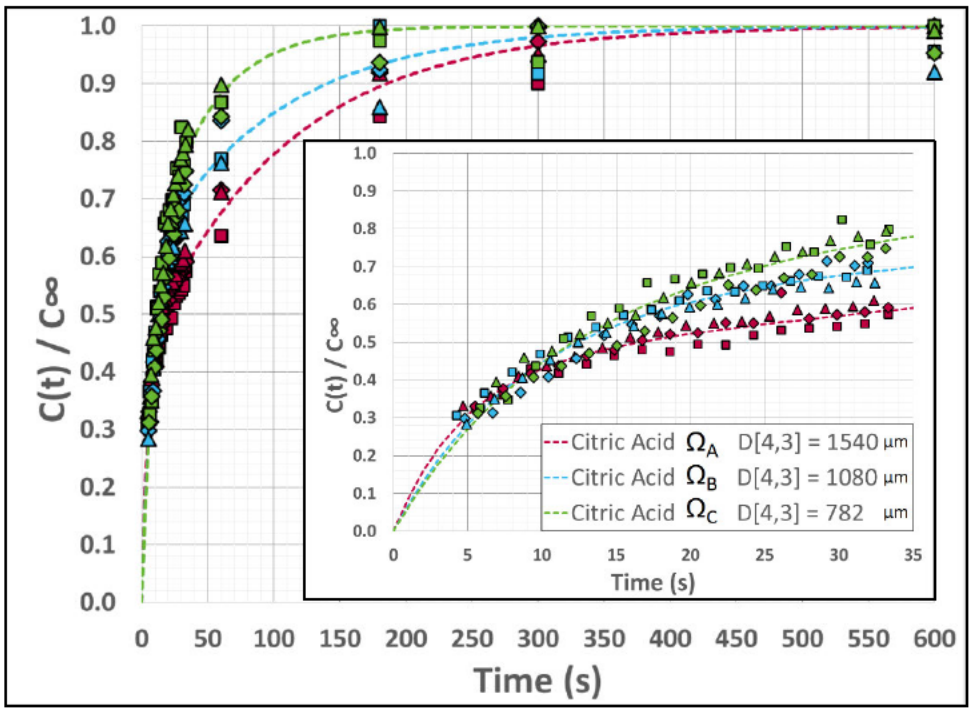

Figure 5.20: Citric acid extraction kinetics for light roast materials Ω_A, Ω_B, and Ω_C.

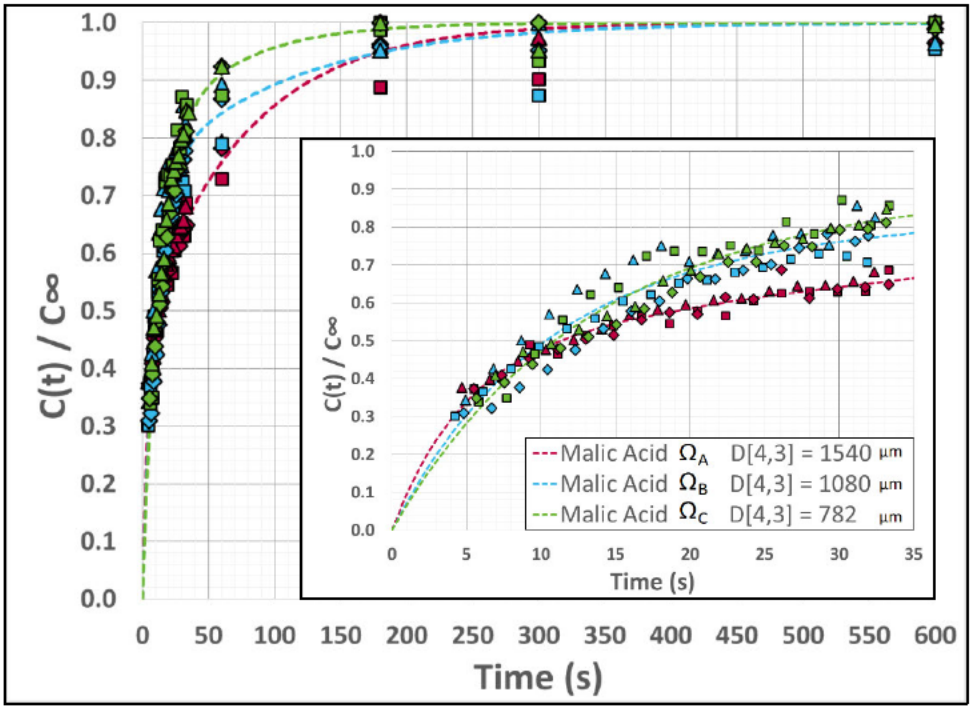

Figure 5.21: Malic acid extraction kinetics for light roast materials Ω_A, Ω_B, and Ω_C.

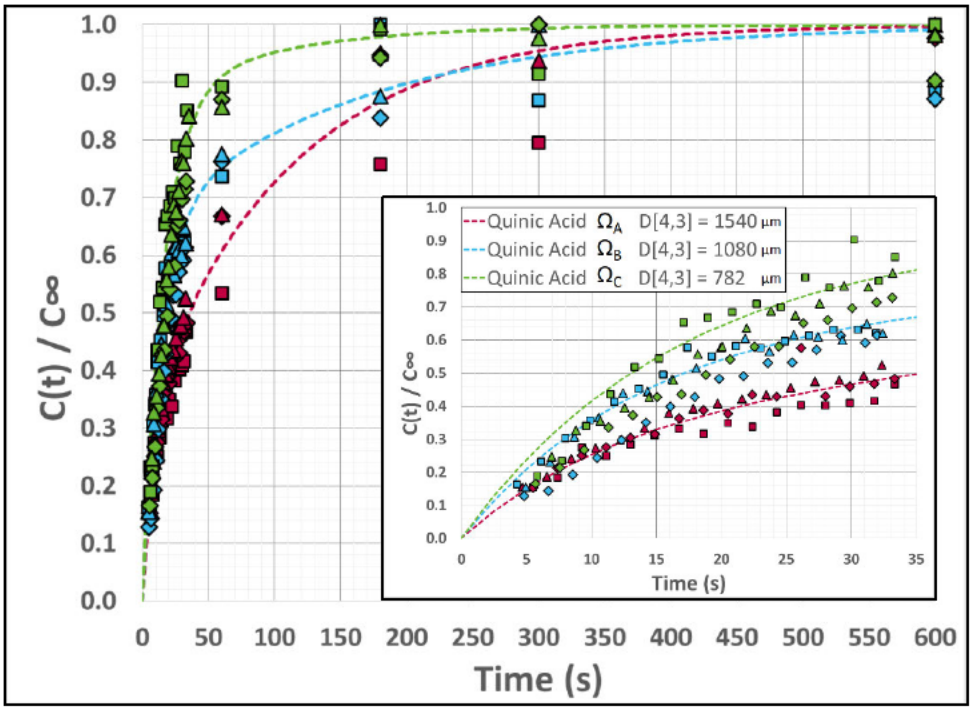

Figure 5.22: Quinic acid extraction kinetics for light roast materials Ω_A, Ω_B, and Ω_C.

The data shows that smaller particles have faster extraction kinetics than larger particles at long times, i.e. ≥ 25 s. This result is expected due to the increase in surface area for the smaller particles and the reduced mass transfer resistance for the extraction of the compounds from within the particle due to shorter diffusion distances. At the earliest time scales, ≤ 15 s, the data demonstrates that the influence of particle size is minimal, as the data points from each of the three materials are overlapping on one another. This observation was consistent for all five chemical compounds. This portion of the extraction kinetic curves has captured the so-called "washing phase" [Zanoni et al. 1992, Spiro 1993] of the surfaces of each coffee particle and the rapid extraction of all fines adhered to the surface of these large particles. This is the first data set to capture this rapid extraction regime or "washing phase" of extraction. Additionally, the delay in extraction for both caffeine and 3-CQA was consistently observed in all three materials.

A consistent order of relative extraction speed was observed for all three sieve fractions, where malic acid had the fastest kinetics, followed by citric acid, quinic acid, caffeine, and 3-CQA. The observed, relative extraction speed order generally aligns well with molecular structure, and solubility of each of the compounds (section 4.3). The molecular weight was not a good predictor of extraction order, as both citric acid and caffeine have nearly identical molecular weights but the extraction kinetics are very different; caffeine extracted much slower than citric acid. Table 5.10 provides a comparison normalized concentrations at approximate times for the three [redacted] coffee materials Ω_A - Ω_C.

Table 5.10: Normalized chemical compound extraction concentrations for coffee materials Ω_A - Ω_C. Time of 60 s and 180 s are the average values across all three replicates. The 10-30 s data is comparative data where the max time differential between the three coffee materials are within 0.5 s of one another and within 1 s of the listed time.

	Caffeine			3-CQA			Citric Acid			Malic Acid			Quinic Acid		
Time (s)	Ω_A	Ω_B	Ω_C	Ω_A	Ω_B	Ω_C	Ω_A	Ω_B	Ω_C	Ω_A	Ω_B	Ω_C	Ω_A	Ω_B	Ω_C
10	0.21	0.30	0.23	0.20	0.29	0.22	0.44	0.45	0.48	0.48	0.57	0.49	0.27	0.37	0.36
15	0.28	0.41	0.32	0.26	0.38	0.30	0.48	0.52	0.55	0.53	0.68	0.57	0.33	0.45	0.43
20	0.37	0.52	0.50	0.33	0.48	0.45	0.54	0.59	0.66	0.60	0.71	0.69	0.41	0.58	0.58
25	0.42	0.59	0.61	0.37	0.53	0.55	0.57	0.64	0.73	0.63	0.74	0.76	0.46	0.57	0.67
30	0.45	0.62	0.67	0.39	0.56	0.60	0.59	0.65	0.77	0.65	0.77	0.80	0.48	0.61	0.76
60	0.63	0.80	0.90	0.55	0.71	0.81	0.69	0.79	0.87	0.77	0.85	0.91	0.62	0.76	0.92
180	0.90	0.97	0.99	0.80	0.91	0.95	0.89	0.93	0.97	0.94	0.97	1.00	0.89	0.90	0.98

The spread in the extraction kinetic values between the three coffee materials, Ω_A - Ω_C, varies between the five chemical compounds, and at different points in the extraction curve. The spread in normalized concentration for citric and malic acid is smaller than the spread for quinic acid, 3-CQA, and caffeine. The data shows a maximum range of 0.15 for malic acid and 0.18 for citric acid at 30 s. In contrast, the maximum range was 0.27 for caffeine, 0.26 for 3-CQA, and 0.30 for quinic acid, all occurring at 60 s. Comparison of model parameters in chapter 6 will explore these observed differences further.

5.4: [redacted]

5.4.1: [redacted]

[redacted]

Figure 5.23: [redacted]

Figure 5.24: [redacted]

Figure 5.25: [redacted]

Figure 5.26: [redacted]

Figure 5.27: [redacted]

[redacted]

[redacted]

[redacted]

[redacted]

[redacted]

[redacted]

Figure 5.28: [redacted]

Figure 5.29: [redacted]

[redacted]

Figure 5.30: [redacted]

Figure 5.31:

Figure 5.32:

5.4.2: [redacted]

[redacted]

[redacted]

[redacted]

[redacted]

[redacted]

[redacted]

Figure 5.33: [redacted]

Figure 5.34: [redacted]

Figure 5.35:

5.4.3: Effects of Degree of Roast on Extraction Kinetics

The effect of degree of roast on extraction kinetics was explored, but only for a single sieve fraction . Figure 5.36 shows the extraction kinetics for caffeine, 3-CQA, citric acid, and malic acid for light and dark roast controls, Ω_B and Ω_D, respectively.

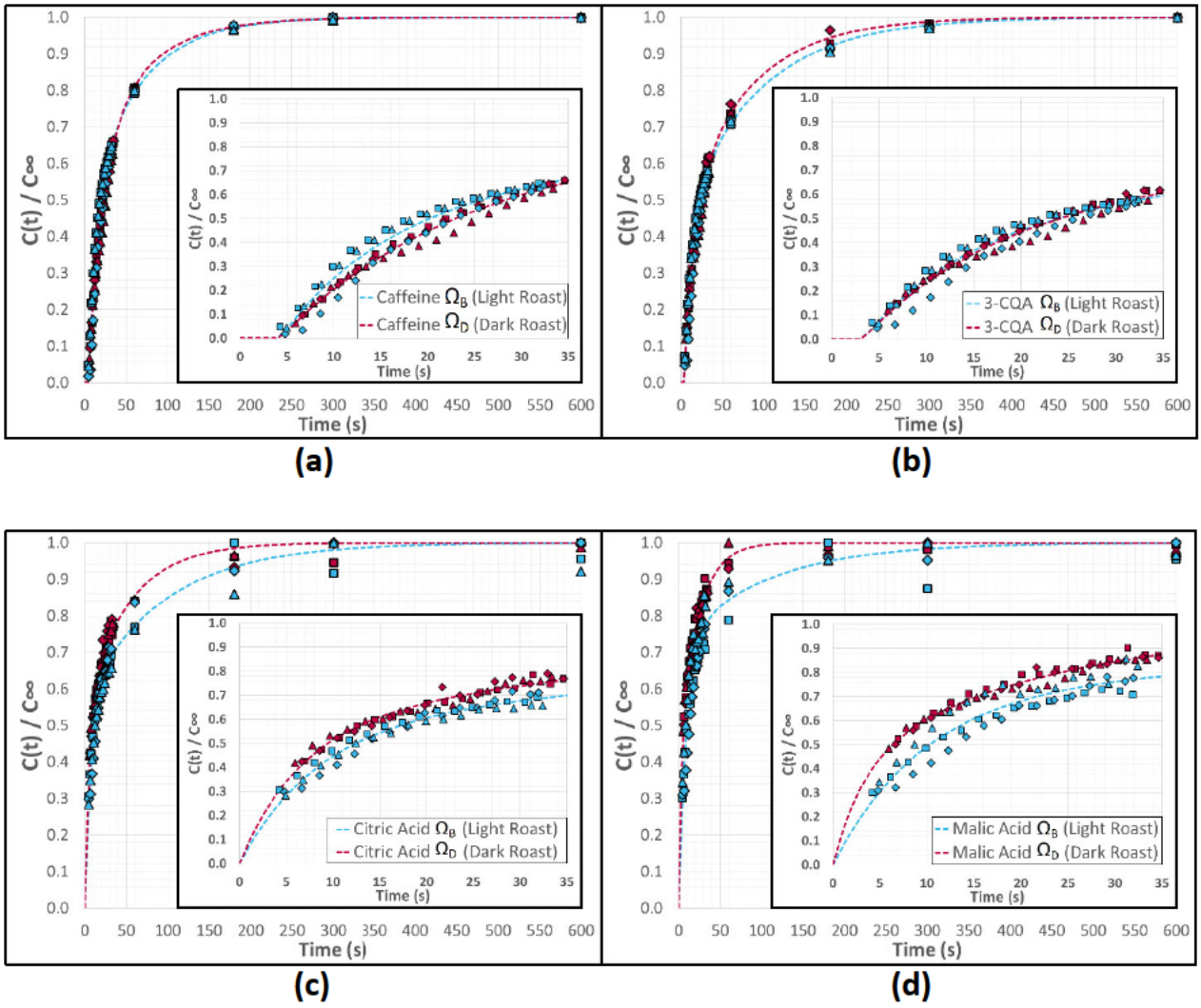

Figure 5.36: Comparison of [redacted] sieved, light roast coffee material Ω_B and sieved, dark roast coffee material Ω_D extraction kinetics for (a) caffeine, (b) 3-CQA, (c) citric acid, and (d) malic acid.

The extraction kinetics of the equivalent light and dark roast particle sizes were compared for the two control materials. There was no difference in extraction kinetics observed for caffeine, 3-CQA, and very small differences in the extraction kinetics for the organic acids, most notably in the malic acid curves (Figure 5.36 (d)). The minimal difference in results are in contrast to the previously reported differences in coffee structure between light and dark roast coffees (section 5.2), where the dark roast material had 40% larger mesopore diameters within the coffee cell walls. These small differences in extraction kinetics between

[redacted] sieved, light and dark roast coffees is evidence that the changes in the mesoporous structure have only a minimal effect on coffee extraction kinetics.

[redacted]

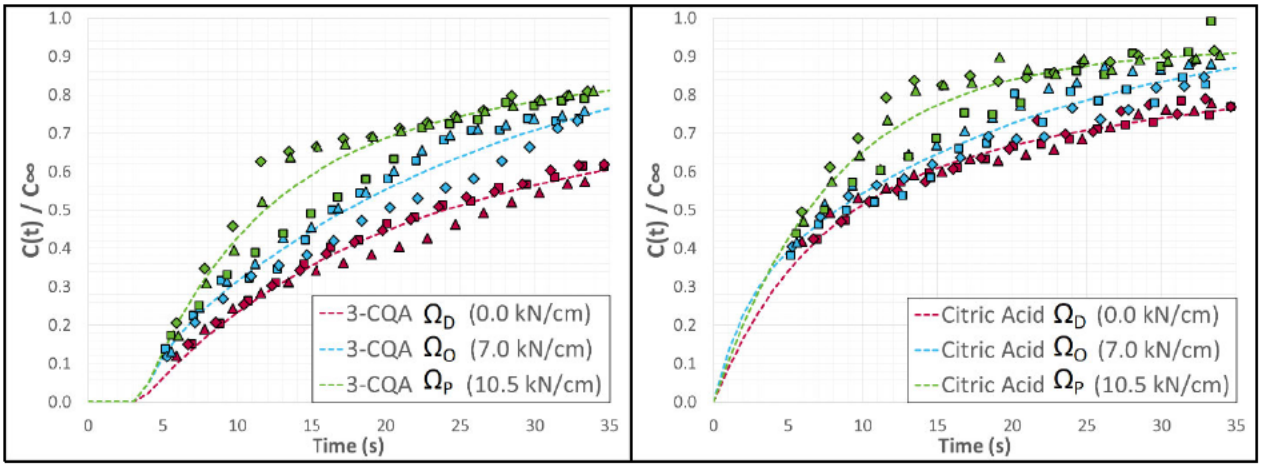

Figure 5.37: [redacted]

[redacted]

Figure 5.38:

5.5:

The absolute concentrations for each of the last three time points for each set of replicate extractions for a single material were averaged and compiled in Table 5.11. In most cases, the maximum absolute concentration was observed at either 300 or 600 s, and the maximum observed value in each replicate was used to normalize the data from that specific extraction event. In rare cases, the maximum chemical concentration was measured at an earlier time, such as 60 or 180 s.

Table 5.11: Average and standard deviation of absolute concentrations for each chemical compound, for each coffee material at 180, 300, and 600 s.

Sample ID	Caffeine (mg/L)			3-CGA (mg/L)			Citric Acid (mg/L)			Malic Acid (mg/L)			Quinic Acid (mg/L)		
Time (s)	180	300	600	180	300	600	180	300	600	180	300	600	180	300	600
Ω_A	346 ± 13	383 ± 4	384 ± 13	164 ± 5	189 ± 10	204 ± 6	135 ± 9	142 ± 12	151 ± 20	54 ± 2	55 ± 2	57 ± 5	195 ± 16	201 ± 22	222 ± 48
Ω_B	340 ± 3	349 ± 5	351 ± 6	179 ± 2	191 ± 2	197 ± 3	144 ± 23	150 ± 16	148 ± 10	61 ± 9	59 ± 4	61 ± 7	172 ± 20	181 ± 11	169 ± 4
Ω_C	355 ± 8	359 ± 6	360 ± 5	204 ± 5	212 ± 4	214 ± 4	147 ± 17	148 ± 11	149 ± 20	62 ± 6	59 ± 5	62 ± 6	175 ± 22	172 ± 14	172 ± 25
Ω_D	349 ± 6	358 ± 6	359 ± 4	87 ± 1	90 ± 2	92 ± 2	104 ± 5	107 ± 4	108 ± 6	39 ± 0.1	39 ± 1	39 ± 0.2	142 ± 6	144 ± 4	143 ± 7
Ω_E	339 ± 2	357 ± 2	372 ± 15	169 ± 1	184 ± 2	193 ± 2	104 ± 4	107 ± 4	108 ± 2	48 ± 4	46 ± 1	45 ± 1	141 ± 10	149 ± 18	139 ± 8
Ω_F	353 ± 1	362 ± 1	363 ± 2	175 ± 1	185 ± 1	188 ± 1	126 ± 4	128 ± 2	130 ± 4	48 ± 3	52 ± 4	50 ± 7	145 ± 5	143 ± 4	142 ± 7
Ω_G	357 ± 4	360 ± 3	359 ± 2	186 ± 11	191 ± 11	191 ± 12	133 ± 12	135 ± 12	131 ± 9	43 ± 6	44 ± 6	45 ± 8	158 ± 14	154 ± 6	150 ± 12
Ω_H	340 ± 1	353 ± 2	355 ± 2	180 ± 1	190 ± 1	195 ± 1	107 ± 2	113 ± 8	115 ± 1	44 ± 2	49 ± 0.5	47 ± 1	128 ± 2	142 ± 12	141 ± 2
Ω_I	360 ± 15	371 ± 15	372 ± 15	198 ± 0.3	209 ± 0.2	212 ± 2	136 ± 6	138 ± 6	140 ± 7	55 ± 4	56 ± 4	53 ± 1	143 ± 9	143 ± 6	142 ± 9
Ω_J	356 ± 9	353 ± 2	352 ± 2	194 ± 3	197 ± 2	196 ± 2	131 ± 3	134 ± 13	118 ± 1	57 ± 3	57 ± 7	55 ± 5	155 ± 2	164 ± 18	163 ± 0.5
Ω_K	346 ± 2	356 ± 2	358 ± 0.1	179 ± 1	187 ± 1	190 ± 0.4	110 ± 6	113 ± 7	117 ± 11	50 ± 6	53 ± 3	54 ± 3	149 ± 3	149 ± 12	158 ± 22
Ω_L	353 ± 10	356 ± 1	355 ± 1	184 ± 1	192 ± 1	193 ± 1	131 ± 9	131 ± 6	132 ± 10	55 ± 3	52 ± 3	51 ± 7	163 ± 5	158 ± 11	160 ± 13
Ω_M	344 ± 2	347 ± 2	346 ± 2	185 ± 1	188 ± 1	187 ± 1	130 ± 12	128 ± 7	131 ± 13	52 ± 5	52 ± 1	53 ± 4	144 ± 11	141 ± 3	145 ± 13
Ω_N	349 ± 1	357 ± 2	357 ± 1	78 ± 4	82 ± 5	82 ± 4	104 ± 12	108 ± 17	107 ± 15	37 ± 2	37 ± 2	36 ± 2	138 ± 10	151 ± 12	139 ± 12
Ω_O	352 ± 2	356 ± 3	356 ± 2	80 ± 2	83 ± 1	82 ± 1	104 ± 2	108 ± 11	105 ± 8	37 ± 1	37 ± 2	36 ± 2	135 ± 6	139 ± 7	135 ± 9
Ω_P	354 ± 3	357 ± 4	357 ± 4	78 ± 1	79 ± 1	79 ± 1	100 ± 5	102 ± 6	101 ± 6	36 ± 1	36 ± 1	35 ± 1	134 ± 5	139 ± 9	134 ± 8
Ω_Q	337 ± 2	344 ± 3	344 ± 3	192 ± 1	199 ± 1	200 ± 2	118 ± 2	120 ± 8	119 ± 6	52 ± 3	52 ± 2	52 ± 2	126 ± 5	125 ± 4	127 ± 3
Ω_R	332 ± 3	341 ± 2	342 ± 2	184 ± 1	190 ± 1	191 ± 2	115 ± 8	115 ± 9	119 ± 9	48 ± 2	46 ± 4	49 ± 3	124 ± 5	128 ± 3	129 ± 9
Ω_S	350 ± 7	351 ± 1	349 ± 1	180 ± 1	184 ± 0.4	182 ± 0.5	133 ± 15	133 ± 1	137 ± 10	53 ± 4	51 ± 1	52 ± 2	173 ± 13	156 ± 11	175 ± 18
Ω_T	309 ± 19	323 ± 21	332 ± 29	169 ± 11	182 ± 12	191 ± 14	*	*	*	*	*	*	*	*	*
Ω_U	346 ± 3	347 ± 3	348 ± 3	190 ± 3	194 ± 3	195 ± 3	145 ± 31	148 ± 22	154 ± 45	60 ± 6	58 ± 6	58 ± 6	145 ± 29	141 ± 19	152 ± 37

The maximum concentration values of each compound were found to converge to similar values across the control materials, except for the dark roast coffee control, material Ω_D, which had lower concentrations for each acid. The lower acid values for Ω_D is consistent when comparing dark roast coffees to light roast coffees [Jeon et al. 2017, Clarke (Ed.) 2012a]. This difference is due to the acid degradation during coffee roasting, where greater acid degradation and decomposition is directly proportion to the temperature and time the coffee is subjected to in the roasting process, where longer roasting times are required to yield a dark roast coffee [Clarke (Ed.) 2012a].

Table 5.12:

Table 5.13: [redacted]

[redacted]

Table 5.14: [redacted]

[redacted]

Table 5.15: [redacted]

[redacted]

Table 5.16: [redacted]

[redacted]

[redacted]

Table 5.17: [redacted]

[redacted]

[redacted]

Table 5.18: [redacted]

[redacted]

[redacted]

5.6: Conclusions

[redacted]

[redacted] coffee extraction was found to be independent of particle size in the first several seconds of extraction, but a strong dependence on particle size was observed at times >25 s. This data set is the first to capture the "washing phase" of extraction due to the unique ability to measure early extraction times. [redacted]

[redacted] dark roast coffee had nearly identical extraction kinetics as light roast coffee for the chemical compounds studied. The structural changes of the coffee particle due to thermal treatment are insufficient to materialize differences in extraction kinetics. [redacted]

[redacted]

Chapter 6: An Empirical Model to Describe Coffee Extraction Kinetics

6.1: Introduction

Previous studies have developed mathematical models to describe coffee extraction kinetics in well-mixed batch reactors and in packed beds of coffee (section 2.5). Models developed for a well-mixed batch reactor are based on first order, non-steady state diffusion out of a sphere. However, previous available data has failed to capture the important short time kinetics. This chapter will introduce the application of a new empirical model containing the sum of two exponentials describing the two regimes of coffee extraction. [redacted]

6.2: Empirical Model Development

6.2.1: A Model to Describe Two Extraction Regimes

The extraction kinetic curves in the well-mixed batch reactor experiments demonstrated the presence of two extraction regimes, and as presented in section 4.5.6, a single regime model is insufficient to describe the data set. The semi-log plot in Figure 4.12 (section 4.5.6) demonstrated a distinct change in slope of the data indicative of a transition point, where two, linear lines would intersect. Figure 6.1 is the same extraction kinetic data of 3-CQA for material Ω_A plotted with two linear regression lines. The intersection point differentiates the total contribution of extract concentration from the fast extraction regime and the slow extraction regime.

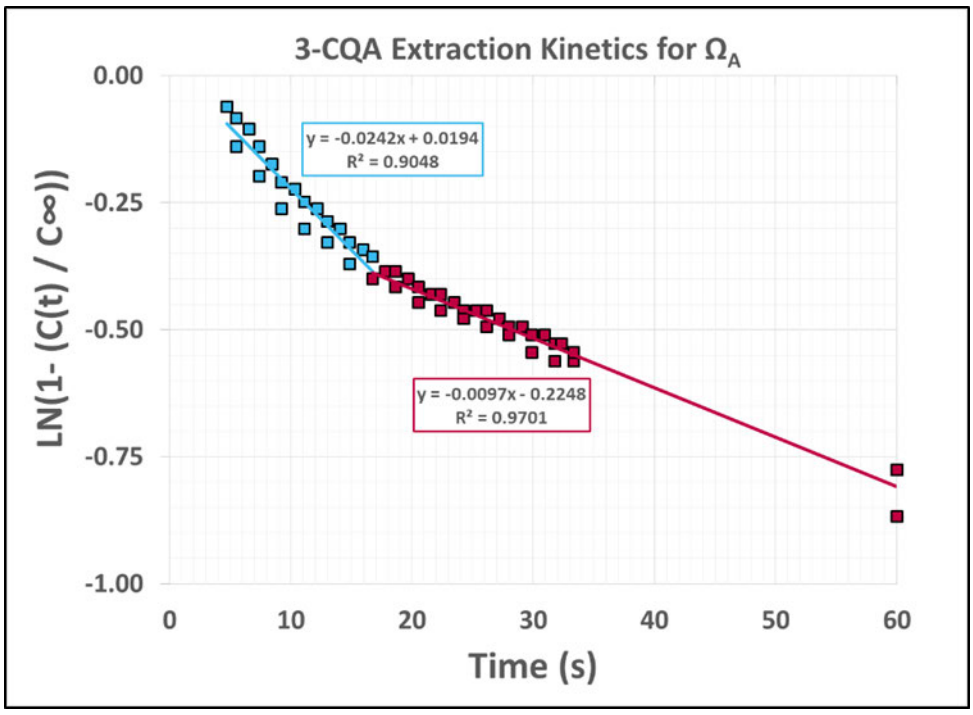

Figure 6.1: Semi-log plot of the 3-CQA extraction kinetics for [redacted] sieved (1180-1000 µm), light roast coffee material Ω_A.

The sum of these two regimes describe the total extraction kinetics:

$$\frac{C_t}{C_\infty} = \varphi\left(1 - e^{\frac{-t}{\lambda_1}}\right) + (1-\varphi)\left(1 - e^{\frac{-t}{\lambda_2}}\right) \quad Eqn.\ 6.1$$

The coffee extraction kinetic model in equation 6.1, is the sum of two, first order exponentials weighted by the concentration contributions from each regime as established by the intersection point; this intersection value is denoted as φ. The two model parameters λ_1 and λ_2 are the time constants for each extraction regime, these correspond to the model presented by Spiro and Selwood [1984].

$$\frac{C_t}{C_\infty} = \varphi\left(1 - e^{\frac{-(t-\tau)}{\lambda_1}}\right) + (1-\varphi)\left(1 - e^{\frac{-(t-\tau)}{\lambda_2}}\right) \quad Eqn.\ 6.2$$

In the observed extraction kinetics of caffeine and 3-CQA, where the extraction kinetics exhibited a delay, an additional parameter is needed. The extraction delay time, denoted as τ, is a shift on the time axis (Eqn. 6.2).

6.2.2: Conceptual and Physical Model Explanation

The model equation 6.2 operates under several key assumptions.

1) The particles are spherical.

2) Hydration is not a rate limiting step and the particles are considered rapidly saturated at the start of the experiment.

3) Very dilute conditions exist in the bulk liquid.

4) The solute completely extracts from the matrix and the solute does not reabsorb to the matrix.

5) The solute diffusion is constant and is treated as an averaged effective diffusivity.

The five assumptions for the empirical model are consistent with modeling coffee extraction kinetics with a first order, steady state diffusion model [Voilley and Simantos 1980, Spiro and Selwood 1984, Sano et al. 2019]. The first assumption of spherical particles greatly reduces the true geometric complexity of ground coffee particles, and simplifies the geometric aspect of the mathematical equations down to a function in terms of only the particle radius.

The second assumption of rapid wetting of the particles establishes a well-defined start to the extraction of all coffee particles. The assumption of rapid hydration, coupled with the assumption of complete saturation, eliminates the possibility of a residence time distribution of the hydration of the particles and of various starting extraction times for the particles. The

validity of this assumption can be checked by approximating the time of hydration as estimated from the Lucas-Washburn equation for wicking in swelling porous materials [Masoodi and Pillai (Eds.) 2012]. The hydration time can be estimated using equation 6.3:

$$h = \sqrt{\frac{\gamma^{lv} R_{pore} \cos(\theta_d)}{2\mu_f} t} \qquad Eqn. 6.3$$

Where h, is the penetration distance into the capillary pore of a solid, γ^{lv} is the surface tension of the liquid, R_{pore} is the capillary pore radius, θ_d is the dynamic contact angle between the liquid and the solid, μ_f is the dynamic viscosity of the liquid, and t is time. The values for the other variables are listed in Table 6.1. The choice of an extremely small capillary pore radius, R_{pore} highlights the extreme case where the time to penetrate would be at a maximum. The value chosen was taken from the measured pore sizes of the plasmodesmata reported by Schenker et al. [2000] for the LTLT roasted coffee.

Table 6.1: Variable values for estimating hydration time of large coffee particles.

Variable	Value	Units	Reference
$h_{\Omega A}$	7.7×10^{-4}	m	This work
$h_{\Omega J}$	3.44×10^{-4}	m	This work
γ^{lv}	6.082×10^{-3}	N/m	Vargaftik et al. 1983
μ_f	9.0×10^{-5}	Pa s	Kestin et al. 1978
R_{pore}	1.12×10^{-8}	m	Schenker et al. 2000
θ_d	80	°	Estimate from Corrochano 2017

The hydration time, the time required for the liquid to penetrate the solid a distance of h, was calculated to be 0.79 and 1.78 s for coffee particles with a radius of 344 and 770 µm respectively, which correspond to the mean volume particle radius of material Ω_J and material Ω_A. These are the smallest and largest particle sizes measured in all of the coffee materials tested. The hydration time for material Ω_A is the worst case scenario as it is the largest particle,

and given that the hydration time is smaller than the ability to measure any coffee extraction, it is reasonable to treat all materials as fully saturated at the start of the experiment. Moreover, the estimated hydration time difference between the largest and smallest particles is one second, which is a very small difference in the overall extraction kinetics.

The well-mixed batch reactor and extraction experiments were intentionally executed with a low coffee to water ratio of 0.028 to ensure a dilute system existed in the bulk liquid, to include at long times where several milliliters of liquid volume were removed in the sample collection process. This assumption of a dilute system and deliberate experimental execution is important as it ensures the external mass transfer resistance due to the bulk liquid concentration over time is as low as possible. A very dilute system also supports a larger partition coefficient of each respective chemical compound, and this model assumes that the partition coefficient is one, which is the fourth assumption of this model.

The final assumption states that the two extraction regimes initially observed in section 4.5.6 and in section 5.3 are assumed to have constant diffusivities with respect to distance, and that the diffusivity is not time dependent. This permits a defined transition point in the extraction curves where the concentration contribution from one extraction regime can be differentiated from the other, and the diffusivity of each regime is a simply a fixed constant rather a function of time and position within the particle. This assumption also assigns the effects of any treatment solely on the slow extraction regime time constant.

Figure 6.2 provides a visual of the physical understanding of the extraction process ultimately described by equation 6.2. The model in equation 6.2 describes the extraction kinetics as the sum of the kinetics from the fast extraction regime and the slow extraction regime. The model parameter φ distinguishes the transition point between the two extraction regimes as mentioned in section 6.2.1. It is necessary to determine the volume of the coffee solids contributing to the total concentration observed within the fast extraction regime versus the volume of the solids contributing to the slow extraction regime.

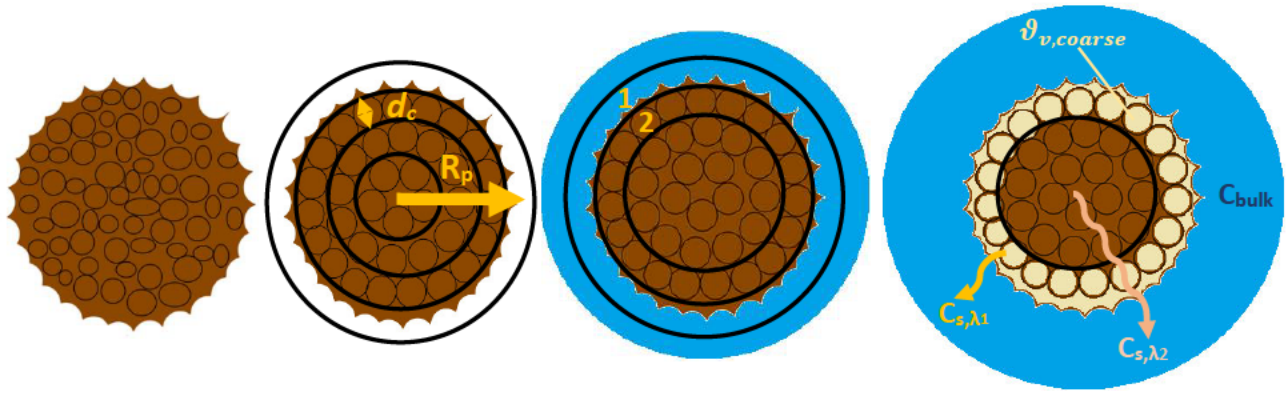

Normal coffee particle assuming spherical geometry.

Assume concentric layers, each the thickness of single coffee cell (d_c).

Coffee particle is wetted rapidly and is fully saturated at the start of the experiment. The first concentric layer is the broken layer, layer 1, and the first intact layer is layer 2.

The particle volume of the broken layer (layer 1) and the first intact layer (layer 2) extract rapidly with the fine particles. This particle volume is highlighted in a lighter color.

Figure 6.2: A conceptual model for two stage coffee extraction.

The volume of coffee solids contributing to fast extraction is a combination of the fine particles adhered to the surface of more coarse particles, in conjunction with the surface layer of the coarse particles themselves. The spherical particle assumption facilitates a consistent way of calculating the surface volume fraction of the coarse particles contributing to the fast extraction regime. This volume fraction can be determined by discretizing a spherical coffee particle into an N number of layers, where the width of each layer is the thickness of an individual coffee cell. Fiori et al. [2009] reported that the first two layers be considered as part of the rapid extraction phase (section 2.5.4.3).

6.2.3: Parameter Reduction

The four parameter model (Eqn. 6.2) was simplified by fixing τ and developing a predictive method for the determination of φ from the particle size measurements. The value of τ was fixed by visual inspection of the extraction data for caffeine and 3-CQA to 4 s and 3 s respectively (section 4.5.5).

The definition of what constitutes a "fine particle" in terms of particle size can be reasonably estimated by calculating the mass transfer Biot number Bi_m, which relates the internal mass transfer resistance to the external mass resistance, and the Fourier number for mass transport Fo_m, which relates time to the time scale of diffusion:

$$Bi_m = \frac{k\, R_p}{D_{eff}} \quad Eqn\ 6.4$$

$$k = \frac{D_{soln}}{\delta} \quad Eqn\ 6.5$$

The Biot number was estimated using equations 6.4 and 6.5, where k is the mass transfer coefficient, R_P is the radius of the particle, and D_{eff} is the effective diffusivity within the particle. The mass transfer coefficient k, can be estimated as the diffusivity of the chemical compound in a bulk fluid, D_{soln}, divided by the thickness δ, of a boundary layer surrounding the particle, shown in equation 6.5.

$$Fo_m = \frac{D_{eff}\, t}{{R_P}^2} \quad Eqn\ 6.6$$

The Fourier number was estimated using equation 6.6, where t, is time, R_P is the radius of the particle, and D_{eff} is the effective diffusivity within the particle. Table 6.2 lists the values of the variables in equations 6.4, 6.5, and 6.6.

Table 6.2: Variable values for estimating Bi_m and Fo_m.

Variable	Value	Units	Reference
D_{soln}	2.3×10^{-9}	m^2/s	Spiro et al. 1989
D_{eff}	7.67×10^{-10}	m^2/s	Estimate from Corrochano 2017
δ	9.0×10^{-5}	m	Assumed
R_P	9.0×10^{-5}	m	Assumed
t	15	s	Time at Transition point

Sufficiently large Fourier numbers, O(>1), describe a mass transport event where adequate time has passed and the concentration gradient within a particle and a bulk solution is near zero. Small Biot numbers, O(0.1-10), where the internal diffusion resistance is less than or approximately equal to the external diffusion resistance, describe a particle which undergoes a fast extraction event [DeWitt et al. 2007]. The Fourier number was estimated to be equal to 1.4 using equation 6.6 and an approximate value of the Biot number was estimated to be equal to 3 with a particle radius of 90 µm. The value of δ was assumed to be equal to the particle radius as it is largest when the particle is considered to be in a stagnant medium and it is typically on a similar length scale of the particle radius [Adrian 2007].

The fines volume fraction is assumed to be the volume fraction of all particles below 186 µm, given the estimated values for the Biot and Fourier numbers. This volume fraction value was taken from the combined particle size distribution data obtained, where the fine fraction was determined with the liquid dispersion method. This maximum fine particle size describes a coffee particle with a radius of two coffee cells, assuming a coffee cell diameter of 45 µm (section 5.2.6). Moreover, the volume fraction of the coarse particles contributing to the fast extraction kinetics needed to be calculated. The proportion of the coarse particle volume contributing to fast extraction was determined by using the combined particle size distribution data, where the coarse volume fraction was determined with the air dispersion method. It is important to note, the Malvern software uses 100 native particle size class bins to calculate particle size distributions.

The fraction of total concentration available for fast extraction is:

$$\varphi = \theta_{v,fines} + \vartheta_{v,coarse} \quad Eqn.\,6.7$$

Where φ is the combination of the fines volume fraction and the surface volume fraction of the coarse particles contributing to fast extraction.

The fines contribution is:

$$\theta_{v,fines} = \sum_{i=1}^{75} v_{i,liquid} \quad Eqn. 6.8$$

Where $\theta_{v,fines}$ is the total volume fraction of all particles below 186 µm, and $v_{i,liquid}$ is the measured particle size distribution (liquid dispersion) volume fraction in each class bin, where the 75th class bin has a mean particle diameter of approximately 186 µm.

The coarse contribution is:

$$\vartheta_{v,coarse} = \sum_{i=76}^{100} v_{i,air} \left(1 - \left(\frac{(\overline{x_i} - 2d_c)^3}{\overline{x_i}^3}\right)\right) \quad Eqn\ 6.9$$

Where $\vartheta_{v,coarse}$ is the total volume fraction of the surface of coarse particles contributing to fast extraction, $v_{i,air}$ is the measured particle size distribution (air dispersion) volume fraction within an individual class-bin, $\overline{x_i}$ is the arithmetic mean diameter of the upper and lower particle sizes of that class bin, and d_c is the diameter of a single coffee cell assumed to be 45 µm.

The value of φ was calculated for each material using equations 6.7, 6.8 and 6.9. A sphere with a diameter of $\overline{x_i}$ was discretized into an N number of concentric layers of d_c , each 45µm thick (Figure 6.2). The volume fraction of the first two layers in each sphere was calculated and multiplied by the class bin volume fraction for coarse particle size distribution; these volume fractions were summed over the 24 coarse particle class bins (Eqn. 6.9). The calculation of the volume of two layers versus a single layer is consistent with the findings of Fiori et al. [2009] who reported a double shell model fit supercritical fluid extraction data more appropriately. Table 6.3 contains the values for $\varphi, \theta_{v,fines}$, and $\vartheta_{v,coarse}$ for all coffee materials modeled.

Table 6.3: Calculated values for $\varphi, \theta_{v,fines}$, $and\ \vartheta_{v,coarse}$.

Sample ID	$\boldsymbol{\theta_{v,fines}}$	$\boldsymbol{\vartheta_{v,coarse}}$	$\boldsymbol{\varphi}$
Ω_A	0.025	0.332	0.356
Ω_B	0.035	0.433	0.468
Ω_C	0.053	0.523	0.576
Ω_D	0.045	0.430	0.475
Ω_E	0.063	0.382	0.445
Ω_F	0.109	0.447	0.556
Ω_G	0.148	0.491	0.639
Ω_H	0.087	0.396	0.483
Ω_I	0.089	0.456	0.545
Ω_J	0.061	0.568	0.628
Ω_K	0.101	0.394	0.495
Ω_L	0.103	0.450	0.553
Ω_M	0.110	0.526	0.636
Ω_O	0.093	0.464	0.557
Ω_P	0.106	0.481	0.587
Ω_T	0.108	0.444	0.551
Ω_U	0.154	0.494	0.648

6.2.4: Influence of Model Parameters and Physical Interpretation

The empirical model in equation 6.2 was simplified into a two parameter regression model, where the parameters are representative of the time constants for each of the two extraction regimes. The impact of each individual parameter on the model for the coffee extraction curve was explored to obtain an initial understanding of the model sensitivity to each respective parameter. The time constant for the fast extraction regime, λ_1 or λ_{fast}, describes the extraction kinetics for the fines and the surfaces of the coarse particles. It is logical that this

value is constant regardless of the value of φ, because there is limited mass transfer resistance due to the absence of coffee structure.

There could be potential variation in this time constant value as the particle size distribution of the fines is treated as lumped value, $\theta_{v,fines}$. Different particle size distributions within the boundary conditions describing fine particles, 0.1—180µm, could exist which would result in different values for λ_{fast} if those distributions were substantially differentiated between materials. The value of λ_{fast} should also be reflective of the extraction kinetics of the individual chemical compound, where slower extracting compounds will have relatively larger values of λ_{fast} than faster extracting compounds. Figure 6.3 shows the effect of λ_{fast} for fixed values of φ and λ_{slow}. It is very clear that smaller values of λ_{fast} achieve the transition point or value of φ in shorter times. As λ_{fast} continues to increase and approach the value of λ_{slow}, a single exponential model begins to form.

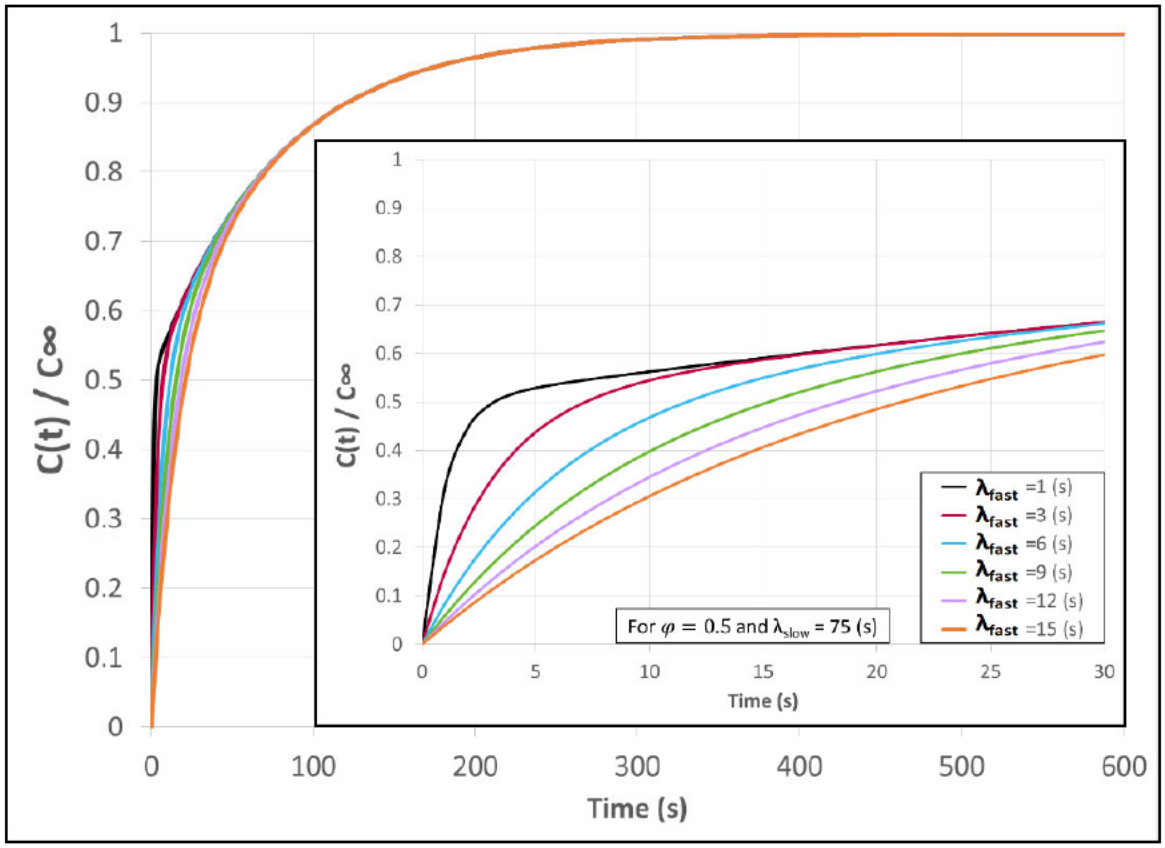

Figure 6.3: Influence of model parameter λ_{fast} on extraction kinetics.

The time constant for the slow extraction regime, λ_2 or λ_{slow}, describes the extraction kinetics for the majority of the volume fraction within the coarse particles. The value of this time constant will change as the coffee structure changes as it is directly related with the mass transfer resistance of diffusion. Figure 6.4 shows the influence of λ_{slow} for fixed values of λ_{fast} for and φ. It is clear from Figure 6.4 that as λ_{slow} decreases, the time to achieve total extraction is reduced. Given the relationship of λ_{slow} with coffee structure, it is expected that as particle size decreases, as particle porosity increases, as surface area increases, or as degree of roast increases (i.e. darker roasts), a decrease in the value of λ_{slow} should be observed, as each of these relationship reduce the complexity of the coffee particle structure and therefore reduce the mass transfer resistance for diffusion.

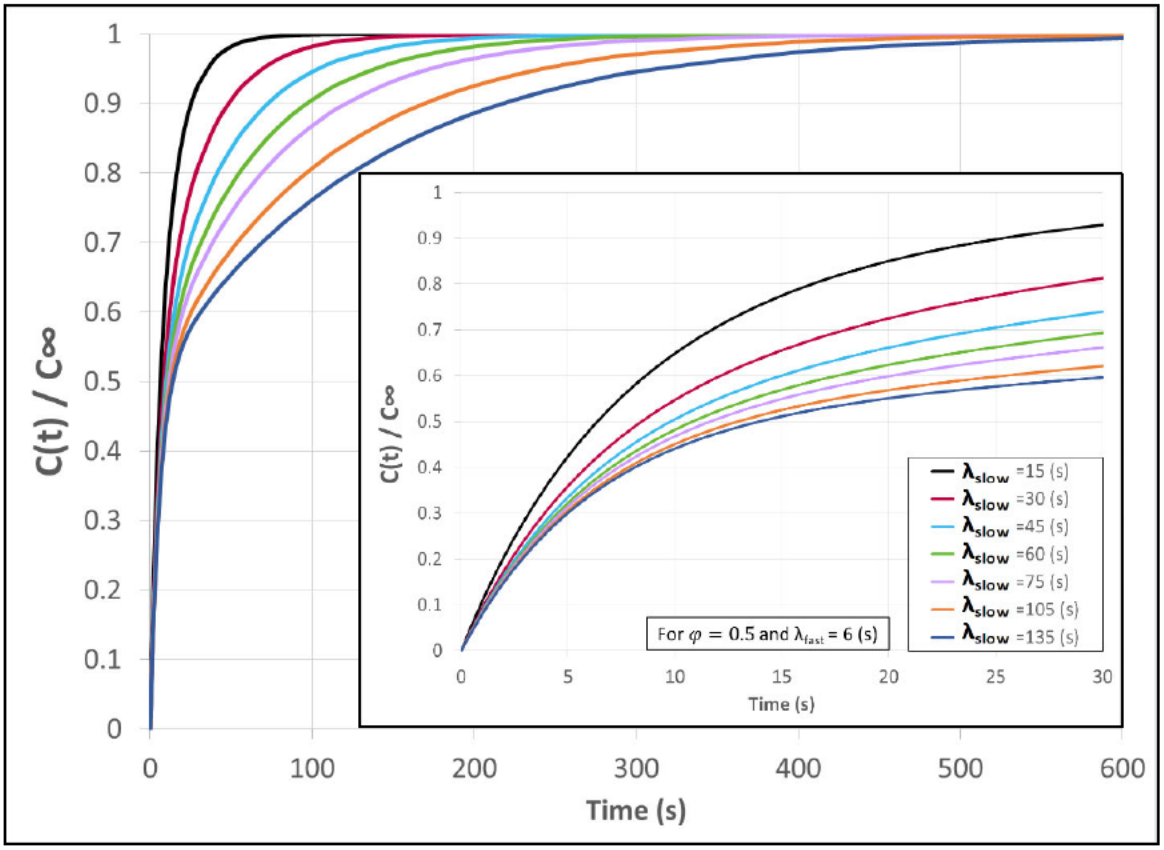

Figure 6.4: Influence of model parameter λ_{slow} on extraction kinetics.

The calculated values of φ are based on the physical measurements of the material and identify the point in normalized concentration where the fast extraction regime transitions to the slow extraction regime. Mathematically, φ bounds model equation 6.2 between a completely fast extraction event, where $\varphi = 1.00$ and a completely slow extraction event where $\varphi = 0$. A real scenario where $\varphi = 1.00$ is the brewing of a Turkish ground coffee, where the median particle size is approximately 100µm [von Blittersdorff, M. and Klatt, C. 2017]. A scenario where $\varphi = 0$ is not practical as every particle has surface area, but φ would be at an absolute minimum value if coffee was extracted as roasted whole bean. This absolute minimum can be estimated from average roasted coffee bean dimensions calculated by Severa et al. [2012] and assuming the coffee bean as an ellipsoid with a result of $\varphi = 0.07$. Figure 6.5 shows the influence of φ for fixed values of λ_{slow} and λ_{fast}.

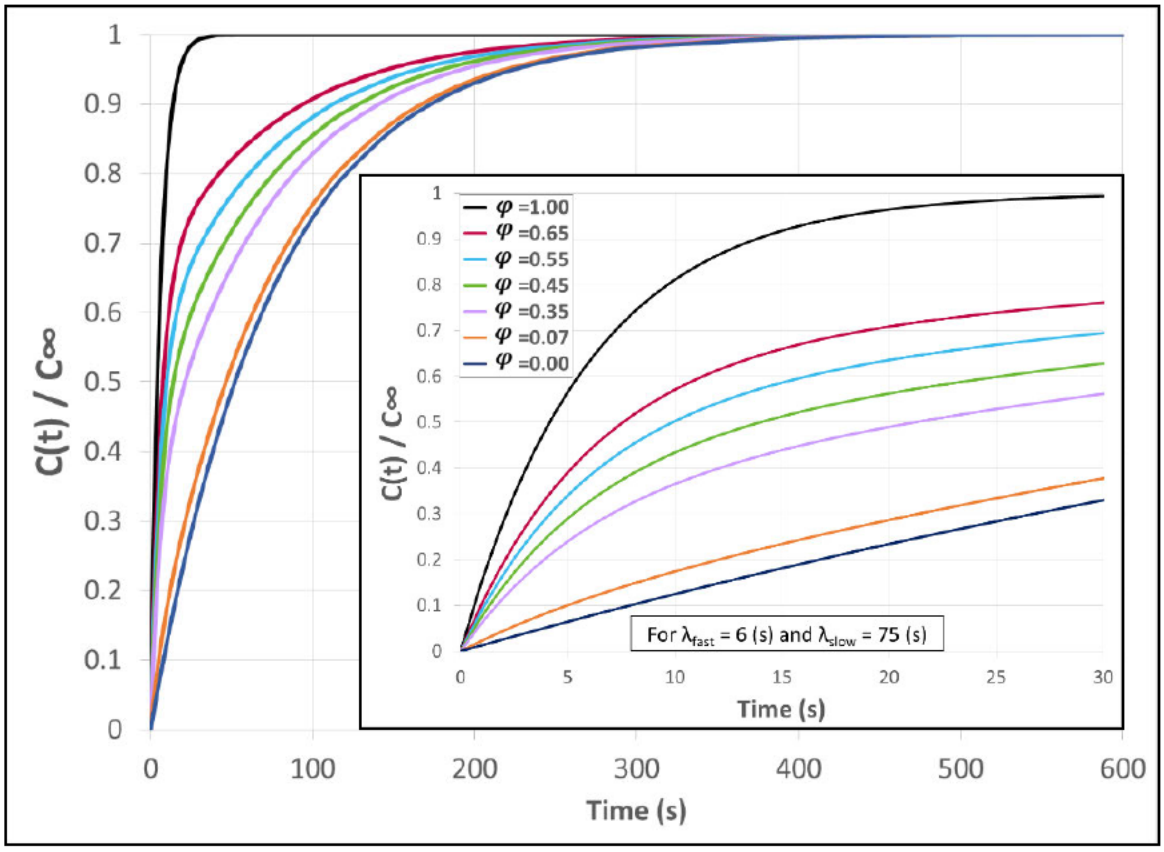

Figure 6.5: Influence of predicted model parameter φ on extraction kinetics.

6.3: Parameter Values and Model Fit

The values for λ_{fast} and λ_{slow}, along with the 95% confidence intervals for each parameter, the coefficient of determination for the model, and the mean absolute percent error of the model are found in Table 6.4 and Table 6.5 for each material and each of the five chemical compounds. In most cases the fit of the model is excellent, resulting in mean percent errors averaging 6% for 3-CQA and 4% for citric acid, and similar values for the other three compounds. A small correlation between the two parameter estimates, λ_{fast} and λ_{slow}, existed within the model for each material. The correlation of estimates is on average between 0.40 and 0.60 for each of the various chemical compounds.

Table 6.4: Model parameter values with 95% confidence intervals, coefficient of determination, and mean percent error for caffeine and 3-CQA extraction kinetic models.

	Caffeine								3-CQA							
Sample ID	**λ_{fast} (s)**	**Lower 95% CI**	**Upper 95% CI**	**λ_{slow} (s)**	**Lower 95% CI**	**Upper 95% CI**	**R^2 (-)**	**MPE (%)**	**λ_{fast} (s)**	**Lower 95% CI**	**Upper 95% CI**	**λ_{slow} (s)**	**Lower 95% CI**	**Upper 95% CI**	**R^2 (-)**	**MPE (%)**
Ω_A	9.2	8.2	10.4	109	99	119	0.95	**6.9**	10.9	10.1	11.2	158	148	169	0.97	**5.5**
Ω_B	10.6	9.3	12.2	57	49	66	0.92	**16.0**	11.2	10.2	12.3	93	81	106	0.94	**10.8**
Ω_C	19.1	14.8	35.5	29	13	43	0.88	**12.6**	18.3	16.0	22.1	59	42	76	0.92	**9.3**
Ω_D	15.7	14.5	17.2	50	45	55	0.98	**3.7**	13.0	12.2	14.0	79	72	87	0.97	**4.0**
Ω_E	5.8	5.4	6.2	104	97	111	0.99	**3.4**	6.8	6.4	7.2	129	121	137	0.99	**3.0**
Ω_F	9.2	8.0	10.6	68	55	84	0.86	**9.3**	10.3	9.3	11.5	97	80	117	0.90	**8.1**
Ω_G	9.1	8.0	10.5	46	36	59	0.85	**9.7**	10.2	9.1	11.5	72	56	93	0.87	**8.9**
Ω_H	4.5	4.1	4.9	67	63	71	0.98	**3.2**	5.4	4.9	5.5	92	85	99	0.99	**3.2**
Ω_I	8.1	7.2	9.2	78	65	93	0.89	**12.9**	9.5	8.6	10.5	97	82	115	0.91	**10.3**
Ω_J	7.8	7.4	8.3	33	31	36	0.98	**3.4**	8.8	8.3	9.4	41	37	46	0.97	**4.1**
Ω_K	2.9	2.6	3.1	50	48	53	0.99	**2.4**	3.7	3.4	3.9	65	62	69	0.99	**2.3**
Ω_L	7.3	7.0	7.6	62	58	65	0.99	**3.1**	8.4	8.1	8.6	78	74	82	0.99	**2.5**
Ω_M	9.0	7.7	10.9	27	20	35	0.85	**9.7**	10.0	8.7	11.9	35	26	45	0.86	**10.3**
Ω_O	12.8	10.9	16.4	33	24	41	0.90	**7.7**	11.8	10.4	13.6	43	35	51	0.92	**6.2**
Ω_P	7.0	6.1	8.1	34	28	40	0.86	**7.4**	7.0	6.2	7.9	38	32	44	0.88	**5.9**
Ω_T	11.2	10.4	12.0	98	86	111	0.98	**3.7**	12.2	11.6	11.9	139	125	155	0.99	**3.2**
Ω_U	8.5	8.0	9.1	35	31	39	0.97	**3.8**	9.1	8.6	9.7	57	50	64	0.97	**3.9**

Table 6.5: Model parameter values with 95% confidence intervals, coefficient of determination, and mean percent error for citric acid, malic acid and quinic acid extraction kinetic models.

	Citric Acid								**Malic Acid**								**Quinic Acid**							
Sample ID	**λ_{fast} (s)**	**Lower 95% CI**	**Upper 95% CI**	**λ_{slow} (s)**	**Lower 95% CI**	**Upper 95% CI**	**R^2 (-)**	**MPE (%)**	**λ_{fast} (s)**	**Lower 95% CI**	**Upper 95% CI**	**λ_{slow} (s)**	**Lower 95% CI**	**Upper 95% CI**	**R^2 (-)**	**MPE (%)**	**λ_{fast} (s)**	**Lower 95% CI**	**Upper 95% CI**	**λ_{slow} (s)**	**Lower 95% CI**	**Upper 95% CI**	**R^2 (-)**	**MPE (%)**
Ω_A	3.0	2.5	3.4	65	62	68	0.97	**3.0**	2.4	1.5	3.2	44	42	46	0.95	**4.0**	12.0	10.6	13.8	90	81	99	0.94	**12.5**
Ω_B	6.3	5.6	7.1	57	52	62	0.93	**5.0**	6.4	5.4	7.5	35	31	39	0.89	**5.5**	11.9	9.5	15.5	60	45	77	0.76	**16.8**
Ω_C	10.0	9.2	10.8	44	40	48	0.97	**3.2**	9.8	8.8	11.1	34	30	38	0.94	**5.4**	*	*	*	*	*	*	*	*
Ω_D	5.2	4.7	5.7	42	41	44	0.97	**2.3**	4.0	3.6	4.5	25	24	26	0.98	**1.8**	14.7	12.6	18.4	35	28	40	0.94	**3.7**
Ω_E	3.1	2.4	3.7	35	32	37	0.96	**3.5**	2.8	1.6	3.8	26	23	30	0.88	**6.0**	6.4	5.1	8.0	61	51	72	0.89	**8.5**
Ω_F	5.8	5.1	6.6	44	39	49	0.91	**4.9**	4.1	2.8	5.5	41	34	51	0.61	**10.0**	10.8	8.9	13.5	41	31	51	0.80	**8.5**
Ω_G	7.3	6.5	8.3	37	31	43	0.91	**5.1**	5.2	4.2	6.4	23	19	28	0.84	**7.0**	12.6	9.9	25.2	27	7	40	0.78	**10.5**
Ω_H	3.3	2.5	4.1	40	36	43	0.96	**4.1**	2.3	*	3.5	25	23	28	0.91	**5.3**	5.4	4.3	6.8	55	47	65	0.92	**6.9**
Ω_I	5.6	5.0	6.3	44	40	48	0.92	**5.0**	4.9	4.1	5.9	33	29	38	0.82	**6.9**	9.9	8.5	12.0	38	31	46	0.85	**8.0**
Ω_J	6.7	6.0	7.4	30	26	33	0.94	**3.1**	6.9	5.4	8.6	23	18	28	0.83	**5.3**	10.3	8.7	12.8	33	24	43	0.84	**5.8**
Ω_K	2.7	1.9	3.4	28	26	31	0.95	**3.8**	2.2	1.0	3.0	25	23	28	0.93	**4.4**	5.3	4.3	6.4	46	41	53	0.92	**5.7**
Ω_L	5.7	5.2	6.2	34	31	36	0.95	**2.6**	4.9	4.1	5.8	32	28	36	0.85	**4.9**	10.3	8.8	12.4	44	65	54	0.84	**6.6**
Ω_M	7.8	6.9	8.9	24	20	28	0.91	**4.0**	6.6	5.7	7.9	21	17	25	0.85	**5.1**	*	*	*	*	*	*	*	*
Ω_O	6.7	5.8	7.7	32	28	36	0.90	**4.8**	4.5	3.8	5.2	21	19	23	0.93	**3.4**	*	*	*	*	*	*	*	*
Ω_P	5.7	4.9	6.6	20	17	22	0.90	**4.1**	4.6	3.7	5.7	13	10	15	0.88	**4.0**	11.3	8.1	20.9	18	7	27	0.70	**9.4**
Ω_U	7.1	5.9	8.7	43	32	57	0.70	**8.7**	7.1	6.3	8.2	16	13	19	0.95	**2.9**	9.1	6.9	*	34	*	54	0.47	**12.7**

The predicted value of φ was plotted on the semi-log plot of the extraction kinetic data to confirm that the predicted value aligned with the change in slope between the two extraction regimes. Figure 6.6 shows the predicted point identified in dotted lines and the actual point identified in solid black lines. In a majority of the cases, the predicted value is well within 5% of the actual value. On occasion the predicted value of φ was not well aligned with the transition point in the kinetics. Figure 6.7 shows an example of where the predicted value and the actual value are approximately 10% different.

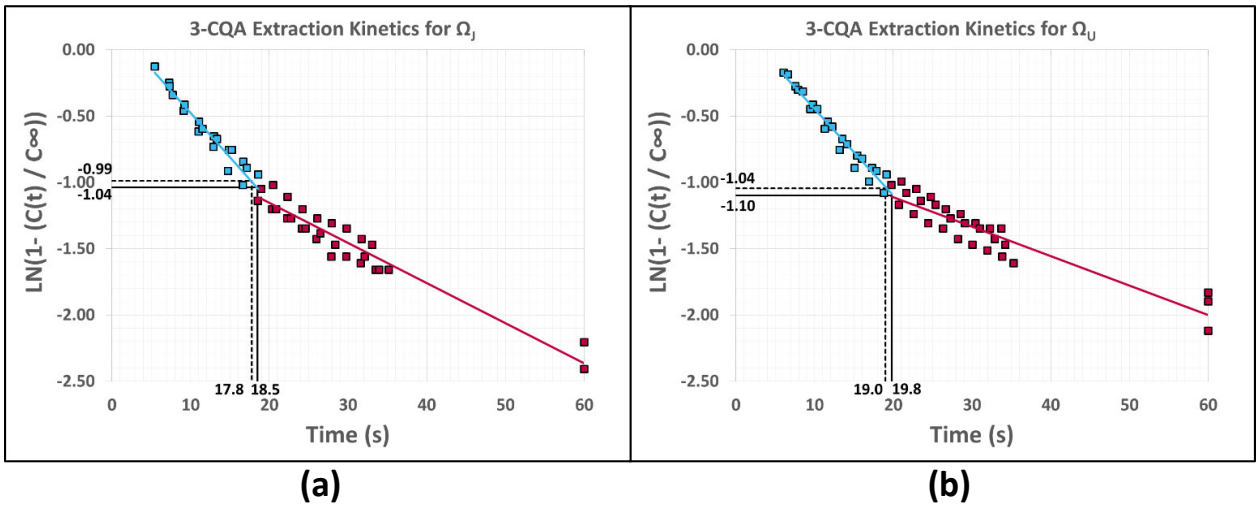

Figure 6.6: Predicted value of φ vs actual for (a) material Ω_J and (b) material Ω_U.

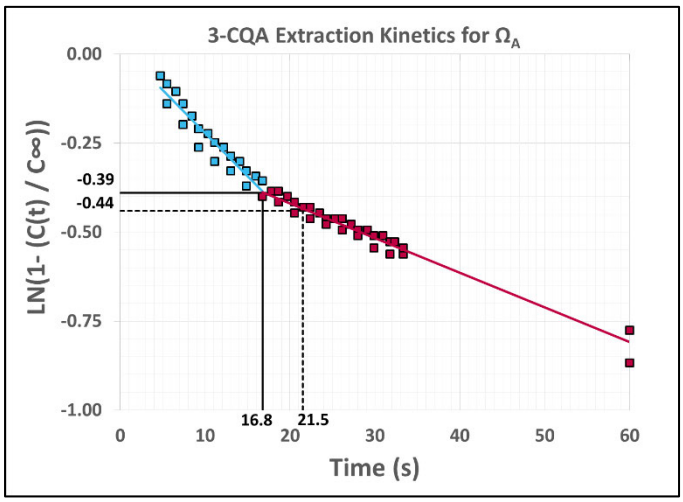

Figure 6.7: Predicted value of φ vs actual for material Ω_A.

Extraction kinetic data presented in chapter 5 are plotted with the respective models, represented in the dotted line, and the upper and lower confidence intervals in the solid lines. Figure 6.8 shows the extraction kinetics of coffee material Ω_A, Ω_B and Ω_C for 3-CQA and citric acid, with the model and confidence intervals.

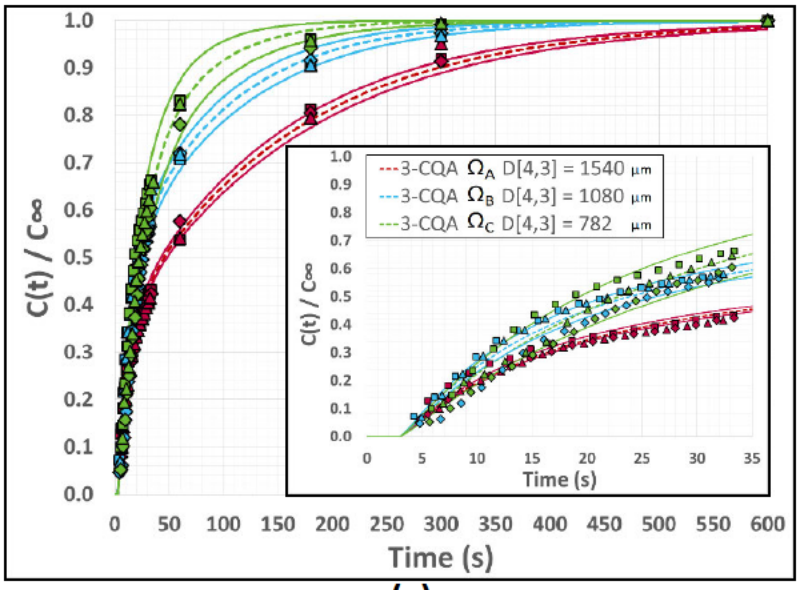

(a)

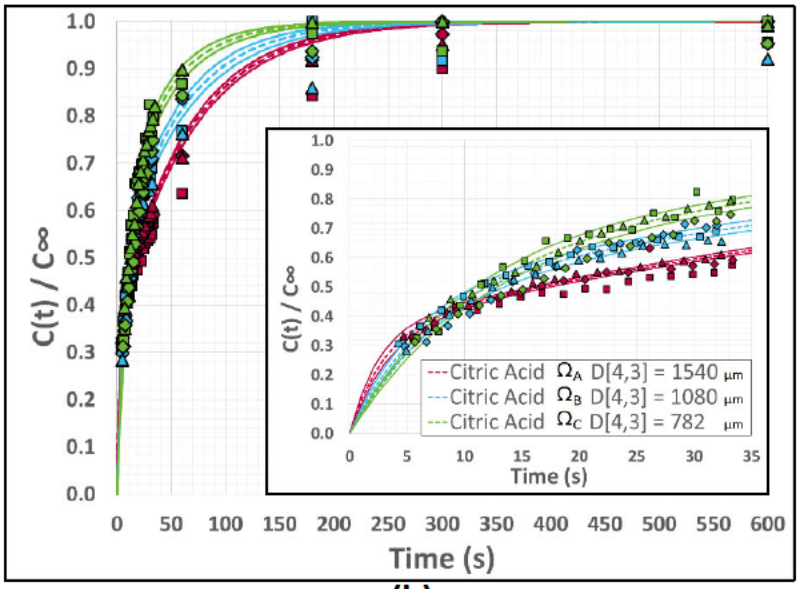

(b)

Figure 6.8: Extraction kinetics of [redacted] light roast, sieved coffee materials Ω_A, Ω_B and Ω_C for (a) 3-CQA and (b) citric acid with the model (dashed lines) and confidence intervals (solid lines).

The empirical model demonstrates a good fit for the three untreated coffee materials. The model fit for the 3-CQA data is excellent, with only minor over/under estimations occurring as specific times in material Ω_A, whereas the model for citric acid generally overestimates the extraction kinetic data at times beyond 60 s for all three materials.

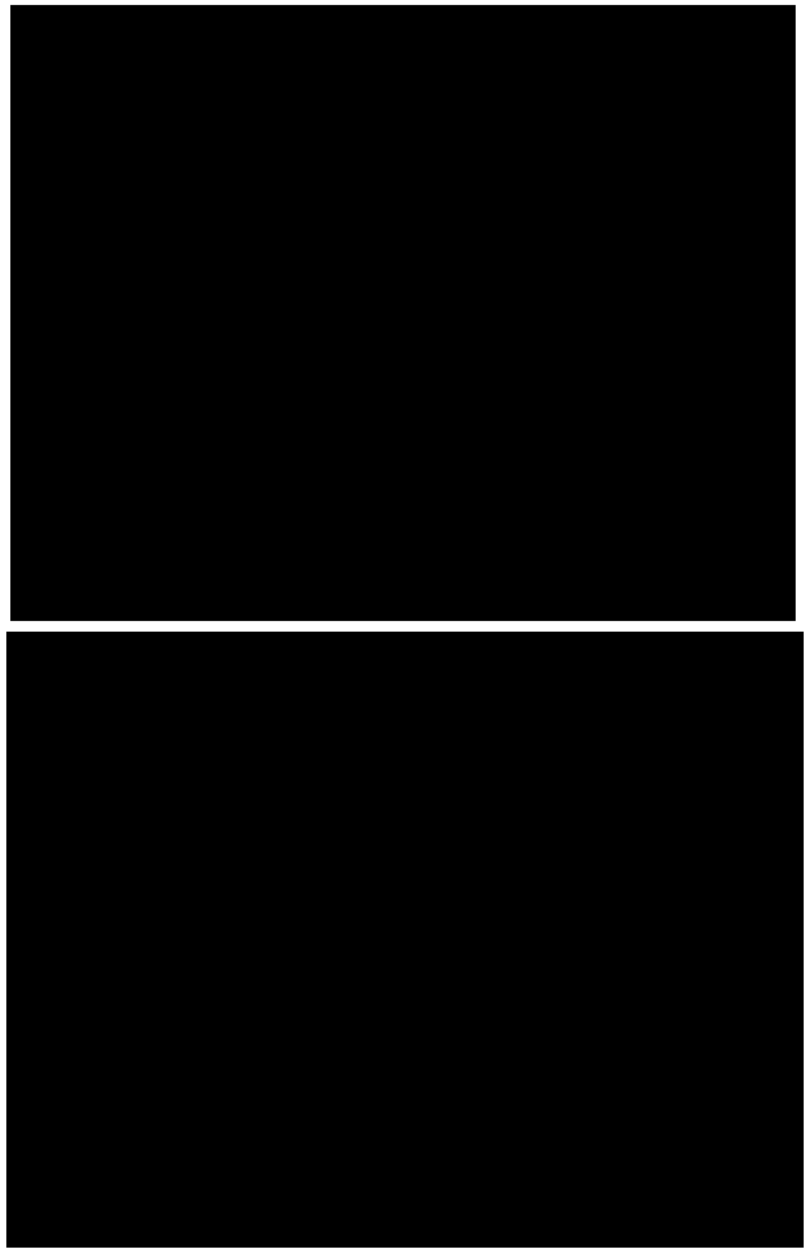

Figure 6.9:

[redacted]

Figure 6.10: [redacted]

[redacted]

[redacted]

[redacted]

[redacted]

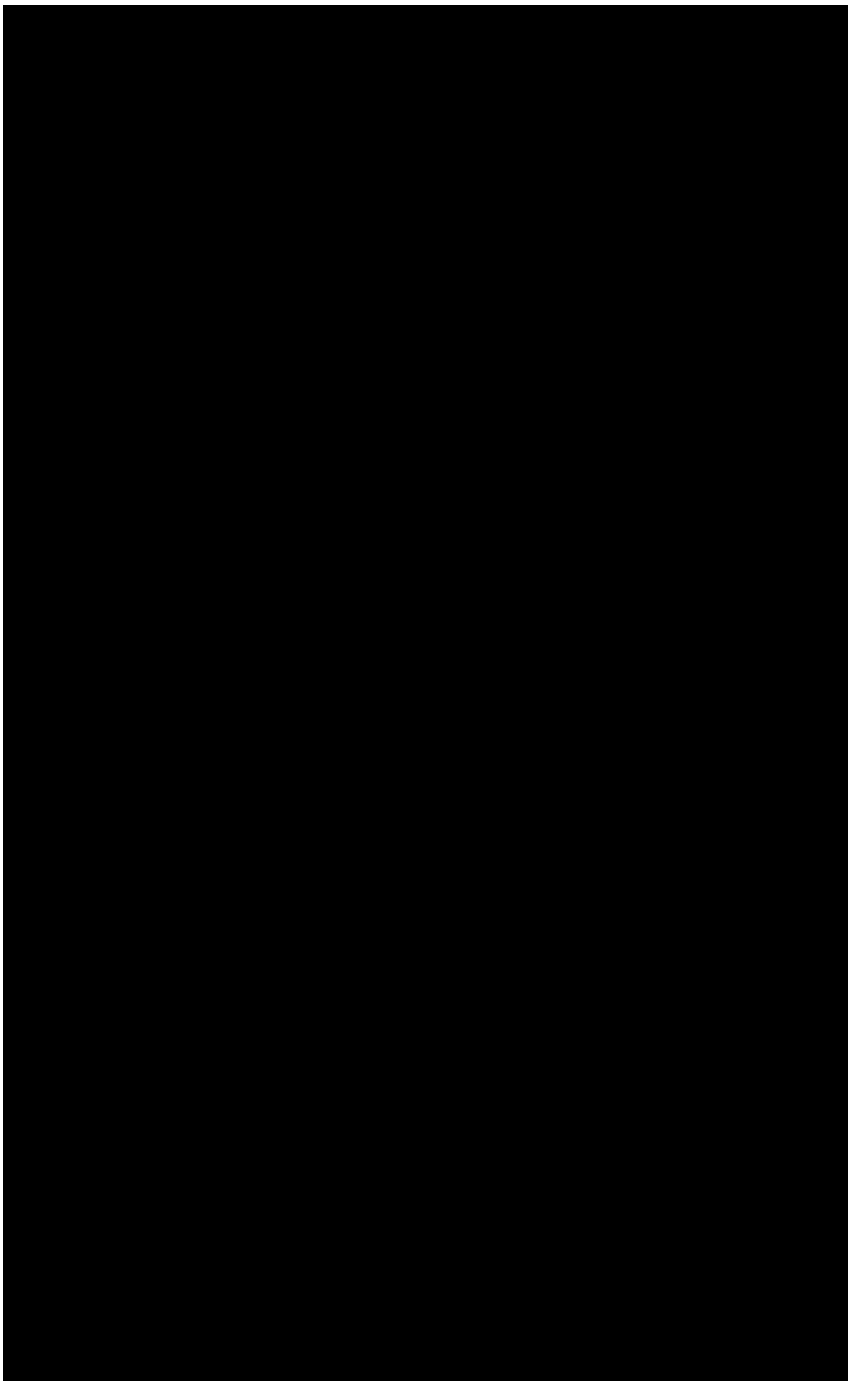

Figure 6.11: [redacted]

[redacted]

[redacted]

[redacted]

Figure 6.12: [redacted]

[redacted]

Table 6.6: [redacted]

[redacted]

[redacted]

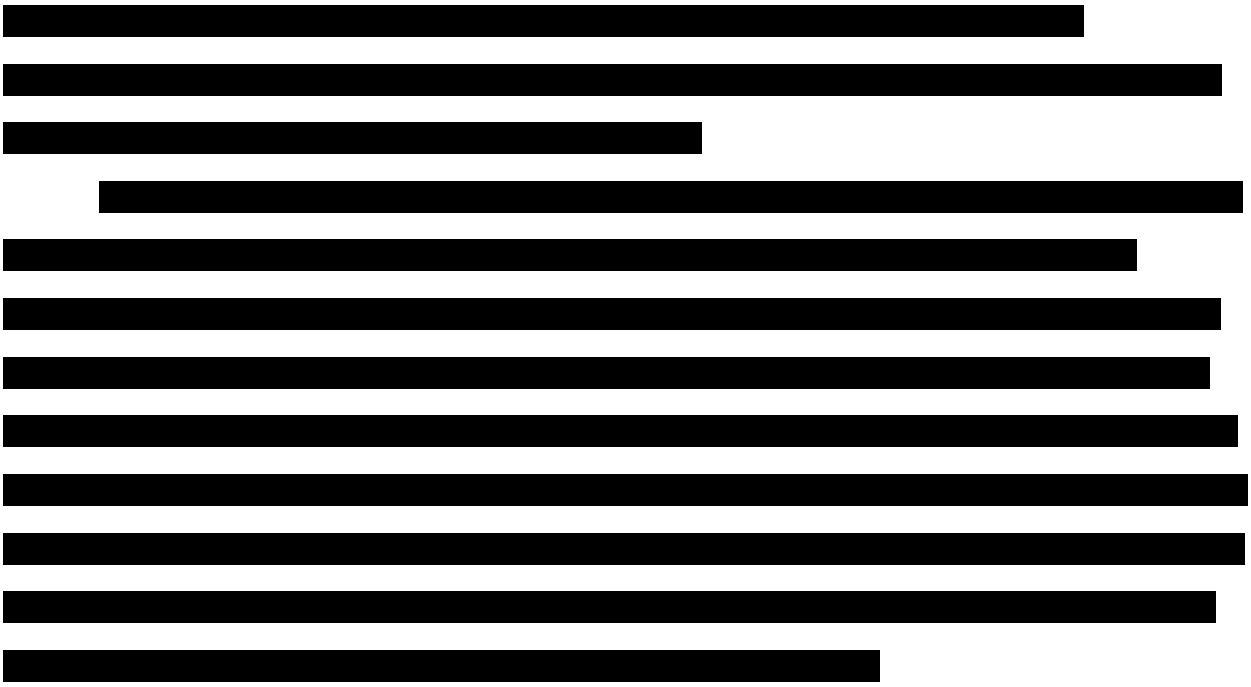

Across many of the aforementioned figures, several data points are outside of the 95% confidence intervals for each of the respective extraction kinetics models. This observation coupled with the slight overestimation in the citric acid could be due to fixing φ to a single value and not carrying through the error propagation from the particle size distribution measurements. If the particle size distribution error was propagated to the model, the 95% confidence interval for the model would broaden. Additionally, the error and difference from the φ calculation to the actual transition point in the data would result in either an overestimation or underestimation.

6.4: Comparison of Parameter Values and Physical Characterization

The two time constant model parameters were plotted against the treatments as well as specific raw material physical characterization values to evaluate the parameter value relationship with coffee material structure. Figure 6.13 are the plots of the two parameter estimates, λ_{fast} and λ_{slow}, for 3-CQA against the volume mean particle diameter, and the measured specific surface area for all modeled coffee materials.

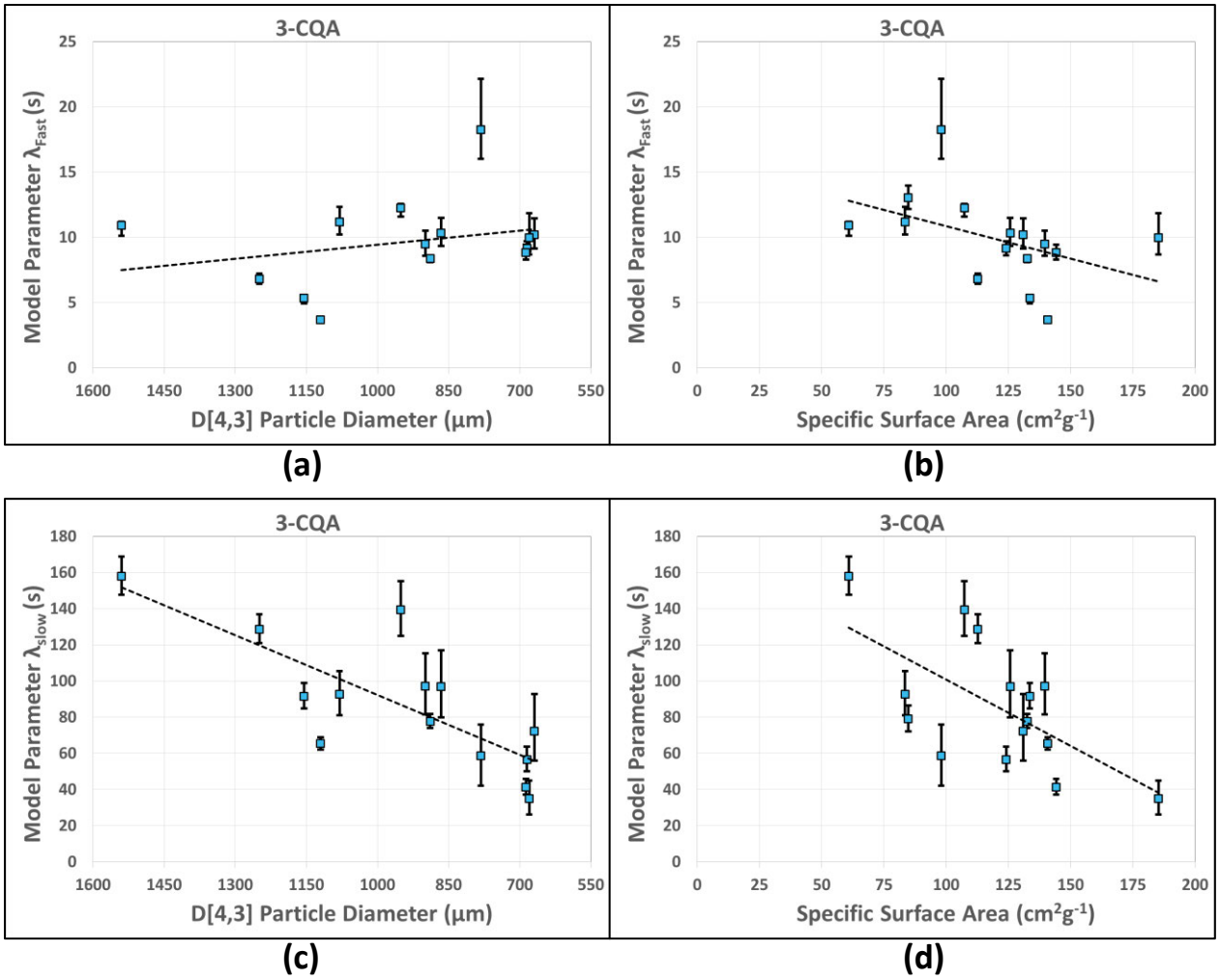

Figure 6.13: Parameter values for 3-CQA models vs physical characteristics. (a) λ_{fast} vs particle size, (b) λ_{fast} vs specific surface area, (c) λ_{slow} vs particle size and (d) λ_{slow} vs specific surface area.

The average value of λ_{fast} for 3-CQA is 9.8 s and the error bars in Figure 6.13 are representative of the 95% confidence interval for the parameter values. As presented in section 6.2.3, λ_{fast} does not have a strong relationship with either particle size or measured specific surface area, and is relatively constant across all materials as predicted. There is some variation in the parameter values of λ_{fast}, which is due to the spread of the data within individual materials and the error from the calculation of φ. The value of λ_{slow} for 3-CQA has a strong dependence on coffee structure as seen in Figure 6.13 (c) and (d), where λ_{slow} decreases by over 60% as particle size decreases from 1550 µm to just under 700 µm and as specific surface area increases from 60 $cm^2\,g^{-1}$ to 185 $cm^2\,g^{-1}$.

Parallel observations are seen in the model parameter values for citric acid. Figure 6.14 are the plots of the two parameter estimates, λ_{fast} and λ_{slow}, for citric acid versus the volume mean particle diameter, and the measured specific surface area. The average value of λ_{fast} is 5.7 s for citric acid. Figure 6.14 (a) shows a strong relationship of λ_{fast} to the mean particle size of materials, whereas no practical relationship exists between λ_{fast} and specific surface area in Figure 6.14 (b). The strong relationship observed in Figure 6.14 (a) is not aligned with the predicted independence between λ_{fast} and coffee structure.

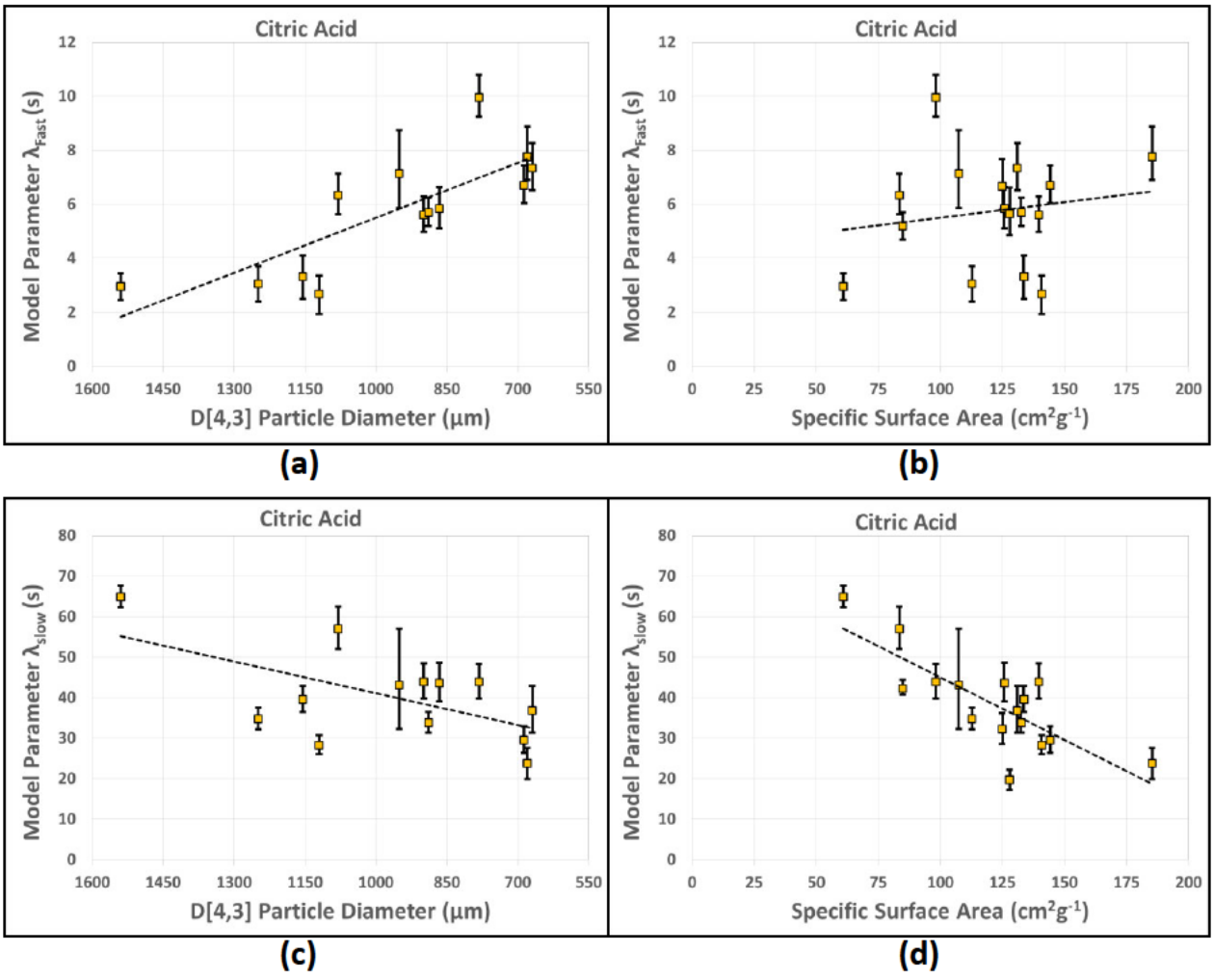

Figure 6.14: Parameter values for citric acid models vs physical characteristics. (a) λ_{fast} vs particle size, (b) λ_{fast} vs specific surface area, (c) λ_{slow} vs particle size and (d) λ_{slow} vs specific surface area.

Figure 6.15 is the plot of λ_{fast} parameter values for citric acid versus mean particle size, where materials Ω_A, Ω_E, Ω_H and Ω_K are plotted independent of the other materials. Further investigation of the values for λ_{fast} versus particle size for citric acid showed that the values for the coarsest particles, materials Ω_A, Ω_E, Ω_H and Ω_K, had much lower λ_{fast} values and were likely exhibiting leverage on the overall data set. When the coarsest materials are plotted independent of the other materials, the predicted independence of λ_{fast} and particle size is clear in both cohorts of materials, with only a weak relationship between λ_{fast} and coffee structure in the other materials. The average value for λ_{fast} in materials Ω_A, Ω_E, Ω_H and Ω_K is 3 s, whereas the remaining materials had an average value of 6.7 s.

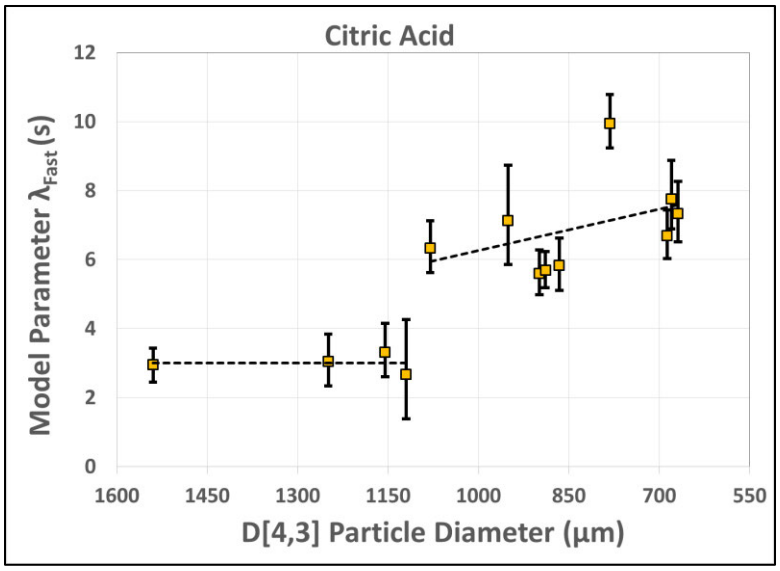

Figure 6.15: Figure 6.14(a) replotted into two distinct groups of materials.

The time constant for the slow extraction regime, λ_{slow} for citric acid also has a strong correlation on coffee structure as seen in Figure 6.14 (c) and (d), where λ_{slow} decreases by over 50% as particle size decreases and as specific surface area increases.

[redacted]

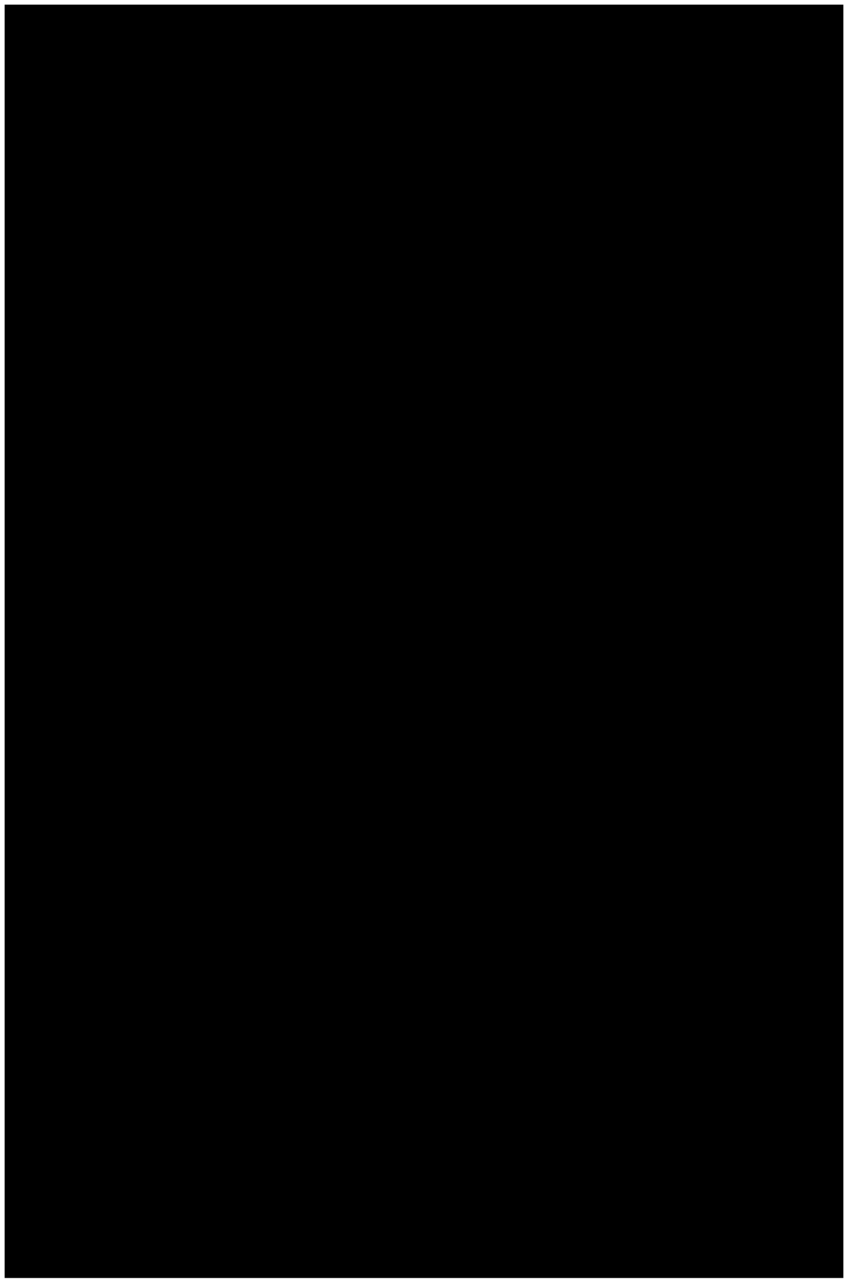

Figure 6.16: [redacted]

[redacted]

Figure 6.17: [redacted]

[redacted]

[redacted]

[redacted]

[redacted]

Figure 6.18: [redacted]

[redacted]

[redacted]

[redacted]

6.5: Conclusions

An empirical mathematical model of a sum of two exponentials was developed to describe the extraction kinetics of any chemical compound extracting from coffee in a well-mixed batch reactor. The model originated as a four parameter model comprised of two time constants, a time shift parameter to reflect observed delays in extraction, and a parameter identifying the transition between fast and slow extraction regimes for the chemical compound. The transition point between extraction regimes was successfully predicted by identifying the total volume fraction contributing to each regime. This total volume fraction is based on the data from the measured particle size distribution of the coffee.

The empirical model fits generally had excellent agreement with the observed data with mean percent errors of less than 10% across all five chemical compounds. The values of the time constants, the correlation (or lack thereof) with physical measurements of the material, aligned well with the physical and conceptual understanding of the coffee extraction process in a well-mixed batch reactor.

In most cases there was no relationship between the physical structure of the material and the fast extraction time constant as predicted. Strong dependencies were found between coffee structure and the slow extraction time constant parameter[redacted]

These results provide a high degree of confidence in the value and application of the empirical model developed in this body of work. This model has demonstrated that it can be

used to measure the efficacy of various coffee treatments aimed at altering extraction kinetics.

[redacted]

Chapter 7: Conclusions and Future Work

There are no previously developed experimental methods which could fundamentally measure and capture the efficacy of various coffee processing treatments on roast and ground coffee, and their effects on coffee extraction at time scales under 60 seconds.

7.1: Major Conclusions

A well-mixed batch reactor coupled to an automated sample splitter provided a robust and very repeatable method to sample extraction kinetics of brewed coffee at time scales between 5 - 30 s and beyond. The sample aliquots collected were analyzed for specific chemical compound concentrations, yielding a time resolved extraction curve for five individual chemical compounds. Two distinct coffee extraction regimes were present for each compound, and future models of coffee extraction should reflect these two regimes going forward.

Individual chemical compounds with nearly identical molecular weights have vastly different extraction kinetics as exhibited by the caffeine and citric acid extraction curves. These kinetic differences were likely due to chemical structure and the specific functional groups of these compounds. Effective diffusivities calculated by fitting models to extraction data solely

grouped by molecular weight, or any other lumped parameter would not appropriately capture the behavior of important, individual chemical compound extraction kinetics.

Caffeine and 3-CQA exhibited a delay in extraction, an observation that has not been reported previously. Moreover, the extraction kinetics of citric and malic acid revealed that up to 50% of the absolute citric acid concentration and 60% of the absolute malic acid concentration was extracted within 10 s in regular roast and ground coffee. These results clearly identify the importance of understanding early extraction kinetics and were obtained as a direct result of the uniquely developed well–mixed batch reactor extraction system.

An empirical model comprised of the sum of two, first order exponentials weighted by the concentration contribution from the two extraction regimes fitted to the experimental data yielded an excellent representation of the extraction kinetics with mean percent errors under 10% for all five chemical compounds modeled. The empirical model effectively described the important early time scale extraction kinetics, which previously published, single-term diffusion models failed to capture.

7.2: Future Work

7.2.1: Improvements to the Extraction System and Method

The work in this thesis established a robust, initial prototype to continuously sample coffee during an extraction event in a well-mixed system extraction, but it did have some limitations. Further refinements to improve the precision of the extraction setup include:

1) Improving the accuracy of the time measurement from the initial drop of the coffee into the WMBR when the slide gate opens, to the time the first sample is collected.
2) Consideration of adopting a linear track of test tubes on a belt conveyor to collect aliquots of sample. The setup employed was limited to 16 test tubes and fixed RPM intervals built into the rotary sample splitter. A belt conveyor with multiple test tubes could also collect aliquots at a variable rate, and it would be much easier to expand the number of collection tubes in a linear direction, whereas a rotary system the diameter is the limiting dimension. Moreover, the use of photogates or similar sensors could capture all relevant times of start, beginning of collection, and each collection time of each test tube. This would improve the temporal resolution and accuracy.
3) Upgrading the coffee hopper to be a stainless-steel mass flow hopper intentionally designed for the flow properties of finer, more cohesive coffee grinds. The extraction system is currently limited to more granular, free flowing coffee grinds.
4) It was observed in early extraction rig design process that the coffee would occasionally float on the surface of the water as it struggled to be completely entrained in the agitated liquid. One option could include adding a surfactant to the water to promote the wetting of the coffee powder upon initial contact. A small amount of Isopropyl alcohol was used in the liquid dispersion particle size measurements for this exact problem. Caution would need to be exercised in the selection of an appropriate surfactant, so as to not interfere with the chemical analysis of the coffee extract.

7.2.2: Additional WMBR Extraction Studies

The compounds studied in this body of work were relatively limited to a narrow range of molecular weights. It would be useful to study the time-resolved kinetics of larger compounds with slower diffusion rates. [redacted]

Furthermore, expanding upon the research presented in this work, studying coffee extraction at commercial cold brew processing temperatures could provide significant value into improving and formulating ready-to drink coffees and coffee concentrates for commercial use, as many commercial processing units are large continuously stirred batch reactors. Moreover, the application and viability of the empirical model needs to be challenged with higher coffee to water ratios. Higher ratios are more representative of ready-to-drink manufacturing (~5% coffee to water) and coffee concentrate manufacturing (15-20% coffee to water).

7.2.3: [redacted]

[redacted]

7.2.4: [redacted]

[redacted]

Figure 7.1:

Figure 7.2:

[redacted]

Appendix A: Corrected System Concentration Calculations

The WMBR experiments constantly remove liquid extract during the sampling process which increases the measured concentration of the system during the experiment. The system concentration needs to be corrected at each sample time to account for the volume removed. This correction requires the calculation of the absolute mass of the chemical compound at each specific sample time.

The volume of liquid in the system at sample time t_j is:

$$V_{sys,j} = V_{sys,0} - \sum_{i=1}^{j-1} V_{aliquot,i} \quad Eqn\ A.1$$

Where

$$V_{aliquot,0} = 0 \quad Eqn\ A.2$$

$$\therefore V_{sys,1} = V_{sys,0} \quad Eqn\ A.3$$

$V_{sys,0}$ is the total volume of liquid in the WMBR at the start of the experiment, and $V_{aliquot,i}$ is the volume of the liquid aliquot removed previously at interval i. The system volume at the first sample time is equal to $V_{sys,0}$ (equation A.3) as no previous aliquot is removed.

The absolute mass of a chemical compound in the system at sample time t_j is:

$$m_{sys,j} = (C_{aliquot,j})(V_{sys,j}) + \sum_{i=1}^{j-1} (C_{aliquot,i} * V_{aliquot,i}) \quad Eqn\ A.4$$

Where

$$C_{aliquot,0} = 0 \quad Eqn\ A.5$$

Where $C_{aliquot,j}$ is the measured chemical compound concentration of the aliquot removed and $C_{aliquot,i}$ is the concentration of the liquid aliquot removed at each interval preceding t_j.

The corrected concentration of a chemical compound in the system at sample time t_j is:

$$C_{sys,j} = \left((C_{aliquot,j})(V_{sys,j}) + \sum_{i=1}^{j-1} (C_{aliquot,i} * V_{aliquot,i}) \right) \Big/ V_{sys,0} \quad for\ 1 \leq j \leq 20 \quad Eqn\ A.6$$

Appendix B: Time Correction of Aliquot Samples

The volume of the first aliquot collected with the rotary sample splitter is often not the same volume obtained during the steady state sampling of the subsequent aliquots. This is due to two factors, the first is the initial position of the sample tube relative to the first test tube in the sample splitter. The second factor is when the rotary sample splitter is turned on (too early or too late). These two factors could result in an initial aliquot volume being smaller or larger than the steady state sampling volumes, which means the sample time of when the aliquot is collected is not equal to the number of test tubes divided by the rotational rate. The volume of the last aliquot obtained is similarly compromised if the air pressure to the WMBR is shut off prematurely or too late. This error would also result in the volume of the last aliquot being lower than steady state flow (premature shut off) or larger than steady state flow (too late) being collected. The average volume of aliquots removed during steady state flow and sampling is:

$$V_{ss} = \sum_{i=3}^{14} V_{aliquot,i} \Big/ 11 \quad Eqn\ B.1$$

The corrected sample time for the first aliquot collected with the rotary sample splitter is:

$$t_{1,corrected} = t_0 + \left(1.88 * \left(V_{aliquot,1} / V_{ss}\right)\right) \quad Eqn\ B.2$$

Where t_0 is the measured time from adding the coffee to the WMBR and flow first flowing out of the sampling tube, $V_{aliquot,1}$ is the volume of the first aliquot removed, and V_{ss} is the average volume of aliquots removed during steady state flow and sampling.

The corrected sample times for the 2nd to the 15th aliquots are:

$$t_{i,corrected} = t_1 + \left(1.88 * (i-1)\right) \quad Eqn\ B.3$$

Where

$$i \in \mathbb{Z} : 2 \leq i \leq 15$$

The corrected sample time for the last aliquot collected with the rotary sample splitter is:

$$t_{16,corrected} = t_{15,corrected} + \left(1.88 * \left(\left(V_{aliquot,16} / V_{ss}\right)\right)\right) \quad Eqn\ B.4$$

References

Adrian, D. (2007). Course materials for 10.37 Chemical and Biological Reaction Engineering, Spring 2007. MIT OpenCourseWare (http://ocw.mit.edu), Massachusetts Institute of Technology. Downloaded on [24 January 2022].

Allen, T. (1997a). Particle size measurement: Volume 1: Powder sampling and particle size measurement. 5th Ed. Chapman & Hall.

Allen, T. (1997b). Particle size measurement: Volume 2: Surface area and pore size determination. 5th Ed. Chapman & Hall.

Angeloni, G., Guerrini, L., Masella, P., Bellumori, M., Daluiso, S., Parenti, A., & Innocenti, M. (2019). What kind of coffee do you drink? An investigation on effects of eight different extraction methods. Food research international, 116, 1327-1335.

Bichsel, B. (1979). Diffusion phenomena during the decaffeination of coffee beans. Food Chemistry, 4(1), 53-62.

Buffo, R. A., & Cardelli-Freire, C. (2004). Coffee flavour: an overview. Flavour and fragrance journal, 19(2), 99-104.

Bustos-Vanegas, J. D., Corrêa, P. C., Martins, M. A., Baptestini, F. M., Campos, R. C., de Oliveira, G. H. H., & Nunes, E. H. M. (2018). Developing predictive models for determining physical properties of coffee beans during the roasting process. Industrial crops and products, 112, 839-845.

Calderone, J. (2016, March 8). The Science Behind Why Pod Coffee Tastes So Bad. Retrieved September 2019 from https://www.businessinsider.com/why-instant-coffee-machines-taste-gross-2016-3

Clarke, R. J. (Ed.). (2012a). Coffee: Volume 1: Chemistry. Springer Science & Business Media.

Clarke, R. J. (Ed.). (2012b). Coffee: Volume 2: Technology (Vol. 2). Springer Science & Business Media.

Corrochano, B. R., Melrose, J. R., Bentley, A. C., Fryer, P. J., & Bakalis, S. (2015). A new methodology to estimate the steady-state permeability of roast and ground coffee in packed beds. Journal of food engineering, 150, 106-116.

Crank, J. (1975). The mathematics of diffusion 2nd Edition. Oxford Science Publications, 32.

De Melo, M. M. R., Silvestre, A. J. D., & Silva, C. M. (2014). Supercritical fluid extraction of vegetable matrices: applications, trends and future perspectives of a convincing green technology. The Journal of Supercritical Fluids, 92, 115-176.

Del Valle, J. M., Germain, J. C., Uquiche, E., Zetzl, C., & Brunner, G. (2006). Microstructural effects on internal mass transfer of lipids in prepressed and flaked vegetable substrates. The Journal of supercritical fluids, 37(2), 178-190.

DeWitt, D. P., Incropera, F. P., Bergman, T. L., & Lavine, A. S. (2007). Fundamentals of Heat and Mass Transfer 6th Edition. John Wiley.

E. E. Lockhart, C. L. Tucker, M. C. Merritt, (Manuscript received June 21, 1955). Presented at the Fifteenth Annual Meeting of the IFT, Columbus, Ohio, June 13, 1955. Contribution No. 264 from the Department of Food Technology, Massachusetts Institute of Technology. Coffee Brewing Institute, Inc., New York, N. Y.

Espinoza-Pérez, J. D., Vargas, A., Robles-Olvera, V. J., Rodrı, G. C., & Garcı, M. A. (2007). Mathematical modeling of caffeine kinetic during solid–liquid extraction of coffee beans. Journal of Food Engineering, 81(1), 72-78.

Farah, A., & dos Santos, T. F. (2015). The coffee plant and beans: An introduction. In Coffee in health and disease prevention (pp. 5-10). Academic Press.

Farah, A., de Paulis, T., Trugo, L. C., & Martin, P. R. (2005). Effect of roasting on the formation of chlorogenic acid lactones in coffee. Journal of Agricultural and Food Chemistry, 53(5), 1505-1513.

Farah, A., Monteiro, M. C., Calado, V., Franca, A. S., & Trugo, L. C. (2006). Correlation between cup quality and chemical attributes of Brazilian coffee. Food Chemistry, 98(2), 373-380.

Fiori, L., Basso, D., & Costa, P. (2009). Supercritical extraction kinetics of seed oil: A new model bridging the 'broken and intact cells' and the 'shrinking-core'models. The Journal of Supercritical Fluids, 48(2), 131-138.

Frisullo, P., Laverse, J., Barnabà, M., Navarini, L., & Del Nobile, M. A. (2012). Coffee beans microstructural changes induced by cultivation processing: An X-ray microtomographic investigation. Journal of food engineering, 109(1), 175-181.

Fuller, M., & Rao, N. Z. (2017). The effect of time, roasting temperature, and grind size on caffeine and chlorogenic acid concentrations in cold brew coffee. Scientific reports, 7(1), 17979.

Geiger, R. (2004). Development of coffee bean structure during roasting-Investigations on resistance and driving forces (Doctoral dissertation, ETH Zurich).

Geiger, R., Perren, R., Kuenzli, R., & Escher, F. (2005). Carbon dioxide evolution and moisture evaporation during roasting of coffee beans. Journal of food science, 70(2), E124-E130.

[redacted]

Gloess, A. N., Schönbächler, B., Klopprogge, B., Lucio, D., Chatelain, K., Bongartz, A., ... & Yeretzian, C. (2013). Comparison of nine common coffee extraction methods: instrumental and sensory analysis. European Food Research and Technology, 236(4), 607-627.

Gonzalez, A. (2014, February 15). Single-serve coffee revolution brews industry change. Retrieved September 2019 from https://www.seattletimes.com/business/single-serve-coffee-revolution-brews-industry-change/

Goto, M., Roy, B. C., & Hirose, T. (1996). Shrinking-core leaching model for supercritical-fluid extraction. The Journal of Supercritical Fluids, 9(2), 128-133.

[redacted]

Hargarten, V. B., Kuhn, M., & Briesen, H. (2020). Swelling properties of roasted coffee particles. Journal of the Science of Food and Agriculture, 100(10), 3960-3970.

[redacted]

Hill, M. (2014, September 15). The Cost of a Cup of Coffee: Where Does the Money Go? Retrieved September 2019 from https://scanews.coffee/2014/09/15/the-cost-of-a-cup-of-coffee-where-does-the-money-go-2/

ISO 6673. (2003). Green coffee: determination of loss in mass at 105 °C.

Jaganyi, D., & Madlala, S. P. (2000). Kinetics of coffee infusion: a comparative study on the extraction kinetics of mineral ions and caffeine from several types of medium roasted coffees. Journal of the Science of Food and Agriculture, 80(1), 85-90.

Jeon, J. S., Kim, H. T., Jeong, I. H., Hong, S. R., Oh, M. S., Park, K. H., ... & El-Aty, A. A. (2017). Determination of chlorogenic acids and caffeine in homemade brewed coffee prepared under various conditions. Journal of Chromatography B, 1064, 115-123.

[redacted]

Johnston, G. P., Smith, D. M., Melendez, I., & Hurd, A. J. (1990). Compression effects in mercury porosimetry. Powder technology, 61(3), 289-294.

Juma, C. (2016). Innovation and its enemies: Why people resist new technologies. Oxford University Press.

Kassing, M., Jenelten, U., Schenk, J., & Strube, J. (2010). A new approach for process development of plant-based extraction processes. Chemical Engineering & Technology: Industrial Chemistry-Plant Equipment-Process Engineering-Biotechnology, 33(3), 377-387.

[redacted]

Kestin, J., Sokolov, M., & Wakeham, W. A. (1978). Viscosity of liquid water in the range− 8 C to 150 C. Journal of physical and chemical reference data, 7(3), 941-948.

Kuhn, M., Lang, S., Bezold, F., Minceva, M., & Briesen, H. (2017). Time-resolved extraction of caffeine and trigonelline from finely-ground espresso coffee with varying particle sizes and tamping pressures. Journal of Food Engineering, 206, 37-47.

Lee, T. A., Kempthorne, R., & Hardy, J. K. (1992). Compositional changes in brewed coffee as a function of brewing time. Journal of food science, 57(6), 1417-1419.

Lingle, T. R. (2011). The coffee brewing handbook: a systematic guide to coffee preparation. Specialty Coffee Association of America.

Litster, J. (2016). Design and processing of particulate products. Cambridge University Press.

[redacted]

Ludwig, I. A., Sanchez, L., Caemmerer, B., Kroh, L. W., De Peña, M. P., & Cid, C. (2012). Extraction of coffee antioxidants: Impact of brewing time and method. Food Research International, 48(1), 57-64.

Maille, M. J., Sala, K., Scott, D. M., & Zukswert, H. (2021). Critical examination of particle swelling during wetting of ground coffee. Journal of Food Engineering, 295, 110420.

[redacted]

Markets and Research (2024, March 22). Global Coffee Analysis Report 2024: Market to Reach $161.66 Billion by 2030 from $116.14 Billion in 2023, Driven by Coffee's Evolution into a Beverage Revolution. Retrieved April 16, 2024 from https://www.prnewswire.com/news-releases/global-coffee-analysis-report-2024-market-to-reach-161-66-billion-by-2030-from-116-14-billion-in-2023--driven-by-coffees-evolution-into-a-beverage-revolution-302095855.html

Masella, P., Guerrini, L., Spinelli, S., Calamai, L., Spugnoli, P., Illy, F., & Parenti, A. (2015). A new espresso brewing method. Journal of food engineering, 146, 204-208.

Masoodi, R., & Pillai, K. M. (Eds.). (2012). Wicking in porous materials: traditional and modern modeling approaches. Crc Press.

Mateus, M. L., Rouvet, M., Gumy, J. C., & Liardon, R. (2007). Interactions of water with roasted and ground coffee in the wetting process investigated by a combination of physical determinations. Journal of agricultural and food chemistry, 55(8), 2979-2984.

Matthews, G. P. (2010). Analytical Report FR1002301 Mercury Porosimetry of certified Silica-Alumina reference material Micromeritics P/N004/16822/00. In M. Foulkes & G. P. Matthews, University of Plymouth (pp. 1–8). https://www.porexpert.com/docs/Example%20ISO9001%20report.pdf

McMurry, J. (2008). Organic chemistry. 7e. Thomson Brooks/Cole.

[redacted]

Melrose, J., Roman-Corrochano, B., Montoya-Guerra, M., & Bakalis, S. (2018). Toward a new brewing control chart for the 21st century. Journal of agricultural and food chemistry, 66(21), 5301-5309.

Melrose, J. R., Corrochano, B., & Bakalis, S. (2019). Polydisperse diffusion kinetics of Coffee Brewing-modelling batch data. Pre-print: www.reserachgate.com under John Melrose, Coffee Brewing project. DOI, 10.

Mestdagh, F., Glabasnia, A., & Giuliano, P. (2017). The brew—Extracting for excellence. In The craft and science of coffee (pp. 355-380). Academic Press.

Moeenfard, M., Erny, G. L., & Alves, A. (2016). Variability of some diterpene esters in coffee beverages as influenced by brewing procedures. Journal of food science and technology, 53(11), 3916-3927.

Moroney, K. M., Lee, W. T., Suijver, F., & Marra, J. (2015). Modelling of coffee extraction during brewing using multiscale methods: An experimentally validated model. Chemical Engineering Science, 137, 216-234.

Moroney, K. M., Lee, W. T., O'Brien, S. B., Suijver, F., & Marra, J. (2016). Coffee extraction kinetics in a well mixed system. Journal of mathematics in industry, 7(1), 3.

National Center for Biotechnology Information (2023). PubChem Compound Summary for CID 2519, Caffeine. Retrieved November 21, 2023 from https://pubchem.ncbi.nlm.nih.gov/compound/Caffeine.

National Center for Biotechnology Information (2023). PubChem Compound Summary for CID 1794427, Chlorogenic Acid. Retrieved November 21, 2023 from https://pubchem.ncbi.nlm.nih.gov/compound/Chlorogenic-Acid.

National Center for Biotechnology Information (2023). PubChem Compound Summary for CID 311, Citric Acid. Retrieved November 21, 2023 from https://pubchem.ncbi.nlm.nih.gov/compound/Citric-Acid.

National Center for Biotechnology Information (2023). PubChem Compound Summary for CID 525, Malic Acid. Retrieved November 21, 2023 from https://pubchem.ncbi.nlm.nih.gov/compound/Malic-Acid.

National Center for Biotechnology Information (2023). PubChem Compound Summary for CID 6508, Quinic acid. Retrieved November 21, 2023 from https://pubchem.ncbi.nlm.nih.gov/compound/Quinic-acid.

National Coffee Association of U.S.A. (2024). 2024 National Coffee Data Trends Spring Report.

Navarini, L., & Rivetti, D. (2010). Water quality for Espresso coffee. Food chemistry, 122(2), 424-428.

Nicoli, M. C., Rosa, M. D., & Lerici, C. R. (1990). Influence of some processing conditions on solid-liquid extraction of coffee. Lebensmittel-Wissenschaft+ Technologie= Food science+ technology.

Oliveira, E. L., Silvestre, A. J., & Silva, C. M. (2011). Review of kinetic models for supercritical fluid extraction. Chemical Engineering Research and Design, 89(7), 1104-1117.

Oliveros, N. O., Hernández, J. A., Sierra-Espinosa, F. Z., Guardián-Tapia, R., & Pliego-Solórzano, R. (2017). Experimental study of dynamic porosity and its effects on simulation of the coffee beans roasting. Journal of Food Engineering, 199, 100-112.

Oshita, S., Hashimoto, A., Miyata, T., & Okado, T. (1994). Extraction Rate for Soluble Solids During Coffee Brewing. In Developments in Food Engineering (pp. 361-363). Springer, Boston, MA.

Palzer, S. (2011). Agglomeration of pharmaceutical, detergent, chemical and food powders—similarities and differences of materials and processes. Powder technology, 206(1), 2-17.

Parenti, A., Guerrini, L., Masella, P., Spinelli, S., Calamai, L., & Spugnoli, P. (2014). Comparison of espresso coffee brewing techniques. Journal of Food Engineering, 121, 112-117.

Perrone, D., Donangelo, C. M., & Farah, A. (2008a). Fast simultaneous analysis of caffeine, trigonelline, nicotinic acid and sucrose in coffee by liquid chromatography–mass spectrometry. Food chemistry, 110(4), 1030-1035.

Perrone, D., Donangelo, R., Donangelo, C. M., & Farah, A. (2010). Modeling weight loss and chlorogenic acids content in coffee during roasting. Journal of agricultural and food chemistry, 58(23), 12238-12243.

Perrone, D., Farah, A., Donangelo, C. M., de Paulis, T., & Martin, P. R. (2008b). Comprehensive analysis of major and minor chlorogenic acids and lactones in economically relevant Brazilian coffee cultivars. Food Chemistry, 106(2), 859-867.

Pittia, P., Dalla Rosa, M., & Lerici, C. R. (2001). Textural changes of coffee beans as affected by roasting conditions. LWT-Food Science and Technology, 34(3), 168-175.

Pittia, P., Sacchetti, G., Mancini, L., Voltolini, M., Sodini, N., Tromba, G., & Zanini, F. (2011). Evaluation of Microstructural Properties of Coffee Beans by Synchrotron X-Ray Microtomography: A Methodological Approach. Journal of food science, 76(2), E222-E231.

Povey, M. J., Holmes, M. J., Rafiq, S., Simone, E., Rappolt, M., & Francis, M. (2020). Physics in Food Manufacturing: Case studies in fundamental and applied research. IOP Publishing.

Rajagopalan, R., & Hiemenz, P. C. (1997). Principles of colloid and surface chemistry. Marcel Dekker, New-York, 8247, 8.

Rao, S. (2014). The coffee roaster's companion. Scott Rao.

Reis, N., Vicente, A. A., & Teixeira, J. A. (2010). Liquid backmixing in oscillatory flow through a periodically constricted meso-tube. Chemical Engineering and Processing: Process Intensification, 49(7), 793-803.

Reverchon, E., & Marrone, C. (2001). Modeling and simulation of the supercritical CO2 extraction of vegetable oils. The Journal of Supercritical Fluids, 19(2), 161-175.

Rhodes, M. J. (Ed.). (2008). Introduction to particle technology. John Wiley & Sons.

Robards, A. W., & Lucas, W. J. (1990). Plasmodesmata. Annual review of plant biology, 41(1), 369-419.

Roman Corrochano, B. (2017). Advancing the engineering understanding of coffee extraction (Doctoral dissertation, University of Birmingham).

Sage, E. (2013, July 8). Dissecting SCAA's Water Quality Standard. Retrieved September 2019 from https://scanews.coffee/2013/07/08/dissecting-scaas-water-quality-standard/

Salamanca, C. A., Fiol, N., González, C., Saez, M., & Villaescusa, I. (2017). Extraction of espresso coffee by using gradient of temperature. Effect on physicochemical and sensorial characteristics of espresso. Food chemistry, 214, 622-630.

Samoggia, A., & Riedel, B. (2018). Coffee consumption and purchasing behavior review: Insights for further research. Appetite, 129, 70-81.

Sano, Y., Kubota, S., Kawarazaki, A., Kawamura, K., Kashiwai, H., & Kuwahara, F. (2019). Mathematical model for coffee extraction based on the volume averaging theory. Journal of food engineering, 263, 1-12.

Schenker, S., Handschin, S., Frey, B., Perren, R., & Escher, F. (2000). Pore structure of coffee beans affected by roasting conditions. Journal of Food Science, 65(3), 452-457.

Scott, D. M. (2019). Interpreting Laser Diffraction Results for Non-Spherical Particles. Horiba Webinar Series.

Severa, L., Buchar, J., & Nedomová, Š. (2012). Shape and size variability of roasted Arabica coffee beans. International Journal of Food Properties, 15(2), 426-437.

[redacted]

Singh, P. C., Singh, R. K., Bhamidipati, S., Singh, S. N., & Barone, P. (1997). Thermophysical Properties of Fresh and Roasted Coffee Powders 1. Journal of food process engineering, 20(1), 31-50.

[redacted]

Sovová, H. (2017). Broken-and-intact cell model for supercritical fluid extraction: Its origin and limits. The Journal of Supercritical Fluids, 129, 3-8.

Spiro, M. (1993). Modelling the aqueous extraction of soluble substances from ground roast coffee. Journal of the Science of Food and Agriculture, 61(3), 371-372.

Spiro, M., & Chong, Y. Y. (1997). The kinetics and mechanism of caffeine infusion from coffee: the temperature variation of the hindrance factor. Journal of the Science of Food and Agriculture, 74(3), 416-420.

Spiro, M., & Hunter, J. E. (1985). The kinetics and mechanism of caffeine infusion from coffee: the effect of roasting. Journal of the Science of Food and Agriculture, 36(9), 871-876.

Spiro, M., & Page, C. M. (1984). The kinetics and mechanism of caffeine infusion from coffee: hydrodynamic aspects. Journal of the Science of Food and Agriculture, 35(8), 925-930.

Spiro, M., & Selwood, R. M. (1984). The kinetics and mechanism of caffeine infusion from coffee: the effect of particle size. Journal of the Science of Food and Agriculture, 35(8), 915-924.

Spiro, M., Toumi, R., & Kandiah, M. (1989). The kinetics and mechanism of caffeine infusion from coffee: the hindrance factor in intra-bean diffusion. Journal of the Science of Food and Agriculture, 46(3), 349-356.

Stapley, A. G. F. (2002). Modelling the kinetics of tea and coffee infusion. Journal of the Science of Food and Agriculture, 82(14), 1661-1671.

Sunarharum, W. B., Williams, D. J., & Smyth, H. E. (2014). Complexity of coffee flavor: A compositional and sensory perspective. Food Research International, 62, 315-325.

Tavagnacco, L., Schnupf, U., Mason, P. E., Saboungi, M. L., Cesàro, A., & Brady, J. W. (2011). Molecular dynamics simulation studies of caffeine aggregation in aqueous solution. The Journal of Physical Chemistry B, 115(37), 10957-10966.

Trefis Team. (2016, July 19) K-Cups: The New Growth Driver For Starbucks? Retrieved September 2019 from https://www.forbes.com/sites/greatspeculations/2016/07/19/k-cups-the-new-growth-driver-for-starbucks/#6109ec23a8e2

Uman, E., Colonna-Dashwood, M., Colonna-Dashwood, L., Perger, M., Klatt, C., Leighton, S., ... & Hendon, C. H. (2016). The effect of bean origin and temperature on grinding roasted coffee. Scientific reports, 6, 24483.

[redacted]

Vargaftik, N. B., Volkov, B. N., & Voljak, L. D. (1983). International tables of the surface tension of water. Journal of Physical and Chemical Reference Data, 12(3), 817-820.

Voilley, A., & Simatos, D. (1980). Modeling the solubilization process during coffee brewing. Journal of Food Process Engineering, 3(4), 185-198.

Von Blittersdorff, M., & Klatt, C. (2017). The Grind—Particles and Particularities. In The Craft and Science of Coffee (pp. 311-328). Academic Press.

Wang, N. (2012). Physicochemical changes of coffee beans during roasting (Doctoral dissertation, University of Guelph).

Wang, X., & Lim, L. T. (2014). Effect of roasting conditions on carbon dioxide degassing behavior in coffee. Food Research International, 61, 144-151.

Wang, X., William, J., Fu, Y., & Lim, L. T. (2016). Effects of capsule parameters on coffee extraction in single-serve brewer. Food Research International, 89, 797-805.

Wei, F., & Tanokura, M. (2015). Chemical changes in the components of coffee beans during roasting. In Coffee in health and disease prevention (pp. 83-91). Academic Press.

[redacted]

Zanin, R. C., Corso, M. P., Kitzberger, C. S. G., dos Santos Scholz, M. B., & de Toledo Benassi, M. (2016). Good cup quality roasted coffees show wide variation in chlorogenic acids content. LWT, 74, 480-483.

Zanoni, B., Pagliarini, E., & Peri, C. (1992). Modelling the aqueous extraction of soluble substances from ground roasted coffee. Journal of the Science of Food and Agriculture, 58(2), 275-279.